UNIVERSITÉ DU LUXEMBOURG

PhD-FSTM-2021-063

Faculty of Sciences, Technology and Medicine

DISSERTATION

Presented on 28 / 09 / 2021 in Luxembourg
to obtain the degree of

DOCTEUR DE L'UNIVERSITÉ DU LUXEMBOURG

EN BIOLOGIE

by

Davide G. FRANCHINA
Born on 5 January, 1991 in Messina (Italy),

A dangeROS liaison:
the metabolism-dependent regulation of B lymphocytes

Dissertation defense committee:

Dr Dirk Brenner, dissertation supervisor
Professor, University of Luxembourg

Dr Stephanie Kreis, chair
Professor, University of Luxembourg

Dr med Karl S. Lang, vice-chair
Professor, University Hospital Essen

Dr Julia Jellusova
Professor, Technical University Munich

Dr Hans-Martin Jäck
Professor, University Hospital Erlangen

Davide G. Franchina

Experimental and Molecular Immunology group,
Department of Infection and Immunity,
Luxembourg Institute of Health

Submitted for PhD in Biology in July 2021 (Semester 9).

A dangeROS liaison: the metabolism-dependent regulation of B lymphocytes

In memoria di mio padre

…

Affidavit

I hereby confirm that the PhD thesis entitled “A dangeROS liaison: the metabolism-dependent regulation of B lymphocytes” has been written independently and without any other sources than cited.

Luxembourg, _____

_____

Davide G. Franchina

Acknowledgements

During the past five years, I have been incredibly fortunate to have been supported by many colleagues and associates, and copious amounts of thanks are owed for making this work possible.

I am thankful to my supervisor Dirk Brenner, firstly for employing me as a completely inexperienced, insecure new graduate into his lab, and then encouraging me to take on the B cell challenge and build my confidence and independence. Thank you for your continuous support and patience.

The other EMI members have all played a part in this project. The PostDocs and lab techs have been generous with their time, expertise, advice, encouragement and empathy. Melanie and Carole deserve special recognition for the team effort that made our viral-endpoint factory feasible. Carole Weis, who can answer any administrative or organizational related question known to man, and who works hard to support the lab.

Among my colleagues, who all deserve thanks from me, some have made particular contributions that must be acknowledged hereafter. Henry, on every occasion that I have encountered a problem that I believed to be insoluble, a discussion with you has solved it. Luana and Lynn, you wisely advised me on almost everything I know about research and hands-on lab practice, and have done so with inexhaustible kindness and patience. Leticia and Anouk, thank you for the many hours of excellent support and good humor.

Aside from the colleagues in our lab, Christophe Capelle provided invaluable general laboratory advice and regular pep talks. François Hafezi, Nathan Reynders and Max Meyrath guided me expertly through the vagaries of western blotting and instructed me on luminesce-based assays. I am also very grateful to the staff of the National Cytometry

Platform for training and technical support for the microscopy experiments and cell sorting. The animal house staff at LIH and University of Luxembourg have been most supportive in ensuring the welfare of our mice.

Niels Vandamme, for expert advice on single cell sequencing preparation and analysis. Anaïs Carpentier, for working hard to make the electron microscopy possible and Anna Rita Minafra for carrying out the nontrivial VSV infection models.

I am thankful to Dr Elisabeth Letellier and Prof. Hans-Martin Jäck, my examiners for my *Comité d'Encadrement de Thèse* yearly meetings, who pointed out flaws in my thinking and provided helpful discussions to guide me in the right direction.

This project was funded by the *Fonds National de la Recherche* (FNR) and conference travels were supported by funding from the *Società Italiana di Immunologia, Immunologia Clinica e Allergologia* (SIICA) and the Doctoral School in Science and Engineering (DSSE) from the University of Luxembourg.

My friends also earned my gratitude for the virtual drinks and pizza nights, and for their understanding of plans abandoned when the lab called.

I owe a debt of gratitude to my family, who raised me to enjoy learning and for providing continuous support. My brother, the first Dr Franchina, demonstrated beautifully how the task should be accomplished: efficiently, with passion and without drama.

Finally, more than anyone, to Rebeca, my perpetual source of moral support. I couldn’t have done any of this without you.

Abstract

Marginal and follicular B cells (MZB and FoB) possess diverse developmental, phenotypic, functional and transcriptomic attributes at steady state. The engagement of distinct redox systems contributes to the metabolic reprogramming of immune cells. However, the function of the main intracellular antioxidant glutathione (GSH) in the context of B cells redoxtasis is unknown. By using mice with B cell-specific ablation of the catalytic subunit of glutamate cysteine ligase (*Gclc*), we show that GSH loss affects the homeostatic persistence of MZB and that GSH-dependent redox regulation is critical for the control of MZB versus FoB metabolic dependencies. Although *Gclc* ablation does not prevent the formation of FoB, *Gclc*-depleted mice exhibit ineffective germinal center reactions and null antibody response upon *in vivo* viral infection. Similarly to wild-type MZB, *Gclc*-deficient FoB show increased ATP levels, glucose metabolism, mTOR activation, and protein synthesis but accumulate defective mitochondria. Moreover, blocking of glucose uptake *in vitro* limits ATP production and accelerates apoptosis in *Gclc*-deficient FoB. Thus, GSH-dependent redox control is crucial for B cell activation and determines the metabolic identity of MZB and FoB.

Table of content

Abbreviations

2-NBDG	2-[N-(7-nitrobenz-2-oxa-1,3-diazol-4-yl) amino]-2-deoxy-D-glucose
3PG	3-Phosphoglyceric acid
Ab	Antibody
Ag	Antigen
Ant	Antimycin A
APC	Antigen presenting cell
Asc	Ascorbate
ASC	Antibody secreting cell
ATA	Anti–Thy-1 autoantibody
ATP	Adenosine triphosphate
B6	C57BL/6
BAFF	B cell activating factor
BAFFR	BAFF receptor
BCR	B cell receptor
BLIMP-1	B lymphocyte-induced maturation protein-1
BM	Bone marrow
C	Constant
CD	Cluster of differentiation
cDNA	Complementary DNA
CDR3	Complementarity-determining region 3
CI-II-III-IV	Complex I-II-III-IV
CL13	Clone 13
CLP	Common lymphoid progenitor
CLR	C-type lectin receptor
CMP	Common myeloid progenitor
CR1	Complement receptor 1
CR2	Complement receptor 2
CS	Citrate synthase
CSR	Class-switch recombination
CTL	Cytotoxic T lymphocyte
CXCL	C-X-C motif chemokine ligand
CXCR	C-X-C motif chemokine receptor
DC	Dendritic cell
DNA	Deoxyribonucleic acid
DZ	Dark zone
ECAR	Extracellular acidification rate
ELISA	Enzyme-linked immunosorbent assay
ER	Endoplasmic reticulum
ETC	Electron transport chain
FACS	Fluorescence-activated cell sorting
Fc	Fragment crystallizable
FDC	Follicular DC
FoB	Follicular B cell
FOI	FoB I
FOII	FoB II
GC	Germinal center

GCL	Glutamate cysteine ligase
GCLC	GCL catalytic subunit
GCLM	GCL modifier subunit
Glu	Glutamate
GLUT1	Glucose transporter 1 (SLC2A1)
Gly	Glycine
Gp	Glycoprotein
GPX	GSH peroxidase
GR	GSH reductase
GRX	Glutharedoxin
GS	GSH synthase
GSEA	Gene Set Enrichment Analysis
GSH	Glutathione, reduced
Gsk3	Glycogen synthase kinase 3
GSSG	Glutathione, oxidized
GST	GSH-S-transferase
H&E	Hematoxylin and eosin
H_2O_2	Hydrogen peroxide
HIF-α	Hypoxia-inducible factor 1-α
HIV-1	Human immunodeficiency virus-1
i.p.	Intra-peritoneal
i.v.	Intra-venous
Ig	Immunoglobulin
IgH	Immunoglobulin heavy chain
IgL	Immunoglobulin light chain
IL-	Interleukin-
ILC	Innate lymphoid cell
ITAM	Immunoreceptor tyrosine-based activation motif
KLH	Keyhole limpet hemocyanin
LCMV	Lymphocytic choriomeningitis virus
LZ	Light Zone
M	Mature
MAC	Membrane attack complex
Mal	Malate
MAS-B	Mannitol and sucrose–BSA
MFI	Mean fluorescence intensity
MHC	Major histocompatibility complex
MID	Mass isotopomer distribution
mtDNA	Mitochondrial DNA
Myc	Myelocytomatosis virus oncogene cellular homolog
MZB	Marginal zone B cell
NA	Natural antibody
$NADP^+$	Nicotinamide adenine dinucleotide phosphate, oxidized
NADPH	Nicotinamide adenine dinucleotide phosphate, reduced
nDNA	Nuclear DNA
NFκB	Nuclear factor kappa-light-chain-enhancer of activated B cells
NK	Natural killer
NLR	NOD-like receptor

NOX	NADPH oxidase
O_2	Molecular oxygen
$O_2^{\cdot -}$	Superoxide
OCR	Oxygen consumption rate
OCT	Optimum cutting temperature
Oligo	Oligomycin A
OXPHOS	Oxidative phosphorylation
PAMP	Pathogen-associated molecular pattern
PBS-T	Phosphate buffered saline-Tween
PC	Phosphorylcholine
PCs	Plasma cells
PER	Proton efflux rate
PPP	Pentose phosphate pathway
PRR	Pattern recognition receptor(s)
PtC	Phosphatidylcholine
PTP	Tyrosine phosphatase
Pyr	Pyruvate
RAG	Recombinant activating gene
RBCs	Red blood cells
RLR	RIG-I-like receptor
RNA	Ribonucleic acid
RNA-seq	RNA sequencing
ROS	Reactive oxygen species
Rot	Rotenone
RT	Room temperature
S1P	Sphingosine-1-phosphate
S1PR	Sphingosine-1-phosphate receptor
scRNA-seq	Single cell RNA sequencing
SDH	Succinate dehydrogenase
SHM	Somatic hypermutation
sIgD	Surface IgD
sIgM	Surface IgM
SLO	Secondary lymphoid organ
Syk	Spleen tyrosine kinase
T1	Transitional B cell 1
T2	Transitional B cell 2
T3	Transitional B cell 3
TB	Transitional B cell
TCA	Tricarboxylic acid
TCR	T cell receptor
TD	T lymphocyte or thymus-dependent
TdT	Terminal deoxynucleotidyl transferase
TEM	Transmission electron microscopy
Th	T helper
Thy-1	Thymocyte Ag 1
TI	T lymphocyte or thymus-independent
TLR	Toll-like receptor
TMPD	N,N,N′,N′-Tetramethyl-p-phenylenediamine
TNP	2,4,6-Trinitrophenyl
TRAF3	Tumor necrosis factor receptor-associated factor-3

Tregs	T regulatory cells	**V**	Variable
Trx	Thioredoxin	**VSV**	Vescicular stomatitis virus
TrxR	Trx reductase	**XBP1**	X-box binding protein 1
tSNE	T-distributed stochastic neighbor embedding	**$\Delta\Psi_m$**	Mitochondrial membrane potential

List of figures

Chapter 1

Chapter 3

Chapter 4

Chapter 5

Chapter 6

Chapter 7

Chapter 1: Introduction

1.1 Overview of the Effector Mechanisms of the Immune Response

The extreme biodiversity of microorganisms constantly threatens the survival of higher order animals due to the ever-evolving evolutionary-driven conflict of survival (Dobzhansky, 1973; Strassmann et al., 2011). The minimal need of organic energy allows the fast reproductive cycle of microorganisms, which is inherently associated with the ability to accumulate mutations (O'Neill, 2000). Together with environmental factors, this may result in the evolution of mechanisms or behavior modifications that lead to evasion of host clearance, endowing microorganisms with pathogenic potential. In mammals, the answer to limit the constant threat of potential pathogens (virus, bacteria, fungi and parasites) is a complex and multifaceted variety of molecules and effector cells that together make up the immune system. Both innate and adaptive mechanisms synergize to ensure host survival and reproduction of the species.

Protection against pathogens relies on several layers (Figure 1). Anatomic and chemical barriers, such as the skin and mucosal surfaces, are the initial defenses against infection. At these sites, chemical and enzymatic systems act as physical resistance. If anatomical barriers are breached, the components of the innate immune system come into action, and inflammatory inducers unique to microbes or chemicals by damaged cells are released. These molecules act on sensor cells to inform about the infection. Activated sensor cells amplify the signals of cellular recruitment and activation and, in a cascade mechanism, other innate cells are recruited and activated. These cells then migrate into target tissues to provide specific effector activities, such as cell killing or production of cytokines, aimed to

reduce or eliminate the infection. In particular, different effector activities in target tissues can induce several types of inflammatory cells that are especially suited for eliminating viruses, intracellular bacteria, extracellular pathogens, or parasites (Janeway CA Jr et al., 2016b).

Adaptive immunity is initiated when the innate immune response fails to control the expansion of the microorganism. The adaptive immune system is based on the specific recognition of elements or molecules referred to as antigens (Ags), which are specific to the individual pathogen. This recognition is based on the presence of a virtually unlimited repertoire of Ag receptors, which are found on the surface of the two types of lymphocyte of the adaptive system: B and T cells. B cells, whose name comes from the *bursa fabricii* or bone marrow (BM) in mammals (Cooper et al., 1965), recognize soluble Ags through their B cell receptor (BCR). T cells, which develop in the thymus (hence the name), express the T cell receptor (TCR) and recognize protidic Ags presented on the surface of other cells (infected cells or Ag-presenting cells, APCs). Each B and T cell carries several molecules of one Ag receptor type (BCR or TCR) capable of binding a single Ag specificity. During the course of the immune response, if the BCR or TCR is engaged by the Ag, the cell bearing that specificity is selected and amplified (Burnet, 1959). This mechanism allows the host to generate a number of adaptive immune cells that are specifically targeted to the invading pathogen and can limit its proliferation and harmful consequences (*i.e.* development of pathology), thus promoting the survival of the host (Figure 1).

Once the pathogen is cleared, some of the adaptive immune cells are able to confer immunological memory. This is the ability of the adaptive branch of immune system, which can recall the original Ag and mount an immune response in case of reencounter, thus avoiding the manifestation of the disease and providing long-term protection (Ahmed and Gray, 1996; Zinkernagel et al., 1996).

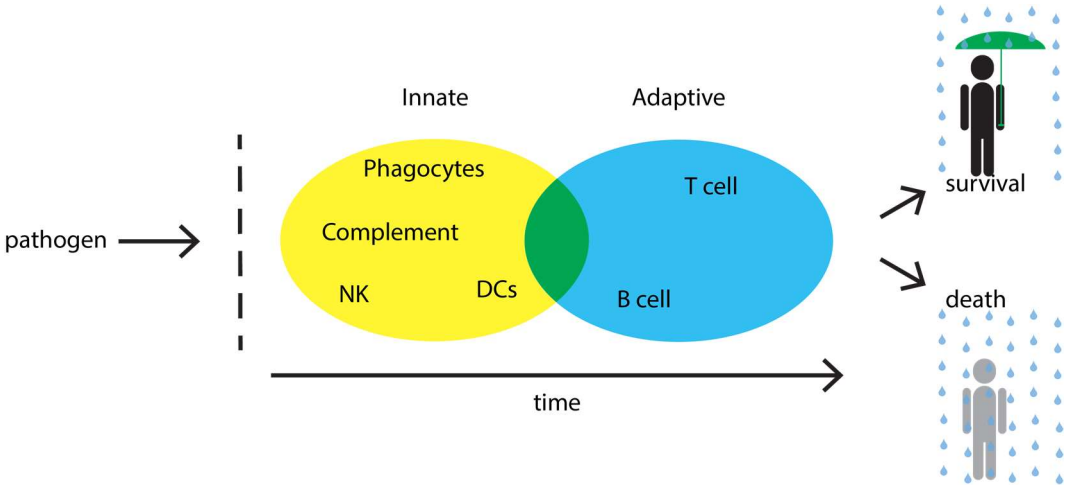

Figure 1: Schematic and simplified overview of the immune defense layers and outcomes.

A pathogenic microorganism breaches the physical barriers of the body (dotted line) and is naturally recognized by the innate arm of the immune system (yellow area). If the pathogen and the inflammatory stimuli persist, the adaptive cells are activated (blue area) in the process of clonal expansion. If the expanded cells can overcome the pathogen, the inflammation is terminated and allows the survival of the host. NK: natural killer cells; DCs: dendritic cells.

1.2 Principles of the Innate Immune Response

Innate immunity uses a defined number of secreted proteins and receptors to detect the infection. These mechanisms are referred to as inborn and are genetically inherited. Once a pathogen overcomes the passive defenses (*i.e.* physical barriers and antimicrobial proteins), it encounters the proteins of the complement system, a group of circulating heat-sensitive proteins that was originally named *alexines* (Beumer, 1962). Complement can be activated directly by pathogens or indirectly by pathogen-bound antibodies (Abs). These Abs, alternatively named immunoglobulins (Igs), are capable of coating (or opsonizing) the surface of the pathogen, thus facilitating killing and inducing inflammatory responses that help to fight infection. Cells of the innate immune system express several receptors that recognize the pathogen or complement proteins attached to it. The engagement of such receptors in neutrophils, macrophages and dendritic cells (DCs) can rapidly trigger a process known as phagocytosis, during which the cell uses its plasma membrane to engulf and eliminate the pathogen (Flannagan et al., 2009). In addition, innate cells express membrane receptors that activate intracellular signaling pathways. These pathways induce the synthesis and secretion of a range of proteins, such as cytokines and chemokines that help maintaining local inflammation and help to recruit more cells to the site of infection.

This process sets the stage for the initiation of the adaptive immune response by APCs, which are recruited to the infection site and internalize the pathogen or its components. By acting fast, the aim of the innate immune system is to hinder the establishment of a focus of infection. Indeed, activated APCs represent the bridge toward the induction of the adaptive immune response, should the innate phase not fulfill its function. APCs are capable of starting the adaptive phase of the immune response by migrating to the

secondary lymphoid organs (SLOs) where most of the B and T lymphocytes reside in a naïve status.

1.2.1 Overview of the Complement System and Natural Antibodies

The complement system includes more than 20 proteins whose main function is to induce and increase inflammation, phagocytosis activity and membrane bursting of the target. These proteins are often proteases secreted by liver cells in an inactive form known as zymogen. Proteins that recognize and opsonize the pathogen trigger one of the three complement pathways. The detection of the target activates the first zymogen, triggering a cascade of proteolysis in which complement zymogens are activated sequentially, each of them becoming an active protease that cleaves and activates many molecules of the next zymogen, amplifying the signal as the chain unfolds (Merle et al., 2015). In addition, complement proteins indirectly boost the adaptive immune response. Indeed, opsonized pathogens are more easily recognized and phagocytized by APCs, thus enhancing the presentation of Ags to T lymphocytes. Notably, a specific B cell subset named Marginal Zone B cells (MZB) cooperate with the complement system. MZB are strategically located in the spleen, at the interface with the blood circulation and express complement receptors 1 and 2 (CR1 and CR2) (Pillai and Cariappa, 2009). These cells contribute to both the innate response and Ag presentation for the subsequent adaptive phase (Haas et al., 2002; Ferguson et al., 2004; Cinamon et al., 2008).

As mentioned above, body fluids contain several complement proteins. These are grouped in three main activation pathways: classical, alternative and the lectin pathway. Each route is marked by a specific chain reaction that ultimately funnels into the activation of the same protein, the complement protein 3 (C3), which triggers the lytic resolution of the target. Particularly, the proteolysis of C3 culminates into the splitting of the C5, which

in turn is cleaved into C5b and C5a. C5b opsonizes the target and promotes the activation and binding of the proteins C6, C7, C8 and C9. Altogether, the C5-9 proteins form the membrane-attack complex (MAC). MAC, also known as lytic complex, is assembled into the outer membrane of the bacteria and contribute to their death by lysis (Merle et al., 2015) (Figure 2).

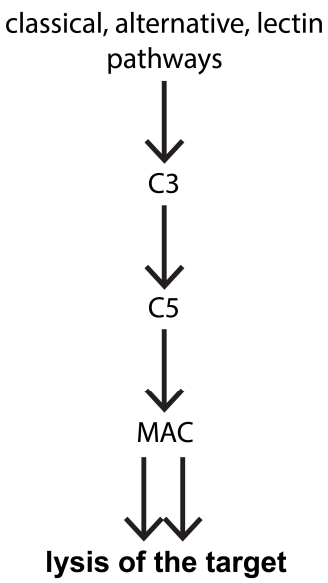

Figure 2: Common players of the three complement pathways.

The ultimate goal of the complement system is the physical destruction of the target. Here, the shared components of the three complement pathways are depicted.

For the purpose of this thesis, the classical pathway deserves more attention as it is inherently connected to the function of B cells and Abs. The classical pathway is initiated by the C1 protein, which is formed by the assembly of three subcomponents C1q, C1r and C1s. Of these, C1q binding to the target induces a conformational change that allows the sequential activation of the proteases C1r and C1s (Janeway CA Jr et al., 2016f). The activated C1s acts on the next components of the classical pathway, ultimately converging in the activation of C3. C1q acts as pathogen sensor of the classical pathway. It can bind the pathogen directly, or indirectly through the C-reactive protein or the constant fragment (Fc) of Abs that are already attached to the pathogen (Figure 3 A) (Janeway CA Jr et al., 2016f). Thus, C1q links the innate phase of the immune response to the effector functions of the adaptive immunity. At this point of the immune response only innate mechanisms are being activated by the detection of the pathogen. Nonetheless, spontaneous Abs are found in the circulation of mice and humans (Avrameas, 1991).

Abs can be subdivided into Ag-dependent and Ag-independent, depending on the type of inducer of the immune response (Ochsenbein and Zinkernagel, 2000). Ag-dependent Abs are generally diversified upon the germinal center reaction, which will be discussed in the next sections. On the other hand, Ag-independent Abs are found in the serum of unimmunized animals and they are spontaneously produced before Ag exposure (Ehrlich and Morgenroth, 1902). Ag-independent Abs are also known as natural Abs (NAs) and are so called because they are capable of binding diverse microbial determinants and autoantigens, protecting the host by favoring opsonization, complement activation and therefore elimination of pathogens and cellular debris (Casali and Schettino, 1996; Baumgarth et al., 2005). NAs are polyreactive Abs, meaning that their Ag-binding pocket is flexible and thus can bind to several Ags, albeit with different affinities (Notkins, 2004; Zhou et al., 2007). The polyreactive nature of NAs may explain why they can recognize a

plethora of foreign and self-Ags, including tumor Ags (Vollmers and Brandlein, 2009). Primarily found as immunoglobulin M or G3 (IgM or IgG3) isotypes, mouse NAs appear to be produced mainly by a specific subset of B cells found in the peritoneal and pleural cavities and named B1 cells (Lalor et al., 1989; Baumgarth et al., 1999; Tumang et al., 2005; Choi et al., 2012) or, to a lesser extent by MZB (Ichikawa et al., 2015). In particular, IgM is the class of Ab most efficient at binding C1q, making NAs an effective mean of activating complement on microbial surfaces (Figure 3 A). The function of NAs becomes crucial when viruses or bacteria are not locally controlled, and, therefore spread in the system.

NAs exert protection against infections in three ways (Figure 3). In some cases, NAs can mediate direct neutralization of the pathogen in the circulation, which is then more efficiently detected and phagocytized (Figure 3 B). Indeed transfer of serum containing NAs were found to be protective for viral (Ochsenbein et al., 1999a) and pneumococcal infections (Briles et al., 1981). NAs-mediated protection can occur also indirectly in two ways, via the complement system. As mentioned above, when an infectious particle spread in the blood, they can be opsonized by NAs. The NA-Ag complex can directly activate the complement and induce the lysis of the target (Figure 3 A). In fact, the Fc portion of the NA binds C1q and initiates the lytic cascade. Otherwise, the NA-Ab particles travel the blood and are more efficiently filtered out by splenic cells. The increased trapping of Ags in the spleen enhances the B and T cell response by activating MZB directly (Figure 3 C) or favoring activation of APCs, respectively. In particular, both MZB and APCs express CR1 and CR2 (Caroll and Prodeus, 1998), which have important implication in the early activation of the adaptive immune response leading to enhanced antigen presentation by APCs and lowering the threshold of B cell activation (Ochsenbein and Zinkernagel, 2000).

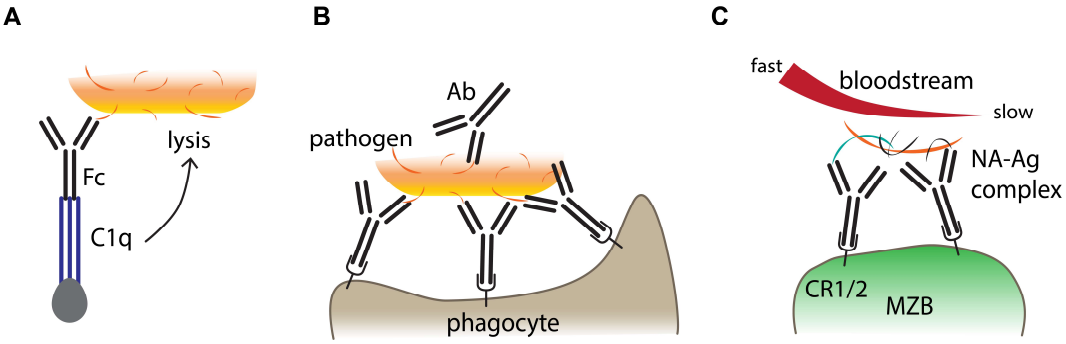

Figure 3: Natural antibodies exert multiple functions across innate and adaptive immune mechanisms.

A. C1q bridges the innate functions of the complement to antibody recognition. **B.** Natural antibodies sterically block the pathogen binding sites and increase phagocytic activity. **C.** Splenic filtration of natural antibody-antigen complexes facilitates MZB activation in the spleen. Fc, constant fragment; Ab, antibody; NA, natural antibody, Ag, antigen; CR1/2, complement receptor 1/2.

As a matter of fact, the action of NAs is not sufficient to block the hematogenic spread of the pathogen. However, the presence of NAs in Ag-inexperienced hosts can be seen as the results of an evolutionary mechanism led by the need of counteracting mechanisms of pathogen elusion of the innate response, therefore creating an additional shortcut to set the stage for the adaptive response. More importantly, NAs are important for the maintenance of B cell tolerance. To this extent, NAs are able to enhance the "eat me" signals by apoptotic cells or exhausted red blood cells. Indeed, one of the canonical signal of cells undergoing apoptosis is the expression of the outer layer of the plasma membrane of the otherwise sequestered phospholipids (Bratton et al., 1997). NAs are indeed able to bind some phospholipids, such as phosphorylcholine (PC), which is the most abundant component of all eukaryotic cells (Cui and Houweling, 2002). In healthy cells PC is not available for immune recognition, but during apoptosis, PC is subject to oxidizing conditions and emerge as neo-Ags (Binder and Silverman, 2005), thus liable of NA recognition. It is important to note that PC is also the major determinant of the pneumococcal cell wall (Briles et al., 1981; Haas et al., 2002), which then explain the cross-reactive properties of such Abs that will be discussed later. The removal of apoptotic bodies and debris is of crucial importance to ensure the active elimination of intracellular Ags that would otherwise accumulate. If the Ag persists, chances are that autoreactive B cells or T cells that have escaped the mechanisms of central tolerance are activated, and promote autoimmune reactions (Nguyen et al., 2015).

1.2.2 Overview of Pattern Recognition Receptors and Innate Immune Cells

Epithelial barriers, antimicrobial peptides, complement proteins and NAs represent the early response of the innate immune response against pathogens. Cellular components of the innate immune system play a crucial role in the initiation of the inflammation, its containment and set the stage for the adaptive response. In particular, phagocytic cells that

scavenge pathogens represent an ancient mechanism of innate immunity. Positioned in the proximity of the epithelial barriers, specialized resident phagocytic cells named macrophages are responsible of pathogen recognition through a series of receptors that are able to bind repeated structure found mainly in microorganisms, which are referred to as pathogen associated molecular patterns (PAMPs). These pattern recognition receptors (PRRs) are germline-coded and expressed non-clonally, that is, they are expressed on all the cells of a given innate cell type such as phagocytes (Akira et al., 2006). PRRs can identify a diverse collection of microbial pathogens, which include bacteria, viruses, parasites, fungi and protozoa.

Since each microorganism has a different way to take over cellular functions, PRRs are strategically located in different parts of the cell and can be classified based on their localization. Membrane bound PRRs include toll-like receptors (TLRs) which recognize bacterial lipids, viral RNA, bacterial DNA or proteins. Upon pathogen detection the intracellular domain of TLRs initiates a signaling cascade that promotes anti-microbial defense and inflammation (Beutler, 2009). The second group of membrane-bound PRRs are the C-type lectin receptors (CLRs), which bind to carbohydrates in a calcium-dependent manner. For instance, mannose is commonly found on fungi and viruses, while fucose is common in bacteria and parasites (Dambuza and Brown, 2015). Intracellularly, PRRs are subdivided into nucleotide oligomerization-like receptors (NLRs) and retinoic acid-inducible gene I-like receptors (RLRs). While NLRs recognize intracellular bacterial peptidoglycan motifs, RLRs help recognizing viral RNA (Baccala et al., 2009). Lastly, a number of PRRs can be secreted by cells and directly bind to invading microorganisms. Some examples of these proteins are collectins, pentraxin and ficolins (Bottazzi et al., 2010).

As discussed above, PRRs are expressed in other phagocytic cells, such as granulocytes and DCs. Granulocytes, mainly represented by neutrophils, but also eosinophils and basophils are short-lived cells that continuously stem from the BM and circulate freely in the blood unless recruited at the site of infection (Amulic et al., 2012). Although DCs are good at engulfing pathogens or their product, their main role is to break down pathogenic peptides for the presentation to B and T cells. For this reason, DCs are considered professional APCs and are crucial for the induction of the adaptive immune response (Stockwin et al., 2000). Innate cells are defined by their properties so far discussed in the context of the immune response and arise from a common myeloid progenitor (CMP). However, some cells with innate functions share the common ancestor of the adaptive immune cells, which is the common lymphoid progenitor (CLP). These cells are known as innate lymphoid cells (ILCs) and their name derives from the fact that they mirror phenotypic and functional characteristics of T cells, but lack specific rearranged Ag receptors (Eberl et al., 2015). In particular, ILCs are categorized into groups according to the transcription factors mediating their development and cytokine production. ILCs include natural killer (NK) cells and ILC1s (often combined to NK cells), ILC2s, ILC3s, which represent the "innate" counterpart of CD8-expressing ($CD8^+$) cytotoxic (CTL), Th1, Th2 and Th17 respectively. ILCs are mainly located at mucosal interfaces and are implicated in immune surveillance, inflammation and tissue remodeling (Vivier et al., 2018).

1.3 Principles of the Adaptive Immune Response

The immune response is a dynamic process that begins with the Ag-independent mechanisms of defense attributed to the innate immunity and becomes more Ag-centered and more effective as the Ag-specific adaptive immune phase matures. As discussed in the previous sections, the innate immunity players not only limit the proliferation of the microorganism, but also anticipate the adaptive B and T cell responses. Adaptive immunity sets off when innate defense mechanisms are eluded or overwhelmed. At this point, loaded APCs that migrated away from the infected tissue enter SLOs, where they initiate the adaptive immune response. Here, both B and T cells are activated and provide Ag-specific targeted weapons to limit the pathogen growth and the possibility of infection.

1.3.1 T Cell Activation and Fates

Naïve T cells are stimulated by recognition, through their TCR, of the antigenic peptide presented on specialized molecules called major histocompatibility complex (MHC) class I and II, expressed on the surface of APCs (Rock et al., 2016). Naïve T cells constantly recirculate between SLOs, blood, and lymphatic circulation. By trafficking through SLOs, T cells encounter APCs which are likely to be presenting foreign Ags on their MHC complexes (Janeway CA Jr et al., 2016a). APCs must deliver two distinct signals in order to activate T cells: one to TCR via the peptide-MHC complex, and a second co-stimulatory signal (Janeway CA Jr et al., 2016c). Importantly, the APC must deliver the Ag signal and the co-stimulatory signal simultaneously to the T cell for activation to occur. In general, DCs deliver the best co-stimulation and are responsible for activating most naïve T cells. Once activated, T cells express other receptors and secrete cytokines with autocrine effect, which overall enhance co-stimulation and potentiate feedback mechanisms to begin clonal proliferation and differentiation into armed effector T cells (Janeway CA Jr et al., 2016c).

After clonal expansion, T cells exert their effector functions without the need of costimulation. However, the primed T cell must bind the peptide-MHC complex in order to release its effector function on the target cell (Bretscher, 1999).

Different T effector cells are specialized to deal with different kinds of pathogens. In particular, three classes of T effector cells can be distinguished: $CD8^+$ cytotoxic T lymphocytes (CTL), $CD4^+$ T helper cells (Th) and T regulatory cells (Tregs). CTL kill infected cells displaying cytosolic pathogen peptides on MHC class I molecules. $CD4^+$ Th1 cells activate macrophages with persistent vesicular pathogens whose peptides are displayed on MHC class II molecules. $CD4^+$ Th2 cells activate B cells that have used their membrane Ig to internalize a specific antigen and display peptides on MHC class II molecules (McGhee, 2005). Th2 cells are heavily involved in responses against extracellular pathogens and parasites. Moreover, a third subset of $CD4^+$ Th cells is distinguished by the production of interleukin-17 (IL-17), and are stabilized by IL-23. Studies have shown that these cells contribute to the response during infection by extracellular and intracellular bacteria and fungi, but are also implicated in autoimmune processes (Cua et al., 2003). Lastly, $CD4^+$ Tregs (Shevach, 2011) control the passive mechanisms of immune-tolerance with an array of suppressive mechanisms. Furthermore, Tregs adapt to inflammatory conditions and exert crucial functions in controlling the end of immune responses (Sakaguchi et al., 2008).

Primary $CD8^+$ T cell responses to pathogens usually require $CD4^+$ T-cell help. However, the pattern described earlier is not fixed, because immune cells and activated T cells retain certain plasticity for adaptation to the ongoing immune response (Murphy and Stockinger, 2010). At the end of the infection, when the pathogen is eliminated, the majority of the clonally expanded effector T cells contracts dramatically and only few long-lived T cells survive to provide long-lasting memory of the infection, thereby providing protective

immunity against re-infections (Ahmed and Gray, 1996; Zinkernagel et al., 1996). However, the integration of cell- and Ab-mediated immunity is critical for effective protection against many types of pathogens. Therefore, B cell-mediated functions, which will be discussed in the following paragraphs, complement the Ag-specific adaptive response.

1.3.2 B Cell Priming and Activation

As detailed in the previous sections, B cells recognize Ags through their BCRs. The BCR is a membrane-bound Ab composed of two functional parts: the variable (V) and the constant (C) region (Figure 4). The V region varies extensively and contains the site of Ag-binding, while the C region has 5 isoforms (known as isotypes) which allow the Ab molecule to engage into 5 different effector mechanisms (Janeway CA Jr et al., 2016e). From a structural point of view, the Ab molecule possesses two different structural units in pairs known as heavy (H or IgH) and light (L or IgL) chains, which are arranged to form a Y-shape (Figure 4). It is important to note that the BCR does not have these effector functions. Its role is to bind the Ag through the V portion and transmit the signal intracellularly through the C part, which will eventually lead to B cell activation, clonal expansion and Ab production. In particular, B cell activation can be initiated by BCR recognition of both unprocessed membrane-associated and soluble Ags (Treanor, 2012).

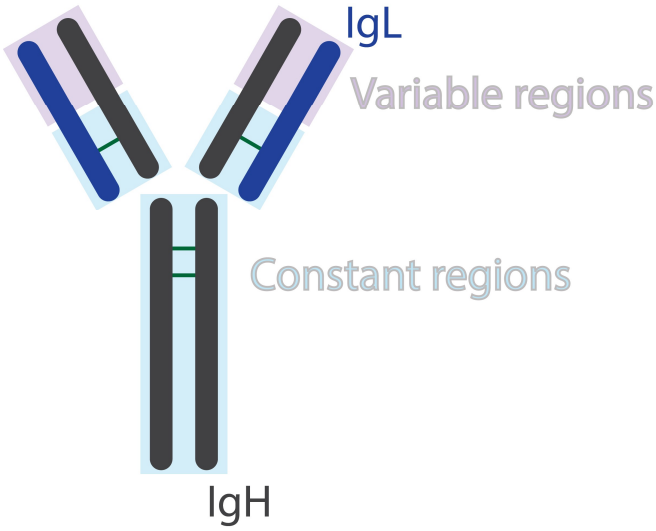

Figure 4: The immunoglobulin molecule possesses distinct functional and structural parts.

Functional and structural components of the generic immunoglobulin molecule are color-coded. Green lines represent disulfide bonds. The light chains (IgL) of an antibody can be classified as either kappa (κ) or lambda (λ) type based on small differences in polypeptide sequence. The heavy chain (IgH) makeup determines the overall class of each antibody.

Ag encounter happens in SLOs, such as lymph nodes and spleen, because they are evolutionary developed to concentrate soluble Ags, APCs and immune cells. In fact, SLOs are well connected to both blood and lymphatic system. Upon entry in resting SLOs, B lymphocytes continuously scan the environment in search of the Ag displayed on MHC complexes matching their BCR. Ag detection by B cells materializes through direct encountering of soluble Ags, or it is mediated through APCs such as macrophages, DCs and follicular DCs (FDCs). Rapid diffusion of small molecules through the splenic subcapsular sinus can happen without the requirement of cell-mediated presentation (Pape et al., 2007). However the existence of pores in the regions of the subcapsular sinus that are adjacent to the lymph-node parenchyma have opened to the possibility of the passive diffusion of soluble Ags (Batista and Harwood, 2009). Thus, Ag priming is usually mediated through cellular assistance.

Macrophage-mediated presentation provides one way for BCRs to bind large soluble and particulated Ags. It is not completely clear if such Ags are retained on the surface of the macrophage or internalized, but subcapsular-sinus macrophages in lymph nodes have limited phagocytic activity, which favor the notion of the direct display of Ags on the cell surface (Szakal et al., 1983). The accumulated Ag is presented in its intact form for BCR recognition, and this mechanism has been reported to be one way of initiating the activation of a neighboring FoB (Phan et al., 2007). Furthermore, DCs are classically considered the most effective class of APCs. Indeed, after Ag collection at the infection site, DCs migrate to the SLOs (Janeway CA Jr et al., 2016b). However, B cells recognize Ags in their unprocessed form, thus DCs necessitate a mechanism to hold and display the Ags on their surface, in a way that is resistant to intracellular degradation (Qi et al., 2006). One more mechanism of cellular-assisted Ag presentation is provided by FDCs. These APCs possess different features compared to DCs, including but not limited to location, ontogeny and

specific organizational functions (Aguzzi et al., 2014). In particular, FDCs are considered the main B cell activators in the primary lymphoid follicles (Tew et al., 2001), which are aggregates of B, T and stromal cells found within the SLOs. Importantly, FDCs are able to retain Ags on their surface via two distinct sets of receptors. On one hand, FDCs express high levels of complement receptors CR1 and CR2, which bind to C3-opsonized particles (Dempsey et al., 1996). Alternatively, FDCs retain Ags through receptors that bind the Fc region (Figure 4) of the IgG isotype, which form immune complexes by opsonizing pathogens (Nossal et al., 1964). It is important to point out that FDCs reside within the lymphoid follicles. Therefore, mechanisms are in place to permit Ags to gain access to FDCs. In particular, a subset of B cells, namely MZB, continuously shuttle Ags to and from follicles in a process that is dependent on chemotactic signals (Cinamon et al., 2004; Cinamon et al., 2008).

Following Ag binding and stimulation, B cells can process and present the Ag through its MHC class II molecules and scan for "cognate" activated $CD4^+$ T cells. To do so, B cells congregate at the boundary of the T cell areas in search of T-cell help (Liu et al., 1991; Garside et al., 1998). Cognate encounters with T cells at the B zone-T zone (B-T) boundary drive initial B cell proliferation. At this point, some responding B cells migrate from the B-T boundary to extrafollicular areas, where they are induced to differentiate into plasmablasts. These short-lived Ab-secreting cells provide an immediate source of antigen-specific Abs and offer rapid protection along with important assistance to stop fast-dividing pathogens such as viruses (MacLennan et al., 2003; Chappell et al., 2012). Alternatively, Ag-primed B cells seed germinal center (GC) reactions in the B cell follicle (MacLennan, 1994). GC B cells can be exported following one of two independent pathways of migration and differentiation. Induced GC B cells rapidly expand and differentiate into plasma cells (PCs) or develop into memory B cells, which confer protection to reinfection. The early

bifurcation of plasmablast versus GC reaction is linked to the migration properties of B cells, which depend on molecular cues that are not fully understood (MacLennan et al., 2003; Victora and Nussenzweig, 2012; Inoue et al., 2018).

1.3.3 The Germinal Center Reaction and B Cell Fates

The GC is a highly diversified and dynamic microenvironment that originates secondary B cell follicles in the course of the immune response. GC is the site of B cell maturation, during which either memory B cells or PCs are generated. Mature GCs are composed by two well defined compartments, the dark and the light zone (DZ and LZ). These compartments were originally identified on the basis of their histological appearance (Nieuwenhuis and Opstelten, 1984). Later studies have unveiled the chemotactic signals governing the GC compartmentalization, which depends on the differential abundance of the C-X-C motif chemokine ligand 12 (CXCL12), CXCL13 and the expression of the receptors CXCR4 and CXCR5 (Allen et al., 2004), together with specific phenotypic markers of the two GC B cell populations (Victora et al., 2010). The DZ is proximal to the T cell area and contains a high density of large, proliferating B cells with downregulated surface immunoglobulin expression and are sometimes referred to as centroblasts. At the distal pole lies the LZ, where B cells are interspersed among the FDC network. LZ B cells, so called centrocytes, are small, non-mitotic B cells expressing surface Igs (MacLennan, 1994).

DZ and LZ B cells are characterized by different functional properties (Victora and Nussenzweig, 2012). In particular, DZ B cells divide and undergo somatic hypermutation (SHM). SHM introduces random mutations that result in changes in the V region of the BCR by few amino acids, altering subtly the affinity of the BCR for its antigen (Papavasiliou and Schatz, 2002). DZ B cells then migrate to the LZ and compete with each

other for Ag binding, which is being displayed on FDCs. If SHM was successful in improving the BCR affinity, this B cell clone outcompetes other clones and is selected for survival. Positive selected clones internalize and present the Ag through their MHC class II to cognate $CD4^+$ follicular T cells, which provide additional survival and mitogenic signals. Importantly, cytokines secreted by these T cells direct the choice of the Ab isotype in a process called class switch recombination (CSR) (Janeway CA Jr et al., 2016d). B cells that received help can re-enter the DZ, divide more and undergo additional V region mutations. These B cells may migrate between DZ and LZ zones to undergo several more rounds of SHM and CSR, in a process known as interzonal migration or cyclic reentry model (Victora et al., 2010). The ultimate goal of the GC is to produce B cells with a BCR with high affinity for the initial Ag, a global process that is referred to as Ab affinity maturation.

During this process, some B cells are selected to leave the GC as PCs and memory B cells. PCs characteristics include a larger cytoplasmic to nucleus ratio than naïve B cells and increased amounts of rough endoplasmic reticulum (ER) (Shaffer et al., 2004; Tellier et al., 2016). This fate choice depends on specific transcriptional programs activated *ad hoc* during GC reactions, which involve the expression of the X-box binding protein 1 (XBP1) and the B lymphocyte-induced maturation protein 1 (BLIMP-1) (Reimold et al., 2001; Shaffer et al., 2002; Shaffer et al., 2004; Tellier et al., 2016), although not all signals have been resolved (Victora and Nussenzweig, 2012). For instance, the bifurcation to PC generation includes signals via BCR, CD40, and the B cell activating factor (BAFF) receptors (Khodadadi et al., 2019). On the other hand, memory B cell generation appear to be decided early during the GC response (Inoue et al., 2018). Whether B cell activation resolves in the generation of plasma blasts, PCs or memory cells, the overall goal of the humoral response to infection is the production of highly specific antigen-dependent Abs,

which bind to the pathogen and facilitate its elimination by phagocytic cells and molecules of the humoral immune system.

1.4 B cells Development and Functions

During fetal life, specific B cell subsets can be distinguished (Hayakawa et al., 1983). However, most of the B cell lymphopoiesis takes place in the adult BM (Figure 5). As described in the previous sections, the contribution of B cells to the immune response rely on the presence of C and V regions on the Ab molecule. The generation and structural assembly of an Ab molecule, in a process named somatic recombination, mark the stages of the correct B cell development. At a defined stage, naïve B cells leave the BM towards the secondary lymphoid tissues, such as lymph nodes, spleen or mucosal tissues where they complete their maturation process. Here, Ags can activate B cells. The overall maturation process is defined by concrete checkpoints that are triggered by both BCR-dependent and -independent factors (Figure 5). Cells that fail die in a controlled process known as apoptosis or programmed cell death (Hardy and Hayakawa, 2001).

1.4.1 Bone Marrow B cell Development

The specialized microenvironment of the BM provides signals for the development of lymphocyte progenitors from hematopoietic stem cells and for the subsequent differentiation of the B cell. Signaling support is provided by specialized cells named stromal cells, which are in continuous contact with developing B cells. Lymphocyte progenitor cells are referred to as common lymphoid progenitors (CLPs). Interaction of CLPs with BM stromal cells is required for development to the first step of the immature B cell stage, namely early pro-B cell. Adhesive interaction is mediated by integrins, and commitment to the early pro-B stage is marked by the paracrine effect IL-7 secreted locally

by stromal cells (Goodwin et al., 1989; Peschon et al., 1994) (Figure 5). Early pro-B cells express recombinase genes (RAG-1 and 2) and initiate the rearrangement of the IgH locus of the BCR, in particular the segment D and Jh. To produce a complete and functional heavy chain, the last gene rearrangement must occur (Vh segment). This event marks the transition of a developing B cell to the late pro-B cell stage. When the V-D-Jh junction is positively completed the late pro-B cell transitions to the pre-B cell stage. Here, the μ segment (Igμ) is rearranged and expressed with surrogate light chains in a complex called pre-BCR (Vettermann et al., 2006). The pre-BCR also includes the invariant proteins Igα (also known as CD79a or Mb1) and Igβ (CD79b). Igα and Igβ transduce signals of successful rearrangement of the IgH locus, by interacting with intracellular tyrosine kinases through their cytoplasmic tails, thus ensuring the positive selection of the developing B cell (Vettermann and Jack, 2010) (Figure 5). Because of this signal cascade, the cell halts recombination of the IgH locus and proliferates into a clone of B cells all producing the same μ chain. Since dividing cells are larger than resting cells, this stage is referred to as large pre-B cell (Hardy and Hayakawa, 2001) (Figure 5).

Following proliferation, RAG proteins are expressed again in small pre-B cells (no longer dividing), and rearrangements of the IgL locus begins. Each of these cells can make a different rearranged IgL and expresses it together with the Igμ on the cell surface as a surface IgM (sIgM). Thus, cells with many different antigen specificities (shared Igμ, but different IgL) are generated, which makes an important contribution to overall BCR diversity. Developing B cells expressing sIgM are now at the immature B cell stage, where each cell is tested for tolerance to self-Ags. At this stage, B cells whose BCRs bind self-Ags in the BM stroma are deleted by negative selection, while immature B cells that do not encounter Ags mature normally (Cornall et al., 1995) (Figure 5). Among other BCR-dependent factors, the release of immature B cells from the BM into the circulation is also

dependent on their expression of sphingosine-1 phosphate receptor 1 (S1PR1), which binds to the lipid ligand S1P and promotes cell migration towards the high concentrations of S1P that exist in the blood (Allende et al., 2010).

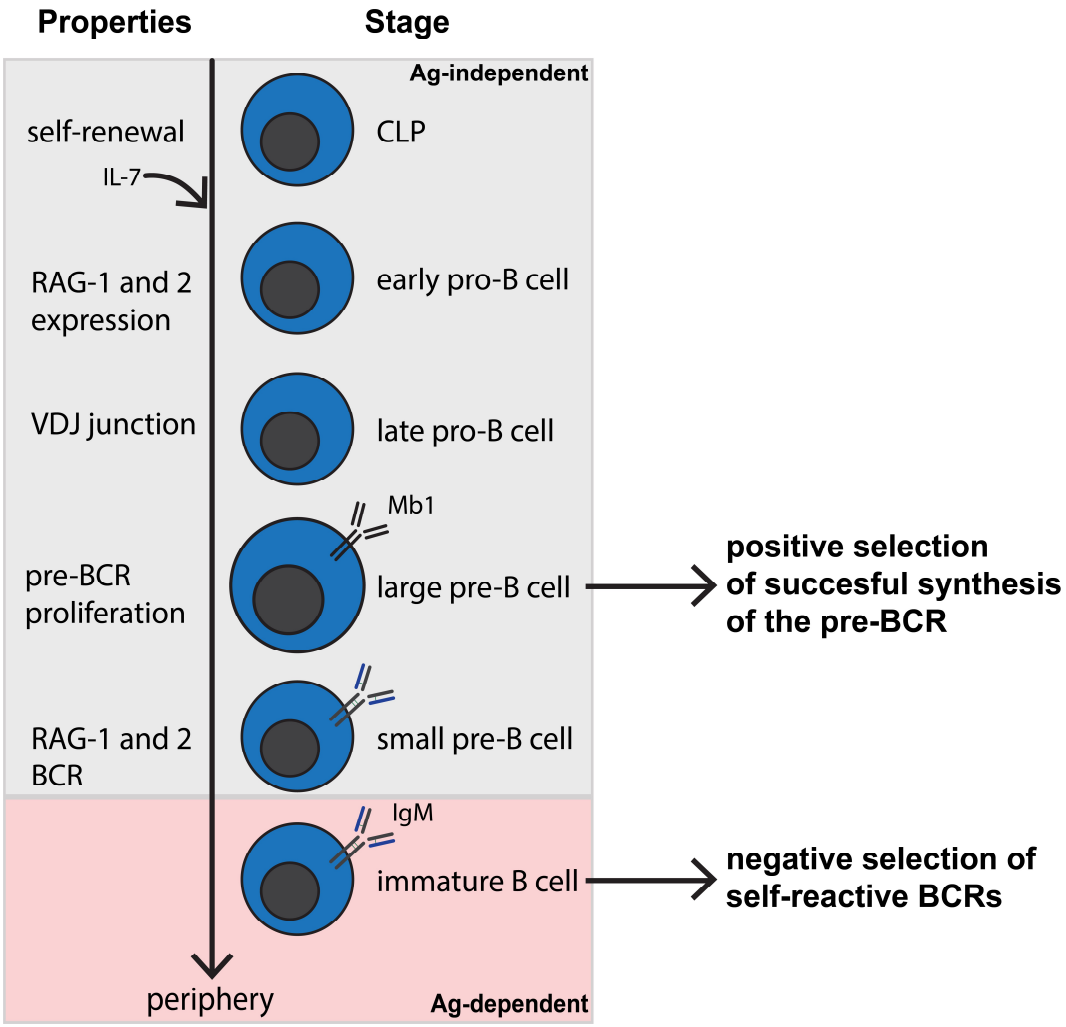

Figure 5: B cell development in the bone marrow.

The main stages of the early B cell development are depicted (right) together with the crucial properties of each cell subset (left). CLP, common lymphoid progenitor; RAG, recombinant activating gene; BCR, B cell receptor; Ag, antigen.

The immature B cell undergoes final stages of development in the spleen to form a mature Ag-inexperienced (naïve) B cell. It must be noted, however, that the mechanism of tolerance in place during the maturation of B cells in the BM is not perfect and some autoreactive B cells escape and are further surveyed by mechanisms of peripheral tolerance (Carsetti et al., 1995). The quasi-perfect nature of this process reflects an evolutionary adaptation of both the ability to respond to pathogen of the immune system and the ability of pathogens to change (which eventually has led to molecular mimicry) (Fujinami et al., 2006). Indeed, the selective pressure against self-reactive B cells is not 100% efficient. If this was the case, too few B cells would gain full maturation and, thus, there would be a smaller Ag recognition diversity. Because of this mutual adaptation, a balance must be reached where it is worth the risk of autoimmunity (which is kept under control by other mechanisms in the periphery, including Tregs (Sakaguchi et al., 2008)), rather than limiting Ag diversity, *i.e.* being unable of pathogen recognition.

1.4.2 Spleen-Dependent Development: the Transition to the Mature B Cell Subsets

By the time immature B cells exit the BM and enter the circulation they are called transitional B cells (TB), and they are characterized by the expression of CD93 (Carsetti et al., 1995). As mentioned above, some emigrated TB can still bear autoreactive BCRs and be activated by self-Ags. If this happens in the absence of inflammatory stimuli, the cell is neutralized by mechanisms of peripheral tolerance. Non self-reactive TB in the spleen have to proceed through two maturation stages, called transitional B cell 1 and 2 (T1 and T2), which have phenotypically and functionally defined properties (Loder et al., 1999). During this late differentiation process, changes in surface markers, chemokine receptors, BCR signals and transcriptional factors correspond to different splenic sublocations (Chung et al., 2003) (Figure 6) and operate as distinct differentiation checkpoints (Su and Rawlings, 2002). A key factor to gain access to primary lymphoid follicles is the interaction of

cytokine BAFF (secreted by FDCs) and its receptor (BAFFR), which is expressed on T1 B cells. Indeed, knock out of the gene or its receptor have been reported to block B cell maturation at the T1 stage (Schiemann et al., 2001). In the mouse system, immune competence is acquired as TB cells transit from T1 to T2, although a third TB population named T3 has been described (Allman et al., 2001). Following to a process of alternative mRNA splicing, B cells express δ chain (Igδ, and therefore surface IgD or sIgD) together with the sIgM and become naïve B cells (Yuan and Tucker, 1984). Generally, these cells are referred to as conventional B2 cells, they derive from progenitors in the BM and can only divide in response to Ag and start the GC reaction.

The majority of B2 cells is represented by FoB, so called as they populate the primary B cell follicles (Figure 6). A second, smaller population is represented by the MZB, which instead is located in a specific area of the spleen known as the marginal zone (Figure 6). The FoB versus MZB bifurcation process is not entirely understood, but a certain degree of consensus has been reached regarding the origin of both B2 cells subsets from T2 cells (Martin and Kearney, 2002; Pillai and Cariappa, 2009) and will be discussed further in the specific sections below. Moreover, as briefly mentioned above, B cell development starts in the fetal liver and gives rise to a distinct B cell population, namely B1 B cells (Hayakawa et al., 1983). In fact, B1 cells are the first B cells to be generated, hence the name, and they have different properties than B2 cells, although they share similarities with MZB that will be discussed in more detail later on (Martin and Kearney, 2000b).

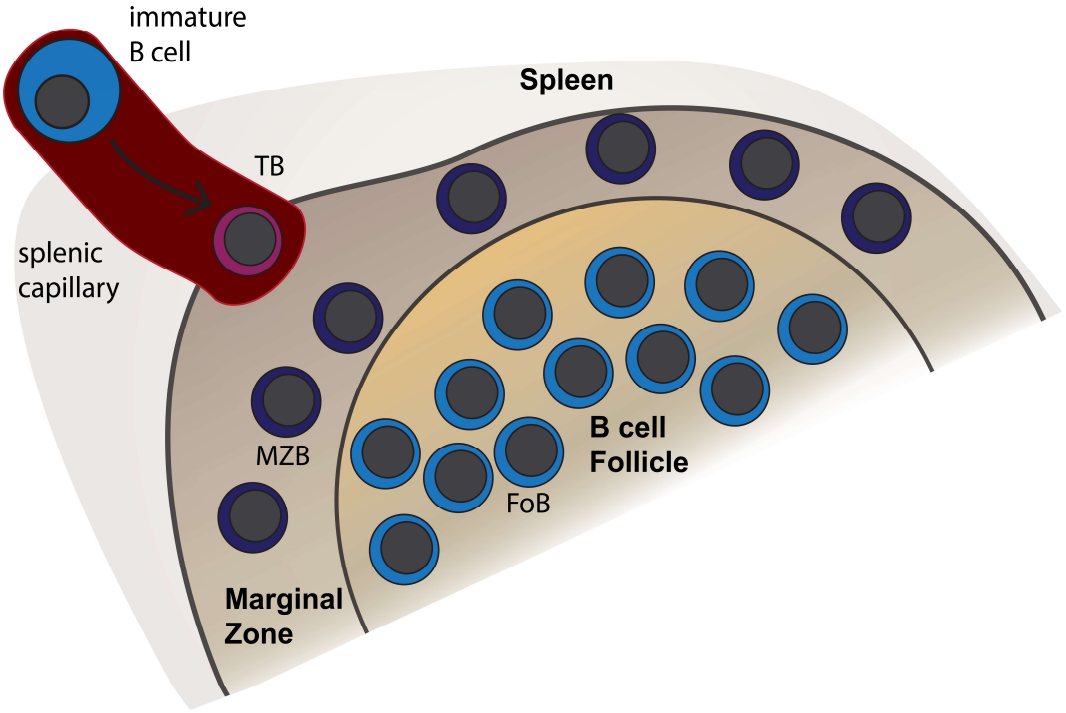

Figure 6: Distinct mature B cell subsets populate specific compartments in the spleen.

Migrating immature B cells from the bone marrow house to the spleen. Here, the late stages of B cell maturation take place. The three main splenic B cells subsets are shown: Transitional B (TB), Follicular B (FoB) and Marginal Zone B (MZB) cell.

1.4.2 I - Follicular B Cells

The follicular niche represents the major site in which FoB can be found in the spleen (Figure 6), however recirculating FoB can wander through other secondary lymphoid sites (*i.e.* BM, lymph nodes and the Peyer's patches). FoB are intrinsically associated with T cell (or thymus-) -dependent (TD) responses because follicles are always adjacent to T cell zones and this arrangement allows activated FoB and activated $CD4^+$ T helper cells to interact at the interface between these two areas. Most FoB express CD23, IgD, IgM while showing an intermediate-to-low expression of CD21. It is thought that FoB activation to TD Ag is achieved by signals delivered through BCR, CD40 and TLRs, although the contribution of the latter to TD immunizations is controversial (Gavin et al., 2006; Allman and Pillai, 2008). BCR diversification at the steady state is extensive in FoB due to the activity of the terminal deoxynucleotidyl transferase (TdT), which provides junctional diversity during the somatic hypermutation of the Igs by adding non-templated (N) nucleotides in the complementarity-determining regions 3 (CDR3) of the IgH chain (Carey et al., 2008). The FoB subset is responsible to recognize soluble or APC-displayed Ags and forms early plasma blasts or initiates GCs reactions. In particular, FoB responses are usually associated to TD antigens of peptidic origin, such as viral proteins (Ochsenbein et al., 1999b; Hangartner et al., 2006). In such case, the Ag is internalized, broken down, and presented on the MHC class II complex to cognate T cells, which provide the necessary help signals in return as described in the previous section. Previous studies have shown that B cells require a tonic BCR signal and BAFFR-mediated activation of the non-canonical nuclear factor kappa-light-chain-enhancer of activated B cells (NFκB) pathway to mature into FoB (Weih et al., 2001; Pillai and Cariappa, 2009). Other analysis of B cell populations suggested that there is a second distinguishable recirculating FoB population identified as FOII B cells, which hold different phenotypic properties, such as high IgM expression

compared to FoB. Moreover, FOII B cells differ from FoB cells in that they develop in an Ag-independent manner and may serve as reservoir for MZB replenishment (Cariappa et al., 2007).

1.4.2 II - Marginal Zone B Cells

MZB are enriched in the marginal zone area of the spleen (Figure 6) and represent a sessile population, which constitutes up to 5-10% of total splenic B cells (Gray et al., 1982; Oliver et al., 1997). MZB compartment is found in germ-free animals (Kumararatne et al., 1982; Martin and Kearney, 2002) and its development is considered to be microbiome-independent. Therefore it is thought that MZB develop as part of the pre-immune B cell repertoire (Hayakawa et al., 1997). Structurally, MZB are spatially separated from the primary follicles and FoB, and this property has direct reflections for MZB effector functions. In particular, MZB are classically associated to the early phases of the immune response, specifically to the early Ab production against T cell (or thymus) -independent (TI) Ags (Mond, 1995; Martin et al., 2001). This function is directly related to the MZB positioning in the marginal zone, where the blood stream is slower due to fenestration and provides direct access to blood borne Ag (Steiniger et al., 2006) (Figure 3 C). Thus, once the Ag reaches the blood, it is captured by MZB within hours directly or through several cell-dependent mechanisms (Cerutti et al., 2013). This allows MZB a faster response rate compared to the FoB-dependent GC reaction (Oliver et al., 1999; Martin and Kearney, 2002; Swanson et al., 2013). Because MZB functionally bridge to the adaptive humoral response, by providing early low-affinity Ag-specific IgM, they are also referred to as “innate-like” B cells. However, there is no absolute restriction of Ag-dependent B cell subsetting. In fact, some evidence shows that MZB are also capable of activation in response to blood borne TD Ags (MacLennan et al., 2003; Song and Cerny, 2003; Chappell

et al., 2012). Indeed, MZB can work as APCs and transit from the marginal zone to the follicle back and forth to participate into FDCs and T helper cell activation in the spleen (Cinamon et al., 2004).

MZB display different characteristics in comparison to FoB. MZB are bigger in size and they have higher surface expression of the co-stimulatory markers CD80, CD86, IgM and CD21 (*i.e.* CR1). Also, MHC class II expression is more pronounced in MZB than FoB, while IgD and CD23 expression is dimmer (Gray et al., 1982; Oliver et al., 1997). Furthermore, MZB express high CR2 (*i.e.* CD35), which favors a more efficient capture of complement opsonized Ag from the bloodstream (Mond, 1995). The involvement of MZB in TI responses is inherently caused by the differential segregation of BCR specificity into the different mature B cell compartments. Indeed, elegant studies with transgenic mice have shown that reduction in the diversity of the BCR led to a dominance of MZB in the spleen (Oliver et al., 1999) and that specific BCR clones selective for TI Ags are funneled into the MZB pool (Yancopoulos et al., 1984). BCR-dependent pathways are involved in the fate decisions of TB cells, and CD19-mediated signaling appears to be crucial for the maintenance of MZB (Martin and Kearney, 2000a). Several other intracellular signaling cascades and environmental cues are implicated in the FoB versus MZB fate commitment and several scenarios have been proposed (Martin and Kearney, 2002; Pillai and Cariappa, 2009; Cerutti et al., 2013; Arnon and Cyster, 2014).

These properties indicate that MZB interact with multiple cells of the innate immune system to mount TI and TD Ab responses. Therefore, the role of MZB in the immune response can be easily integrated into the concept of "geographical immunity" (Zinkernagel et al., 1997), which enforces the notion that the immune system has evolutionary adapted specific cell clones (or subsets), thus restricting functionality for optimization of resources, to specialized sites which are designed to deal with different kind of Ags. In this view,

MZB provide the first line of defense for blood borne Ags, and the restriction into their BCR repertoire ensures a rapid Ab-mediated response to conserved Ags. On the other hand, FoB are featured with a wider array of BCR specificities, and allow the Ag-targeted TD response, including GC reaction, with the formation of PCs and memory. Although highly specific, the GC reaction burden is represented by time, as high-affinity Abs are produced only several days after the start of the GC reaction, and energy consumption, which is also intrinsically linked to heightened metabolic expenditure. In summary, distinct B cell populations retain specific properties to deal with specific Ags depending on their location, and MZB are thought to provide a diversionary tactic against blood borne pathogens and fill the temporal gap necessary for GC reactions to take off (Swanson et al., 2013; Lam et al., 2020).

1.4.2 III - B1 Cells

As briefly mentioned in the beginning, a small portion of B cells develop during early life in the liver (Hayakawa et al., 1985). Yet, some evidence that CLPs can give rise to B1 cell progenitors in the BM has been found, suggesting an alternative developmental pattern for B1 cells (Esplin et al., 2009). B1 cells where first described in the early 80's (Hayakawa et al., 1983) and they were grouped by the expression of the CD5 marker (originally known as Ly-1 in mice and Leu-1 in humans). B1 cells are mainly found in body cavities and predominate the peritoneal cavity of adult mice. Further studies led to the detailed characterization of B1 cells and shown that also $CD5^-$ B1 cells exist (Kantor et al., 1992; Stall et al., 1992; Baumgarth, 2016). Therefore, B1 cells were finally segregated into two subsets: $CD5^+$ B1a and the counterpart $CD5^-$ B1b (Hayakawa et al., 1997; Baumgarth, 2016). On the basis of this differential expression, B1a and B1b cells stick to a "division of labor" model, where B1a constitutively produce Abs and B1b secrete Abs once activated

(Haas et al., 2005). However, discrepancy has resulted from other studies and a deeper investigation is needed (Baumgarth, 2016). In general, the literature supports the notion that the B1 cell pool contains cells with different functional properties that will be outlined below. It is worth to mention that B1 cells share similarities with MZB. For this reason, B1 cells are also included in the innate-like B cell pool.

B1 cells are self-renewing cells and possess a germline-skewed BCR repertoire, which is less diversified than the BCR of FoB (Hayakawa et al., 1999). Moreover, B1 cells lack N-nucleotides at the V-D-J junctures, which is consistent with lack of TdT expression in neonatal tissues (Feeney, 1990). Seminal studies have uncovered that B1 cell development strongly depends on self-Ag (Hayakawa et al., 2003), and in particular most of B1 cells are reactive against components of the cell membrane such as PC (Shaw et al., 2000) and phosphatidylcholine (PtC) (Arnold et al., 1994). This led to the partial conclusion that B1 cells are positively selected based on their ability to bind to self-Ag. This points out a fundamental difference between B1 and B2 cells, that is the positive or negative selection based on self-reactivity, respectively.

The major function of B1 cells is to spontaneously produce NAs, mainly of the IgM and IgG3 class (Casali and Schettino, 1996). However, steady state secreting B1 cells do not upregulate X-box binding protein 1 (XBP1) and BLIMP-1, which instead are hallmarks of Abs secretion in PCs (Tumang et al., 2005; Choi et al., 2012). B1-derived NAs are known to bind both self-Ags such as the thymocyte Ag 1 (Thy-1), PC and PtC and conserved structural motifs which share properties with self-Ags, like Ags from *S. Pneumoniae*, *Salmonella* etc. Spontaneous production of Abs puts B1 cells in stark contrast to B2 cells and FoB in particular, which need T helper cell to reach full activation. Many of the properties discussed so far, are related to the self-reactivity of B1 cells. The notion of self-

reactivity is often linked to autoimmune inflammation and tissue damage, therefore the evolutionary maintenance of B1 cells and their development seems counterintuitive.

Nevertheless, we should consider the developmental requirements of B1 cells in the context of the notion of the "layered immunity" proposed in the late 80's (Herzenberg and Herzenberg, 1989), which examines the B1 and B2 populations as a product of different mechanisms of selection based on time (*i.e.* age of the host) and different host needs. Indeed, B cells come in waves or "layers" during ontogeny: first B1 cells, selected positively by self-Ags (also because non-self-Ags do not easily reach embryonic tissues) until shortly after birth (Montecino-Rodriguez and Dorshkind, 2012); then BM stem cells provide precursors for the development of B2 cells, when the non-self Ag exposure is maximized. Therefore, in the BM a B cell should not be selected for autoantigens (*i.e.* through the negative selection and central tolerance mechanisms). This way, early in life the immune system provides an innate mechanism of protection (Ag-independent) based on polyreactive Abs produced by B1 cells, which play a role in protecting several embryonic and neonatal tissues (Montecino-Rodriguez and Dorshkind, 2012). A fetal versus adult developmental switch integrates the co-existence of B1 and B2 cells, with the latter providing means of coping with external Ags, when they occur. Finally, the notion of distinct B cell populations homing to distinct tissues in order to deal with different types of Ags can easily be integrated in the "geographical" view of immune reactivity outlined above (Zinkernagel et al., 1997).

1.5 Redox Remodeling and Control of B cell Functions

Redoxtasis is necessary to ensure normal functioning of aerobic organisms and cells (Finkel, 2011). For this to happen, the circuits of redox regulation keep running to prevent deterioration of cellular functions (Birben et al., 2012). When oxidative intermediates, such as reactive oxygen species (ROS), are either too high or too low, the cell undergoes an oxidative or reductive stress that may cause severe cell injury, transformation or eventually cell death (Cairns et al., 2011; Schieber and Chandel, 2014). Due to the hormetic nature of ROS, a sophisticated defense network must act to keep the balance right, and allows ROS regulation of cell cycle, differentiation, and functions (Sies and Jones, 2020). Redox cycles drive attenuation of redox stress in both physiologic and diseased state. These chemical challenges are mastered by intracellular antioxidant systems, which are optimized to use the tripeptide glutathione (GSH), as the most versatile nucleophile in the reduction, direct conjugation and GSH-dependent enzymatic reactions of neutralization of electrophiles (Meister, 1988; Wu et al., 2004; Deponte, 2013).

B cells are central components of the immune system with a variety of functions, yet their main goal is to produce Abs (LeBien and Tedder, 2008). The variety of processes which characterize a B cell`s life, from differentiation to Abs secretion, are marked by dramatic changes in the redox state (Masciarelli and Sitia, 2008; Vene et al., 2010). For example, protein synthesis and release in PCs generate stress which has to be compensated adequately in order to prevent fatal stress and cell death (Haynes et al., 2004). Indeed, protein secretion implies a net loss of amino acids, which must be continuously replenished to ensure cell survival. Moreover, secreted proteins and especially Abs are rich in disulfide bonds (Figure 4). The correct rearrangement of these bonds are necessary to overcome stringent secretory quality control checkpoints to reach the native conformation of proteins

(Vashist and Ng, 2004). *In vitro* studies have demonstrated that linear ROS production in the form of H_2O_2 derives from the number of disulfide bonds formed (Tu and Weissman, 2002; Shimizu and Hendershot, 2009). Upregulation of chaperones, proteasomes and redox buffering capacity is promoted in the Ab factory in order to overcome the dangerous effects of proteotoxicity, adapt to stress and meet the demanding secretory goals (van Anken et al., 2003). This synergy facilitates B cell differentiation and correct functioning during the immune response. On a more translational note, early studies on human immunodeficiency virus-1 (HIV-1)-infected subjects associated GSH deficiency with a poor lymphocytic response and impaired survival following HIV-1 infections (Staal et al., 1992a; Staal et al., 1992b; Herzenberg et al., 1997). This studies set GSH as a potential modulator of immune functions and indicate that a link between GSH functions and B cells activity may exist.

Interestingly, the main site of intracellular ROS production is the mitochondria. Mitochondrial or metabolic ROS (mtROS) integrate instructive signals which have been linked to B cell activation (Jang et al., 2015). Moreover, balanced mtROS are critical for the correct function of the redox-sensitive proteins of the electron transport chain (ETC), which are susceptible to inactivation by these reactive molecules (Zhang et al., 1990; Brand, 2010; Garcia et al., 2010; Wang et al., 2013; Mailloux et al., 2013). In particular, complex I (CI) activity requires adequate levels of reduced GSH in the mitochondria for its function (Balijepalli et al., 1999; Beer et al., 2004). The existence of B cell subsets with distinct properties, such as innate like B cells (MZB and B1 cells) and FoB, allows room for speculation and interesting challenges arise in order to investigate whether these cells differ in their mechanism of coping with ROS-induced stress, metabolic demands and how this affect their lifespan and function.

1.5.1 Overview of Glutathione Synthesis

As briefly anticipated, GSH is the predominant low molecular antioxidant in mammalian cells (Wu et al., 2004). The main intracellular GSH reservoir is the cytoplasm, where GSH exerts a variety of functions including antioxidant defense (Winterbourn and Brennan, 1997), detoxification of xenobiotics and/or their metabolites (Boyland and Chasseaud, 1969), regulation of cell cycle progression (Holmgren, 1976) and apoptosis (Esteve et al., 1999), storage of cysteine, maintenance of redox potential, enzyme cofactor (Forman et al., 2009) and modulation of immune function (Mak et al., 2017; Kurniawan et al., 2020). However, GSH is compartmentalized at several levels intracellularly and compartment-specific GSH-dependent functions are influenced by changes in levels of cytosolic GSH because GSH is synthesized in the cytosol and must be imported to exert its function as antioxidant, for instance into the mitochondria (Martensson et al., 1990; Masini et al., 1992).

GSH is a tri-peptide constituted by glutamate, cysteine and glycine and its synthesis involves two enzymatic processes, which both are ATP-dependent (Figure 7). The first reaction is carried out by the glutamate-cysteine ligase (GCL), and in particular by its catalytic subunit (GCLC) - encoded by the gene *Gclc* - which holds the substrate binding sites (Chen et al., 2005a). GCL contains also a light or modifier subunit (GCLM), on which the enzymatic activity of GCL strongly depends on, as seen in *Gclm*-deficient mice where GSH production dropped by almost 90% (Yang et al., 2002). During this first step, cysteine is conjugated to glutamate to form γ-glutamylcysteine (γ-Glu-Cys in Figure 7). The second step in the *de novo* GSH synthesis is catalyzed by the GSH synthetase (GS), a homodimeric enzyme (Oppenheimer et al., 1979) that adds glycine to γ-glutamylcysteine to form γ-glutamylcysteinylglycine or GSH (Lu, 2013) (Figure 7). The assumption that the first reaction catalyzed by GCLC represents the rate-limiting step in the *de novo* synthesis of

GSH comes from an earlier report showing that in the presence of GS, γ-glutamylcysteine is present at very low concentration (Dalton et al., 2004). Of the three precursors of GSH, cysteine deserves particular attention. In mice and humans, cysteine is mainly obtained by the diet and because it is unstable extracellularly, it is mainly found in its oxidized form (cystine), which can be taken up by cells and used for protein synthesis (Kaplowitz et al., 1985; Bannai and Tateishi, 1986). Most of the cysteine used for GSH comes from protein turnover or it is recycled from methionine intracellularly, otherwise it depends on hepatic GSH for its distribution in the body (Meister, 1991; Wu et al., 2004; Lu, 2013).

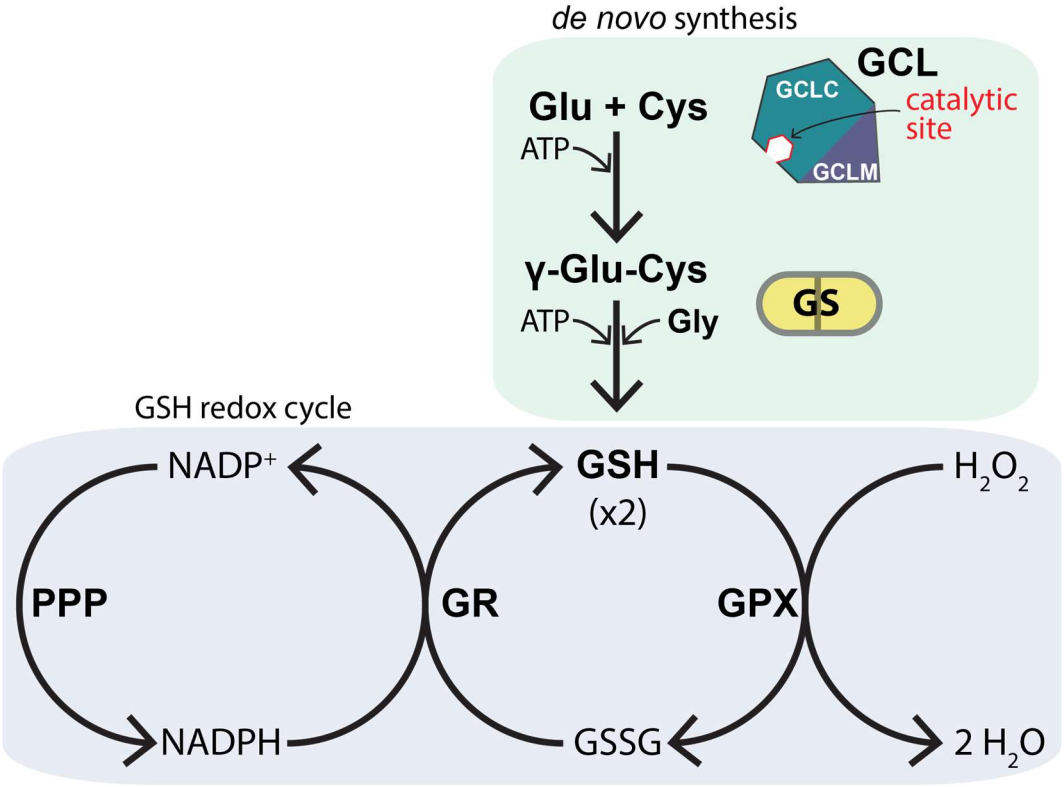

Figure 7: The synthesis of GSH is a multi-step process.

De novo GSH synthesis (green shaded area) and the GSH redox cycle (blue shaded area) contribute to the maintenance of the intracellular level of GSH. GCL. Glutamate-cysteine ligase; Glu, glutamate; Cys, cysteine; GS, glutathione sintase; PPP, pentose phosphate pathway; GR, glutathione reductase; GPX, glutathione peroxidase.

1.5.2 Role of Glutathione in the Regulation of Redox-Dependent Circuits

The balance between oxidized and reduced compounds within the cell is known as redox homeostasis (or redoxstasis) and plays a fundamental role in the maintenance of signaling and cell survival (Forman et al., 2004; Trachootham et al., 2008; Sies and Jones, 2020). Endogenous antioxidants, and GSH in particular, are able to neutralize oxidative species (*i.e.* ROS and derivatives) in order to maintain or restore the redox balance. GSH exists as reduced (GSH) and oxidized (GSSG) form (Kaplowitz et al., 1985) (Figure 7), but GSH constitutes the predominant form. In redox reactions, which can be facilitated by enzymes, one reactant loses electrons (it becomes oxidized) and another gains these electrons and it is converted into its reduced form. In fact, GSH is a nucleophile and reductant molecule able to react with oxidants. If the balance of GSH and ROS is disrupted by an excess or deficiency of either one, the cell undergoes oxidative stress (Sies, 1986). In particular, a more oxidized environment will cause alterations of DNA, RNA, protein, and lipid damage (Vaughan, 1997).

Aerobic cells are inevitably subjected to molecular oxygen (O_2) exposure due to the processes of cellular (and more specifically mitochondrial) respiration, during which partially reduced forms of O_2, namely ROS, are formed. In turn, ROS can lead to the production of toxic macromolecular radicals and induce redox stress and cell injury. The major function of GSH is to donate electrons to ROS in a direct manner or to ROS-destabilized macromolecules. GSH conjugations are either spontaneous or catalyzed (Meister, 1988) and usually result in the neutralization of the oxidized species, with a net loss of intracellular GSH and generation of GSSG and H_2O. GSSG is recycled back to its reduced form (GSH) by the GSH reductase (GR) at the expense of NADPH in a redox cycle (Figure 7). As mentioned, GSH can directly react with O_2^- and other ROS, but it is mainly consumed to renovate other antioxidants, and redox-related enzymes. This

generates a complex network of GSH-dependent reactions, which work in loop to ensure the constant replenishment of reductants (Figure 8).

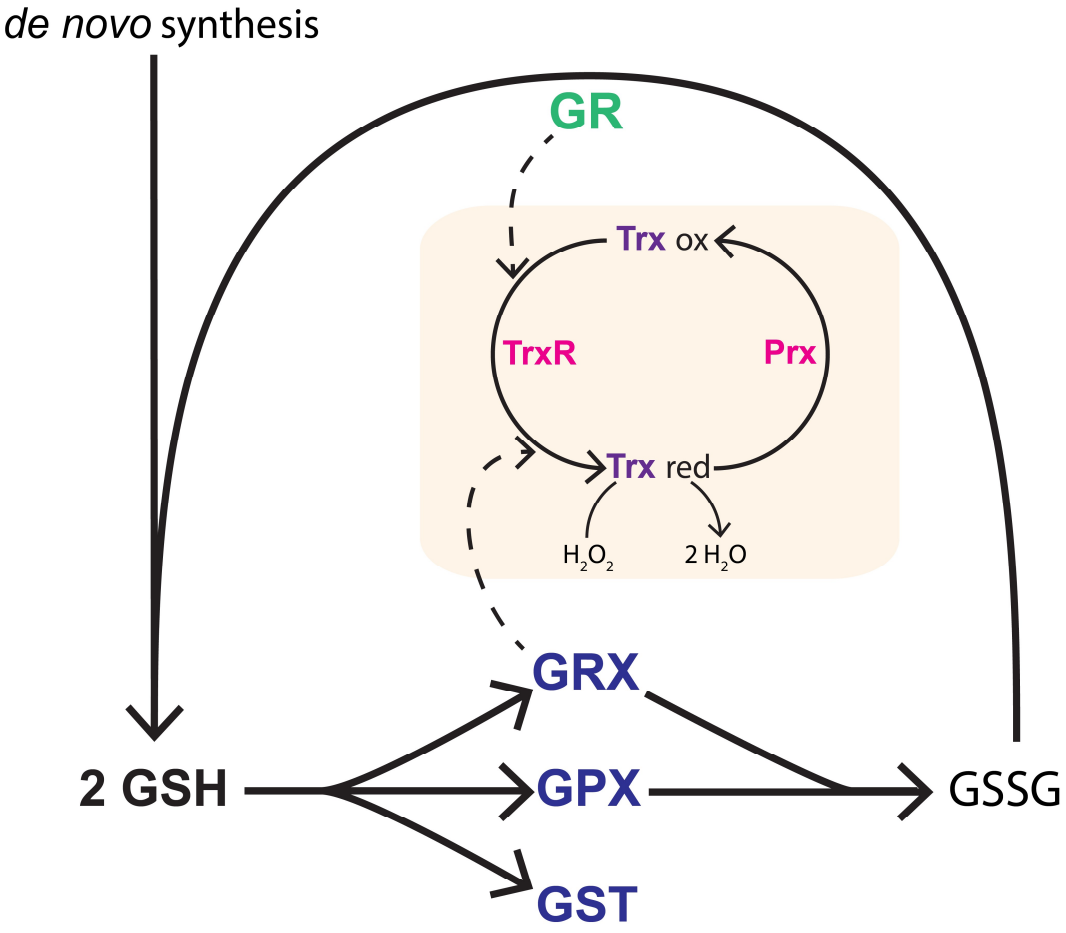

Figure 8: The GSH network ensure cell signaling and redox regulation.

The intricate connection among glutharedoxins (GRXs), peroxiredoxins (Prxs), thioredoxins (Trxs) and GSH-dependent antioxidant enzymes is shown. Trx reduction (yellow shaded area) can be catalyzed by other reductases than Txr reducatase (TxrR) (alternative pathways are indicated by dotted lines). Blue color indicates GSH-consuming enzymes. GRX, glutaredoxin; GPX, glutathione peroxidase; GST, glutathione-s-transferase.

GSH peroxidases (GPXs) are the main producers of GSSG from 2 molecules of GSH (Figure 7) in the process of H_2O_2 detoxification. Eight members and several isoforms of GPXs are known and have subcellular- of tissue-specific expression patterns (Brigelius-Flohe and Maiorino, 2013). Oxidized GSSG is recycled back to 2 molecules of GSH by the GR (Figure 7 and 8), which depends on the reducing agent NADPH, from the pentose phosphate pathway (PPP) (Pollak et al., 2007). GSH is also a crucial co-factor and substrate of other redox enzymes, such as glutaredoxins (GRXs) (Fernandes and Holmgren, 2004) and GSH-S-transferases (GSTs) (Nebert and Vasiliou, 2004) (Figure 8).

However, GSH is not the only intracellular antioxidant and other thiol-specific proteins are capable of peroxidase activity. In particular, peroxiredoxins (Prxs) are thought to be the main reductants of H_2O_2 (Wood et al., 2003). Downstream of Prxs oxidation, thioredoxins (Trxs) specifically target the reduction of Prxs cysteine residues, allowing the regeneration of Prxs. By doing so, oxidized Trxs can be reversibly reduced by the Trx-reductase (TrxR) in a NADPH-dependent manner (Holmgren et al., 2005) (Figure 8). However, it is important to note that the reduction of the disulfide bond of oxidized Prxs can be reduced by other reductases belonging to the GSH-dependent redox reactions (*i.e.* GR) and that Trxs reduction can be performed by GRXs (Espinosa-Diez et al., 2015) (Figure 8). Thus, GSH is directly and indirectly responsible of several redox reactions. Yet, GSH-independent redox enzyme exist, and examples are superoxide dismutases and catalase, which further catalyze the neutralization of H_2O_2 and OH^- (Espinosa-Diez et al., 2015).

As mentioned earlier, metabolic ROS are mainly generated in the mitochondria, and mitochondrial GSH is crucial to maintain the thiol redox status. At steady state condition in particular, the unique biochemical (such as basic pH) and redox properties (exposed protein thiols) of the mitochondrial matrix facilitate glutathionylation reactions (Mailloux et al., 2013), that is, the formation of mixed disulfides between protein cysteines and GSH

cysteines. Therefore, fluctuation of ROS, GSH or GSSG in the mitochondria plays important roles in the context of mitochondrial function and cellular metabolism.

In lymphocytes, GSH increase is often associated with the proliferative burst, which characterize the early phases of immune response (Messina and Lawrence, 1989; Hamilos et al., 1989; Mak et al., 2017). This is often caused by a rewiring of the immune cell metabolism, which generally increases the biosynthetic needs by lifting metabolic pathways (Pearce and Pearce, 2013), and therefore increasing the by-production of ROS (Yang et al., 2013; Franchina et al., 2018a).

1.5.3 Redox Regulation of the Humoral Immune Response

As discussed above, a B cell's life is characterized by a transition of proliferation, quiescent stages and, sometimes, continuous migration. For instance, during early B cell development in bone marrow (Figure 5), the developing B cells experience a variety of metabolic challenges which are discussed elsewhere (Urbanczyk et al., 2018). Moreover, at each of these stages B cells are exposed to a variety of local milieu and intracellular metabolism and transcriptional regulation have to make up the sufficient energy according to nutrient availability (Boothby and Rickert, 2017; Urbanczyk et al., 2018) (Figure 9). Furthermore, metabolic changes are expected to happen upon BCR engagement (or other co-receptors) in naïve B cells, independently of the specific subset. ROS production in B cells can be initiated as a result of three biological processes. First, BCR engagement and the activation of proximal NADPH-oxidases (NOX) (Yang et al., 2013). These non-metabolic ROS induce short-term local oxidation and inactivation of the protein tyrosine phosphatase (PTP). In turn, this allows the intracellular BCR tails (known as Immunoreceptor tyrosine-based activation motifs or ITAMs) to activate the spleen tyrosine kinase (Syk) and the downstream signaling. Another source of non-metabolic ROS in B

cells is indirectly associated with the protein synthesis machinery. In particular protein folding in the ER directly correlates with H_2O_2 production (Tu and Weissman, 2002; Shimizu and Hendershot, 2009). Nonetheless, the major source of ROS is in activated B cells and derives from metabolic processes associated with the powerhouse of the cell, the mitochondria (Murphy, 2009).

The three ways implicated in ROS production in B cells must be contemplated over the multistep process of the B cell's journey towards Ab secretion. Particularly, upon encounter of the Ag, several steps are involved, and so are metabolic pathways (Boothby and Rickert, 2017) (Figure 9), ROS level and redox buffering capacity (Franchina et al., 2018b). Previous studies have unveiled the dynamics underlying B cell differentiation into PCs (van Anken et al., 2003; Kirk et al., 2010). It is conceivable to imagine that the first wave of ROS favors BCR signaling upon BCR engagement. A slow, but constant increase of metabolic proteins is registered through a 4-days activation time, and provide energy for the cellular growth. Mitochondrial ROS seem to be involved to allow full B cell activation and proliferation (Wheeler and Defranco, 2012). Then, sequential changes occur in B cells in accordance to the expression of different protein packages. For instance, molecular chaperones are upregulated early during activation, in order to prepare the cell to sustain the upcoming expansion of the ER machinery and protein synthesis. Later studies have demonstrated that the expansion of the secretory apparatus and increased biogenesis are mainly regulated by the BLIMP-1-XBP1 axis (Shaffer et al., 2004). As discussed earlier, increased Ab synthesis inevitably induces ROS accumulation in the ER. In fact, in this process, B cells linearly upregulate proteins related to redox circuits and ER resident proteins to assist Ab production over time. It is interesting to note that the synthesis of IgM rapidly peaks only after 3 days post-activation, while there is a linear increase of redox proteins from the beginning (van Anken et al., 2003). Thus, B cells prepare carefully for

their secretory role and simultaneously, redox mechanisms are in place, enabling the activity of the downstream cellular machineries involved in the B cell activation.

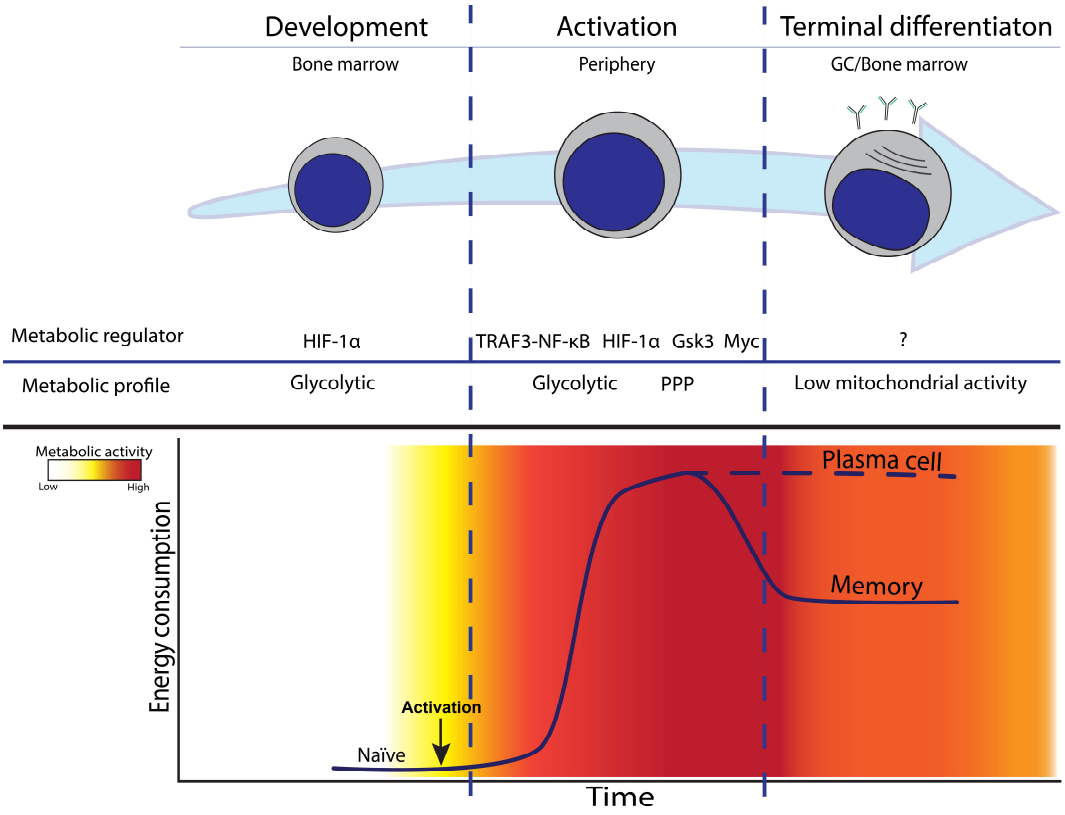

Figure 9: Overview of the metabolic features of B cells during differentiation and activation.

Top: discrete steps of B differentiation are marked by the activity of specific metabolic regulators which define the metabolic profile of the differentiation stage; bottom: energetic profile (y axis) of mature B cells during activation (x axis). HIF-1α, hypoxia-inducible factor 1-alpha; TRAF3, TNF receptor associated factor 3; NF-κB, nuclear factor kappa B; Gsk3, glycogen synthase kinase-3. Myc, myelocatomatosis; PPP, pentose phosphate pathway.

In conclusion, B cells have evolved a multitasking strategy to cope with different kinds of stress (Cenci and Sitia, 2007). In particular, the activated B cell has to overcome the immunological pressure exerted by the fast-replicating pathogen and, at the same time, has to cope with the increasing biosynthetic needs to provide substrates for cell growth, division and immunological functions (*i.e.* Ag presentation and cytokine secretion (DiLillo et al., 2011)). In the midst of this stressful condition, B cells must integrate and survive the stress of the correct synthesis, folding and secretion of thousands Abs per second (Helmreich et al., 1961; Hibi and Dosch, 1986). Therefore, the existence of periodic oscillations in the metabolic redox reactions and the maintenance of a delicate balance between ROS and antioxidants support the concept that maintenance of the redox control could sustain some functions of B cells.

1.6 Mitochondrial Glutathione

GSH is distributed in intracellular organelles such as the endoplasmic reticulum (ER), nucleus and mitochondria (Meister and Anderson, 1983). The latter are source of ROS, most of them originating from the electron transport chain (ETC), and the maintenance of the mitochondrial GSH pool is considered to be an indispensable antioxidant reservoir to avoid oxidative modifications. The concentration of GSH in the mitochondrial matrix is within the range of that found in the cytosol (10-15 mM). However, GSH synthesis is limited to the cytosol (Lu, 2013) and given its anionic nature at physiological pH, GSH cannot freely diffuse through the inner mitochondrial membrane. Consequently, GSH must be actively imported by carrier-mediate transport into the mitochondrial matrix from the cytosol (Martensson et al., 1990; Lash, 2006).

B cells can transit between rapidly proliferating and quiescent states to meet the demands of the adaptive immune response and mitochondria represent central signaling and bioenergetic hubs. Accordingly, regulation of mitochondrial function was shown to be critical for B cell activation (Jang et al., 2015; Waters et al., 2018). However, the function of mitochondria in the context of GSH-dependent redox regulation in the distinct B cell subsets is still understudied (Muri and Kopf, 2020). Taken together, ROS generation associated with electron transfer reactions combined with mitochondrial GSH redox power represent a potential functional link integrating energy metabolism, redox signaling, and control of cellular physiology.

1.7 Hypothesis and Aims of the Project

B lymphocytes are involved at various levels in the immune response. Depending on the type of the Ag and its diffusion through the body, the B lineage has evolved into specific subsets to populate defined compartments and with specific immediate or long-term functions. In general, the lifespan of a B cell can be extremely variable and characterized by peaks of cellular activities, including protein synthesis and its downstream processes. In such phases, secretion of Abs imposes considerable amount of stress on the redox homeostasis network. Therefore, activated B cells employ compensatory mechanisms to overcome the generation of toxic metabolic byproducts. This is the case of upregulation of GSH production to counterbalance ROS and oxidized products (van Anken et al., 2003).

While our current knowledge of B cell immunometabolism is constantly growing, and we begin to appreciate the distinct metabolic requirements of the different B cell subsets (Farmer et al., 2019), it is of interest to study how B cells function in the absence of the main antioxidant, GSH. In fact, although progress has been made and recent studies have elucidated the role of GRXs in B cells (Muri et al., 2019), how GSH rules B cell biology and function has not been addressed. In particular, a disturbance of metabolic functions can be anticipated due to stable role of GSH within the mitochondria.

Based on previous studies that have elucidated the important role of GSH in cellular functions of immune cells (Mak et al., 2017; Kurniawan et al., 2020), we hypothesized that GSH directly empowers B cells differentiation checkpoints or, at least in part, their functions. However, due to the highly variable metabolic profiles of B cells at the different stages of maturation (Franchina et al., 2018b), more studies are needed to determine the specific requirements and cellular adjustments to oxidative stress. We therefore hypothesized that by deleting the main player of the aforementioned redox cycles, namely

GSH, we can directly study how the total GSH-dependent antioxidant response influences B cell immune function and metabolism.

Below is a list of the specific aims of this thesis project:

A. To determine the effect of *Gclc* deficiency in the distribution and maintenance of B cell subsets at the steady state (Chapter 3).

B. To study if the innate humoral immunity is affected in B cell-specific *Gclc*-depleted mice (Chapter 3).

C. To explore the outcome of the germinal center reaction in the absence of *Gclc* (Chapter 4).

D. Should *Gclc* affect B cell properties, to identify the connection between the B cell functional variation and the intracellular metabolic dependencies (Chapter 5).

E. To understand the molecular basis of *Gclc* contribution to B cell metabolic function through analysis of single cell transcriptomic and *in silico* metabolic inference (Chapter 6).

F. To intensify the fundamental understanding of the properties of B cells that would offer novel insights for the study of the role of GSH in the regulation of B cells function and defects during disease, such as viral infections.

Chapter 2: Methods

2.1 Mice

Gclc$^{fl/fl}$ mice were described previously (Chen et al., 2007) and were crossed to *Mb1-Cre* expressing mice (Hobeika et al., 2006) to obtain the *Gclc*$^{fl/fl}$*Mb1-Cre* strain. The mice were housed and bred under specific pathogen-free conditions at the Luxembourg Institute of Health and the BTA facility of the University of Luxembourg. Age-matched mice (7-12 weeks old) were used for all experiments. All protocols were conducted and approved in the accordance to the Animal Welfare Structure guidelines.

2.2 T-independent B cell immunization (TNP-Ficoll)

To study Ag-trapping by MZB, mice were injected i.v. with 100µg TNP-Ficoll FITC (Biosearch Technologies F-1300F) and 30 min later tissues were analyzed with flow cytometry or snap-frozen for immunofluorescence microscopy in Tissue-Tek optimum cutting temperature (OCT, Sakura 4583). To measure the early IgM response, the same dose of TNP-Ficoll (Biosearch Technologies F-1300-100) was administered i.p. and blood was collected one day previous injection and 3, 5 and 7 days post injection (d-1, 3, 5, 7).

2.3 T-dependent B cell immunization (LCMV Cl13 and TNP-KLH)

LCMV Cl13 was propagated in BHK cells as previously described (Battegay et al., 1991a) and mice were i.v. infected with $2x10^6$ pfu. Blood was collected at different time points. At the endpoint, mice were euthanized and blood, spleen, kidney, liver and lung were collected and snap-frozen until further analysis. For ASCs assay BM cells were also harvested and used immediately.

For TNP-KLH immunization, mice were i.p. injected with 50μg of TNP-KLH (Biosearch Technologies T-5060) in 4mg of Imject alum (Fisher Scientific 10475325). Blood was collected at d-1, 7, 14, 21, 28.

2.4 Flow cytometric analyses and sorting

All antibodies for flow cytometry are reactive against mouse antigens, unless otherwise stated. For surface staining, cells were washed and resuspended in PBS 1% FCS 50 μM EDTA (FACS buffer).

Antigen	**Fluorochrome**	**Supplier (reference)**
CD19	FITC	BD (557398)
CD45R/B220	PE	Immunostep (MO45RPE(V100))
TCR beta	APC	Fisher Scientific (15380800)
TOMM-20	/	Abcam (ab186734)
IgM	AF647	Fisher Scientific (10368172)
integrin β1	AF488	BioLegend (102211)
Integrin α4β7	PE	BioLegend (120605)
Integrin β2	AF594	BioLegend (101416)
CD106 (VCAM-1)	PE	Fisher Scientific (15586846)
CD11b	Pacific Blue	BioLegend (101224)
CD138 (Syndecan-1)	BV650	BioLegend (142518)
CD19	BV785	BioLegend (115543)
CD19	PE	BioLegend (115508)
CD1d	Pacific Blue	BioLegend (123517)
CD21/CD35	FITC	BioLegend (123408)
CD21/CD35	APC	BioLegend (123411)
CD23	PE	BioLegend (101608)
CD23	Pacific Blue	BioLegend (101615)
CD24	APC	Fisher Scientific (17-0242-82)
CD267 (TACI)	PE	Fisher Scientific (12-5942-81)

CD35	BUV737	BD (741751)
CD3ε	PerCP/Cy5.5	BioLegend (100328)
CD43	PE	BioLegend (143205)
CD45.1 (Thy1.1)	PE/Cy7	BioLegend (110730)
CD45R/B220	BV510	BioLegend (103248)
CD5	FITC	BioLegend (100605)
CD5	APC-eF780	Fisher Scientific (15539506)
CD54 (ICAM-1)	APC	Miltenyi Biotec (130-104-248)
CD93	BUV737	BD (741800)
CD93	BUV395	BD (740275)
IgD	BV605	BD (63003)
IgG1	FITC	BioLegend (406606)
IgG2b	FITC	BioLegend (406706)
IgG2c	AF488	SouthernBiotech (1077-30)
IgG3	FITC	BD (553403)
IgM	BUV395	BD (566217)
IgM	PE/Cy7	BioLegend (406514)

2.5 Labelling of cell surface antigens with fluorophore-conjugated antibodies and cell sorting

Cells were incubated at 4°-8°C, in the dark with the surface antibody mix. Antibody was washed from the cells with FACS buffer after 20-30mins. All washes were performed by adding FACS buffer to each well and centrifuging samples at 350g for 5mins at 4°C, then tipping off the supernatant. Samples from *in vivo* LCMV experiments were fixed in a volume of at least 100µL 2% formaldehyde. Staining of blood cells was performed on 5-10uL whole blood. RBCs were lysed by adding 100uL of lysis solution (BD 349202) for 10mins at RT. Cells were washed twice with FACS buffer. Flow cytometry was performed using a BD Fortessa instrument (BD). For viability, 7-aminoactinomycin D (7AAD) (Thermo fisher A1310) or Zombie NIR (BioLegend 423106) was stained concurrently with

antibodies in all flow cytometry assays. Unless otherwise specified, FoB cell sorting was performed by MACS pre-enrichment with B cell isolation kit (Miltenyi Biotech 130-090-862). Untouched B cells were then stained with CD19, CD21/35 and CD23. Live $CD23^{+}$ $CD21/35^{-}$ FoB cells were FACS-sorted using Aria IIu (BD).

To stain intracellular thiols, cells were incubated at 37°C for 10 min with 50µM monobromobimane (MBB) (Thermo Fisher Scientific) in complete RPMI 1640 (10% FBS, 1% penicillin/streptomycin, 1% L-glutamine, 55µM 2-mercaptoethanol). Stained cells were washed twice and resuspended in PBS for flow cytometry analysis.

2.6 Intracellular staining

Cells were washed in PBS and fixed in fix/perm buffer (BD 554714) for 20mins at 4°C. Cells were washed twice with perm/wash buffer (BD 554714) and resuspended in fix/perm buffer containing TOMM-20. After 30mins at 4°C, cells were washed in perm/wash buffer and resuspended in perm/wash with secondary Ab anti-Rabbit IgG FITC (Fisher Scientific 15303926).

2.7 Glucose uptake assay and GLUT1 surface detection

Total splenocytes were washed at RT once with glucose-free RPMI medium (Lonza BE12-752F). Pellet was resuspended in glucose-free RPMI medium supplemented with 2-NBDG (Thermo Fisher N13195) at 50µM for 30mins at 37°C. Then, an equal amount of staining solution containing 2-fold Abs for surface detection of FoB was added and mixed. Cells were returned at 37°C for 30mins more and glucose uptake was measured directly with a BD Fortessa instrument. GLUT1 (Abcam ab195359) surface expression was measured on FoB from total splenocytes as described earlier.

2.8 Characterization of mitochondria

For quantification of mitochondrial potential and mass in FoB and MZB, splenocytes were stained with 100nM MitoTracker Deep Red FM, and 10nM MitoTracker Green FM (Fisher Scientific 15754272 and 15784272) as follows. Splenocytes were washed once with warm RPMI 1640, stained at 37°C for 30mins with Abs diluted in RPMI 1640 and washed twice with PBS.

2.10 Measurement of ROS and NADH

To detect intracellular ROS, cells were incubated with dichlorofluorescein diacetate (Carboxy-H2DCFDA; Thermo Fisher 11500146) or MitoSOX Red (Thermo Fisher 11579096) as follows. Splenocytes were washed once with warm RPMI 1640, stained at 37°C for 30mins with Abs diluted in RPMI 1640 and washed twice with PBS. To measure NADH, cells were stained at 4°C in FACS buffer with surface Abs. NADH autofluorescence was detected with BD Fortessa (BD) in the BUV395 channel equipped with a BP465/30.

2.10 Serum ATA titers

Based on previous reports (Hayakawa et al., 1999; Hayakawa et al., 2003), mouse sera were dispensed on thymocytes from C57BL/6J mice previously washed in FACS buffer. Sera were incubated for 30mins at 4°C. After washing twice with FACS buffer, pellets were stained with anti-IgM AF647 and CD45.1 (Thy1.1). Relative anti-Thy1.1 IgM was measured as AF647 mean fluorescence intensity (MFI) gated on live CD45.1 expressing cells.

2.11 ELISA assays

ELISA assays were performed in 96-well NUNC plates (Fisher Scientific 11371605) unless otherwise indicated. Readings were recorded with SpectraMax ELISA plate reader instrument (Molecular Devices). Washes were done manually by submerging plates in a bucket containing PBS Tween 0.05% (PBS-T).

2.12 Detection of total Igs and anti-PC IgM in mouse sera and cell culture supernatants

Plates were coated overnight at 4°C with 100µL/well of capture antibody anti-mouse Ig (SouthernBiotech 1010-01) at 1µg/mL in PBS. After tipping off the supernatant, plates were washed 4 times with PBS-T blotted on paper and blocked with 200uL/well of PBS 1% BSA for 30mins at RT. After tipping off the supernatant, serum samples were diluted 1:100 in 100µL of PBS 1% BSA and 2-fold serially diluted. For standard preparation, 8 to 12-points standard curve for IgM (Sigma PP50), IgG1 (Sino Biological 10690-MNAH), IgG2a (Sino Biological 51094-MNAH), IgG2c (Thermo Fisher 39-50670-65) and IgG3 (Sino Biological 51096-MNAH) was run in duplicate with top concentration of 5-10ng/mL. Samples and standards were incubated for 2h at RT, and plates were washed 6 times as above. Then, 50µL/well of HRP-conjugated detection antibody (anti-IgM-HRP Sigma A8786, anti-IgG1-HRP Sigma SAB3701171, anti-IgG2a-HRP Sigma SAB3701178, anti-IgG2c-HRP SouthernBiotech 1078-05, anti-IgG3-HRP Sigma SAB3701192) diluted 1:4000 in PBS was added for 1h at RT. Plates were washed 6 times as above and developed by adding 50µL of RT TMB solution (ThermoFisher 12750000). Reaction was stopped by adding 50 µL H_2SO_4 2N. Plates were read within 5mins at 450nm.

For detection of anti-PC IgM, plates were coated at 4°C overnight with PC-BSA (Biosearch Technologies PC-1011-10) at 1µg/mL in PBS.

For detection of total IgM in supernatants, total spleen or BM were lysed with Erylysis-buffer (Morphisto 12972) for 3mins at RT and counted. $2x10^6$ cells were seeded in a 96-well plate and washed once with RT complete medium. Cells were resuspended in 200µL complete medium and incubated for 12h at 37°C. Cells were centrifuged for 5mins at 350g at 4°C and supernatant were stored at -20°C. ELISA for IgM was performed as above and 100µL of supernatant was used.

2.13 Detection of Igs in mouse sera from LCMV Cl13 and TNP-KLH immunized mice

Analysis of IgM and IgG anti-LCMV-Gp specific antibodies was performed as previously described (Recher et al., 2004). Briefly, plates were coated overnight with anti-human Fc (Jackson ImmunoResearch Laboratories 109-001-008), blocked for 2h with PBS 2% BSA at RT and incubated with 100µL/well overnight at 4°C of recombinant Gp1-Fc protein derived from HEK293 cells transfected with LCMV glycoprotein vector. 1:30 pre-diluted sera of LCMV Cl13 infected mice were 1:3 serially diluted in PBS 2% BSA and incubated for 90mins at RT. Plates were washed with PBS-T and diluted anti-mouse IgM-HRP or anti-mouse IgG-HRP (Sigma A8786 and A3673) was added for 1h at RT. Plates were washed and a green color reaction was produced with 2,2`azino-bis(3-ethylbenzothiazoline-6-sulfonate) ABST (Sigma 10102946001) diluted in 0.1M NaH2P04 (pH=4). Plates were read at 405 nm and Ab titer was defined as the log2 serum dilution two-fold above background.

For TNP-specific Ig, plates were coated at 4°C overnight with 100µL/well of $NP_{(7)}$-BSA (Biosearch Technologies N-5050L) at 1µg/mL in PBS. ELISA was performed following the protocol of total Igs detection.

2.14 Antibody Secreting Cells (ASC ELISPOT) LCMV assay

ELISPOT assay was performed as previously described (McIlwain et al., 2015). Briefly, filter plates were coated overnight at RT with LCMV-infected BHK-cell lysates. Plates were washed with PBS-T and PBS and blocked with RPMI 10% FCS for 2h at RT. Splenocytes and BM cells were serial diluted onto filter plates and incubated for 8h at 37°C in humidified 5% CO_2 incubator. After washing with PBS and PBS-T, the plates were incubated with biotinylated anti-IgG overnight at 4°C. The plates were then incubated with HRP-conjugated avidin-D for 60mins at RT. Following washing with PBS-T and PBS plates were stained with AEC working solution and rinsed abundantly with dH_2O.

2.15 Virus titer quantification (Plaque assay)

LCMV Cl13 virus titers were determined by plaque-forming assay on MC57 fibroblasts as described previously (Ahmed et al., 1984; Battegay et al., 1991b; McIlwain et al., 2015).

2.16 Magnetic activated cell sorting of lymphocytes and cell culture

FoB were magnetically enriched from mouse spleen using a MZ and FO B Cell Isolation Kit (Miltenyi Biotec 130-100-366) as per manufacturer's protocol. Enriched fractions were counted with CASY cell counter. Most of the experiments were performed with MACS-sorted FoB cells, unless clearly specified.

2.17 B cell culture and activation

Cells were seeded in complete medium consisting of RPMI-1640 supplemented with 10% FCS (Sigma), 1% Penicillin/Streptomycin (GIBCO), 1% L-Glutamine (Sigma), and 55mM β-mercaptoethanol (GIBCO). Cells were seeded in 96-well plates at $2x10^5$ cells/well unless otherwise indicated. FoB were activated with 5µg/mL anti-IgM (Jackson

Immunoresearch 715-006-020), 50ng/mL CD40 ligand (Bio-techne 8230-CL-050) and 10ng/mL IL-4 (Miltenyi Biotec 130-097-757).

2.18 Quantitative Real-Time PCR

RNA was isolated using a NucleoSpin RNA Kit (Macherey-Nagel 740955250). RT-qPCR was carried out using Luna Universal One-Step RT-qPCR Kit (Bioké E3005E) and the primers listed below. Reactions were run on a CFX384 instrument (Bio-Rad). Data were normalized to *Tbp* and analyzed using the ΔΔCt method as previously described (Mak et al., 2017).

Target	**Forward (F) and Reverse (R) primers**
Gclc	F:GGCTCTCTGCACCATCACTT R:GTTAGAGTACCGAAGCGGGG
Tbp	F:GAAGAACAATCCAGACTAGCAGCA R:CCTTATAGGGAACTTCACATCACAG
MTCOI	F: GCCCCAGATATAGCATTCCC R: GTTCATCCTGTTCCTGCTCC
18srRNA	F: TAGAGGGACAAGTGGCGTTC R: CGCTGAGCCAGTCAGTGT

2.19 Immunoblot analysis

For the detection of Gclc (Santa Cruz Biotechnology sc-390811), 1-5x10^6 cells were lysed with lysis buffer (CST 9803S) and protein/phosphatases inhibitors as per manufacturer's protocol and blotted as described (Kurniawan et al., 2020). Briefly, cells were washed and lysed on ice for 30mins and spun. Supernatants were assayed for total protein concentration with Bradford assay (BioRad 5000006) and 50-100ug of protein was mixed with loading buffer and loaded in a 12 or 16% gradient gel (Thermo 1Fisher XP00162). Proteins were transferred onto a NC or PVDF membrane (Fisher Scientific) and blocked with 5% milk for 1hr. OXPHOS complexes were revealed with total OXPHOS

Rodent WB Antibody Cocktail (Abcam ab110413). Lysis was carried out with the addition of 1.5% lauryl maltoside.

2.20 Histology and immunofluorescence of tissues

Hematoxylin and eosin (H&E) and immunofluorescence of tissues were performed on snap-frozen tissue samples in O.C.T. (Sakura 4583). Tissues were sliced in 5-7µm slices on glass coverslips and used for downstream processing. For H&E staining sections were processed following standard laboratory procedures. For immunofluorescence, cryosections were dried for 2h at RT, fixed in pure acetone for 10min and blocked with PBS 10% FCS for 30mins at RT. After washing in PBS, primary antibodies diluted in PBS 10% FCS were incubated at 4°C overnight. Primary antibody was washed in PBS and DAPI mounting medium (SouthernBiotech 0100-20) or secondary antibody staining was performed with the same procedure as above.

2.21 Confocal microscopy

For TOMM-20 mitochondria staining, 10^6 sorted FoB cells were stained in 96-well plate as before. After the last wash, cells were resuspended in DAPI mounting medium (SouthernBiotech 0100-20) and seeded on Cell-Tak (Fisher Scientific 10317081) coated glass slides. Cells were visualized with ZEISS LSM 880. Images were analyzed with ZEISS ZEN Blue and Fiji program.

2.22 Transmission electron microscopy

For ultrastructural microscopy, 10-20x10^6 FoB were fixed in complete RPMI medium 2.5% glutaraldehyde (EMS 16220) for 1h at RT. After spinning, supernatant was removed and pellet was resuspended in 0.1M sodium cacodylate buffer (pH 7,4) with 2.5% glutaraldehyde and stored overnight at 4°C. Then, cells were centrifuged and resuspended

in 0,1 M sodium cacodylate buffer. The cells were post-fixed for 1h with 1% osmium + 0,1 M sodium cacodylate buffer, then dehydrated and embedded in Agar 100 resin. Pelleted cells were sectioned a RMC Boeckeler ultramicrotome using a Diatome diamond knife at a thickness setting of 60 nm. Sections were stained with 2% uranyl acetate, and lead citrate. The sections were examined using a ZEISS GEMINI 300 at 30 kV with the STEM detector.

2.23 Single cell RNA sequencing

For CITE-seq labelling, a total of 2 million cells/genotype were FACS sorted, counted, isolated and spun down. The cell pellet was resuspended and incubated for 30mins on ice with 25µL of staining mix in PBS containing 0.04% BSA, TruStain FcX Block (BioLegend 101320) and the mouse cell surface protein antibody panel containing the following oligo-conjugated anti-mouse antibodies (TotalSeq-A BioLegend) diluted 1:500.

Antigen	**Ref. number**
CD23	101635
IgD	405745
CD1d	123529
CD21/CD35	123427
IgM	406535

Sorted single cell suspensions were resuspended at an estimated final concentration of 1000 cells/µl and loaded on a Chromium GemCode Single Cell Instrument (10x Genomics) to generate single cell gel beads-in-emulsion (GEM). Biological replicates (n=4 for each group) were multiplexed using TotalSeq-A Cell Hashing Antibodies. The scRNA/CITE-seq libraries were prepared using the GemCode Single Cell 3' Gel Bead and Library kit, version 3 (10x Genomics 1000128) according to the manufacturer's instructions with the addition of amplification primer (3nM, 5'CCTTGGCACCCGAGAATT*C*C) during cDNA amplification to enrich the TotalSeq-A cell surface protein oligos. Sequencing

libraries were loaded on an Illumina HiSeq4000 flow cell at VIB Nucleomics core with sequencing settings according to the recommendations of 10x Genomics, pooled in a 85:15 ratio for the gene expression and antibody-derived libraries, respectively. The Cell Ranger pipeline (10x Genomics version 3.1.0) was used to perform sample demultiplexing and to generate FASTQ files for read 1, read 2 and the i7 sample index for the gene expression and cell surface protein libraries. Read 2 of the gene expression libraries was mapped to the reference genome (mouse mm10, v3.0.0) using STAR. For cellular identification and clustering of the gene-barcode matrix the data was passed to the R package Seurat (v. 4.0) (Butler et al., 2018) for all downstream analyses. Analysis was conducted on cells that expressed a minimum of 800 genes, of which less than 15% was of mitochondrial origin. Count data was derived through the SCTransform function. To identify FoB and MZB, Antibody-derived signals (ADT) were used in combination with the SCINA algorithm (Zhang et al., 2019) with the following signatures: CD23-ADT, IgD-ADT for FoB; CD1d-ADT, CD21-CD35-ADT, IgM-ADT for MZB. For principal component analysis (PCA), counts of each cell group/mouse for each genotype where extracted and analyzed using DESeq2 (Love et al., 2014). Cluster-based marker identification and differential expression were performed using Seurat's FindMarkers/DESeq2 comparing specific groups (i.e. MZB vs. FoB for *Gclc*$^{fl/fl}$, or FoB *Gclc*$^{fl/fl}$ *Mb1-Cre*$^{+}$ vs. FoB *Gclc*$^{fl/fl}$). Visualization of differentially expressed genes was done with EnhancedVolcano (Blighe et al., 2020). For gene ontology (GO) analysis, the Seurat's FindMarkers output for the specified groups was used to plot gene ontology terms with the barcodeplot functions from limma (Ritchie et al., 2015). For GSEA analyses, the fgsea package was used (Korotkevich et al., 2021).

scRNA-seq data were analyzed as above and the gene expression matrix of 156 cells/group (MZB and FoB from *Gclc*$^{fl/fl}$ mice) or 1700 FoB/genotype (*i.e.* *Gclc*$^{fl/fl}$ or *Gclc*$^{fl/fl}$ *Mb1-Cre*$^{+}$ mice) was used as input for the Compass algorithm (Wang et al., 2020; Wagner

et al., 2021). Downstream analysis was conducted with the compassR package and differential metabolic states were determined with a Wilcoxon Rank Sum Test on the Compass reactions.

2.24 Isotopic labeling

FoB cells were incubated for 5h in SILAC RPMI containing [U-$^{13}C_6$]-glucose (11 mmol/L; Cambridge Isotope Laboratories). Extraction of intracellular metabolites, GC-MS measurement, MID calculations, determinations of fractional carbon contributions, and subtractions of natural isotope abundance were performed as described (Kurniawan et al., 2020). Total glucose and lactate concentrations from medium were determined using a YSI 2950D. Total cellular glucose was measured by liquid chromatography (Vanquish HPLC Thermo Scientific) coupled to high resolution mass spectrometry (QExactive HF Thermo Scientific). Briefly, extraction of 3-30x10^5 cells was done in a 2:2:1 mixture of acetonitrile:MeOH:H_2O + 0.5% formic acid on ice. Following neutralization with $(NH)_4HCO_3$, samples were frozen at -20°C for 20min, spun and supernatants measured directly.

2.25 Seahorse flux analyses

Assays were performed using an XFe96 Extracellular Flux Analyzer (Agilent). FoB or MZB cells were seeded in XF Seahorse RPMI medium at 10^6/well on Seahorse XFe96 culture plates pre-coated with Cell-Tak. Oxygen consumption rate (OCR) of intact cells were determined using the XF Cell Mitochondrial Stress Test according to the manufacturer's protocol. Briefly, three basal OCR measurements were taken, followed by sequential injections of 1 µM Oligo, 3 µM FCCP, and 1 µM Ant + Rot, taking three measurements following each treatment. GlycoATP and mitoATP were derived from cells sequentially treated with Oligo and Ant + Rot. Activity measurements for each respiratory

chain complex in permeabilized cells were performed according to previous research (Kory et al., 2020; Salabei et al., 2014). Briefly, after enrichment, FoB were washed and resuspended in mannitol and sucrose–BSA (MAS-B) buffer pH 7.2 (70 mM sucrose, 220 mM Mannitol, 10 mM KH2PO4, 5 mM $MgCl_2$, 2 mM Hepes, 1 mM EGTA, and 0.4% fatty acid-free BSA), and flux measurements were started. After three basal measurements, cells were permeabilized by injection of saponin (1µg/mL, Sigma S4521), together with 1 mM ADP (Sigma 01905) and the following respiratory complex substrates: CI, pyruvate/malate (5 mM/2.5 mM); CII, succinate/Rot (5 mM/1 µM); CIII, duroquinol (0.5 mM); CIV, N,N,N,N-tetramethyl-p-phenylenediamine (TMPD)/ascorbate (0.5 mM/2 mM). These were followed by injections with Oligo (1 µM) and respective complex inhibitors (CI, 1 µM Rot; CII and CIII, 20 µM Ant; CIV, 20 mM potassium azide). For calculation of the $state_{apparent}$ see Figure 27.

2.26 Statistical analyses

Data are graphed as the mean ± SD and have at least n = 2-3 per group (refer to Figure Legends for detailed information). P value was determined by unpaired Student's t-test, one- or two-way ANOVA using Prism (GraphPad). Significance is indicated with asterisks * and a minimum P value of 0.05 was considered statistically significant (refer to Figure Legends for details).

Chapter 3: Investigating the role of *Gclc* in B cell-specific *Gclc*-depleted mice

3.1 Introduction

B cells are central components of the immune system with a variety of functions, yet their main goal is to produce Abs (LeBien and Tedder, 2008). Importantly, the variety of processes which characterize B cell life, from differentiation to Ab secretion, are marked by dramatic changes in the redox state (Masciarelli and Sitia, 2008; Vene et al., 2010). These chemical challenges are mastered by intracellular antioxidant systems, which are optimized to use GSH as the most versatile nucleophile in the reduction, direct conjugation and enzymatic reactions of electrophiles (Meister, 1988; Wu et al., 2004; Deponte, 2013).

Many advances in the understanding of B cell immunology have been achieved with the aid of transgenic mouse models. Utilising a reverse genetics approach, the function of a particular protein can be probed using a model in which that molecule is genetically manipulated. A protein of interest may be over-expressed, knocked out or knocked down (Tiscornia et al., 2003; Doyle et al., 2012). Certain aspects of B cells biology are incompletely understood, and, in particular, those related to the intracellular metabolic activities. For instance, the influence of antioxidants and their weight against metabolic ROS is poorly understood. By deleting *Gclc* in the B cell lineage with the *Mb1* deleter (Hobeika et al., 2006), we sought to shed light on the effect of GSH – the prime cellular antioxidant – in B cells.

In this chapter we have discerned in detail the maturation, differentiation and distribution of most B cell populations at the physiological level. Building upon previously published methods such as flow cytometry and ELISA, we identified an ontogenic block in regard to

the development of MZB and B1 cells, and an impairment of the humoral immunity in B cell-specific *Gclc*-depleted mice at the steady state.

3.2 Objective

To investigate if and to which extent the deletion of *Gclc* in the B cell lineage affects B cell development, homeostasis and antigen-independent Ab production.

3.3 Results

3.3.1 Deletion of *Gclc* alters normal B cell progression during splenic development

Recent work from our laboratory has described the role of GSH in tempering ROS activity to allow protective $CD4^+$ T cell responses (Mak et al., 2017) and the maintenance of Treg cell functionality (Kurniawan et al., 2020). In order to explore the relevance of *Gclc* and GSH in B lymphocyte homeostasis and function, we generated $Gclc^{fl/fl}$ *Mb1-Cre* mice by crossing mice with loxP-flanking $Gclc^{fl/fl}$ with mice expressing the gene encoding the recombinase *Cre* under the B cell-specific promoter *Mb1* (*Mb1-Cre*) (Hobeika et al., 2006).

First, we examined the B cell developmental stages to assess the effect of GSH depletion under homeostatic condition. We studied early B cell development in the BM via flow cytometry following Hardy's fractions classification (Figure 5 and 10 A) (Hardy et al., 1991). Hardy's fractions frequencies and numbers were comparable between $Gclc^{fl/fl}$ *Mb1-*Cre^+ and littermate controls ($Gclc^{fl/fl}$), with the only exemption of fraction F (Figure 10 B, right). Fraction F includes mature B cells, which are recirculating through the blood (Hardy et al., 1991; Melamed et al., 1998; Hardy and Hayakawa, 2001) and can also be identified by the expression of the surface markers CD19, IgM and IgD. In line, $CD19^+IgM^+IgD^+$

recycling BM B cells were diminished in *Gclc*$^{fl/fl}$ *Mb1-Cre*$^{+}$ animals (Figure 10 C). Together, these results suggested that *Gclc* deficiency does affect early B cell development. Concurrently with the decrease of mature recycling B cells in the BM (Figure 10 B, C), lower frequencies and numbers of *Gclc*-depleted B cells were found in the blood (Figure 10 D), which is known to contain naïve mature B cells (Loder et al., 1999). These findings overall support the notion that *Gclc* is dispensable for BM maturation of B cells.

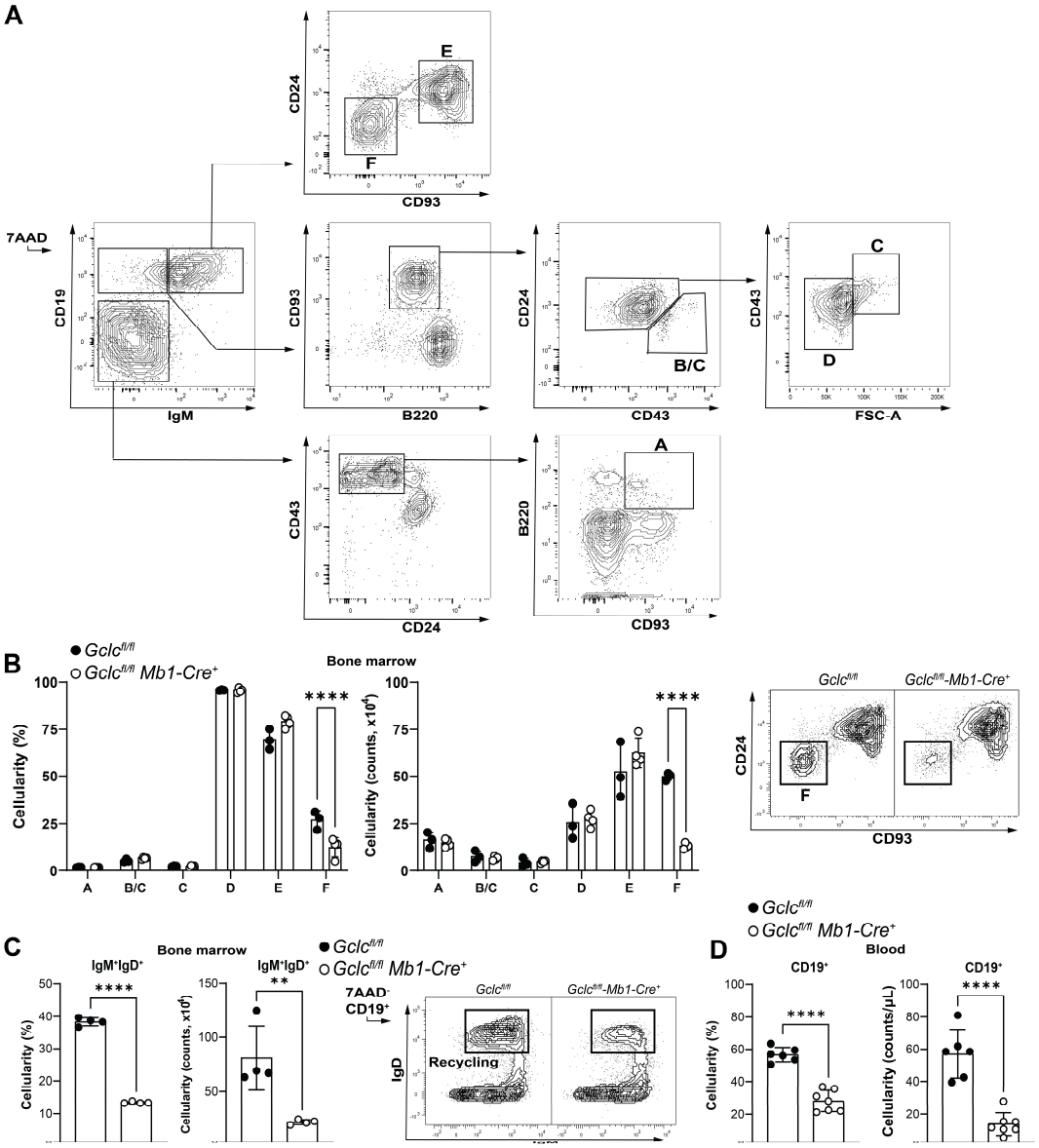

Figure 10: The absence of Gclc does not alter early B cell development.

A. Representative FACS plots showing the gating strategy used for early B cell differentiation in the BM (Hardy's fractions are indicated). **B.** Summary statistics of fractions A-F in percentages and counts. Right: representative contour plot for fraction F is shown. **C.** Cell frequencies and counts for mature recirculating B cells in the BM (pre-gated as $CD19^+$). Representative contour plot is shown on the right. **D.** Summary statistics of frequencies and counts of total B cells in the blood of *Gclc*$^{fl/fl}$ *Mb1-Cre*$^+$ and control mice. For all applicable figure panels, data are mean ± SD and each dot represents one single mouse. Data shown are representative of ≥3 independent experiments with 3-7 mice/group. Significance (P) was calculated with unpaired t-test or tw-way ANOVA (B). **: $P \leq 0.01$; ****: $P \leq 0.0001$.

The product of early B cell development in the BM is the immature B cell (Hardy and Hayakawa, 2001), which continues the maturation process in the spleen (Pieper et al., 2013). Histological examination of the spleen architecture did not reveal abrupt anomalies in B cell-specific *Gclc*-depleted animals, however we could detect loss of cellularity around the follicle's edges (Figure 11 A, insert). mRNA and protein deletion of Gclc was nearly complete in total splenic B cells (Figure 11 B) and so was the GSH content (Figure 11 C). Next, we analyzed the three major resident splenic mature B cell populations (TB, transitional B cells; FoB, follicular B cells and MZB, marginal zone B cells) with flow cytometry (Figure 11 D). *Gclc* deficiency led to a drastic decrease in the MZB compartment, identified as $CD19^{+}CD23^{-}CD21^{+}$ cells (Martin and Kearney, 2002; Arnon et al., 2013), while FoB and TB were only partially affected (Figure 11 E). Moreover, we further checked MZB with flow cytometry by using a combination of other surface markers, such as CD93, CD1d and CD24 (Oliver et al., 1997) (Figure 11 F) and confirmed the data shown in Figure 11 D. Lastly, the absence of MZB in *Gclc*-depleted animals was confirmed by immunofluorescence microscopy of spleen sections (Figure 11 G).

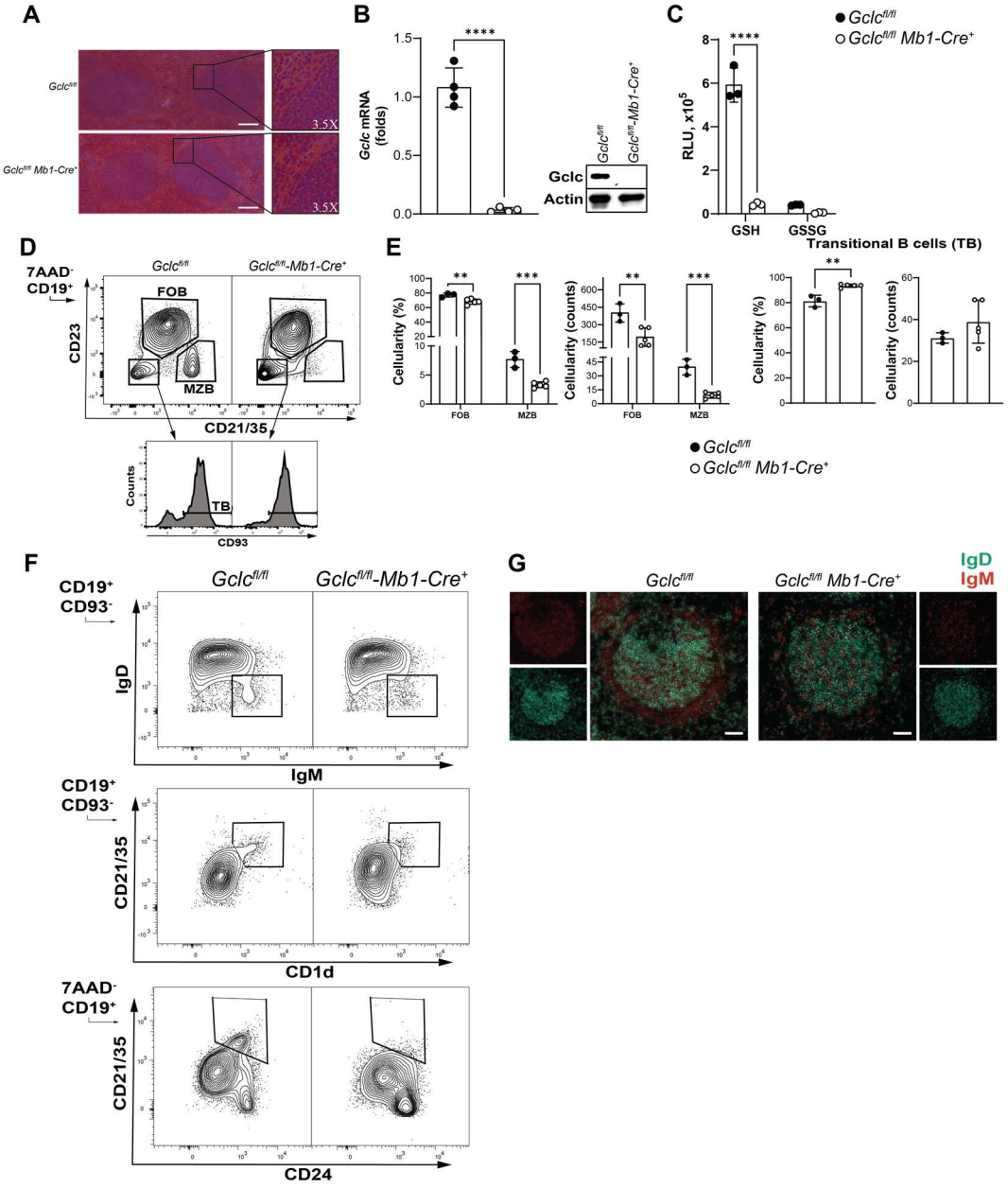

(Legend on next page)

Figure 11: B cell-specific Gclc-deficient mice lack MZB.

A. Representative H&E staining of two follicles of *Gclc*$^{fl/fl}$ *Mb1-Cre*$^{+}$ and control mice. Scale bars: 100µm. **B.** Fold change of mRNA level of *Gclc*. Right: protein level of Gclc in total B cells from *Gclc*$^{fl/fl}$*Mb1-Cre*$^{+}$ and control mice. **C.** GSH and GSSG measurement in freshly enriched total splenic B cells. **D.** Representative contour plot used for identification of splenic B cell populations: TB, FoB and MZB. **E.** Summary statistics of the percentages and counts of the three main splenic B cell populations. **F.** Representative contour plots with alternative identification strategies for splenic MZB of *Gclc*$^{fl/fl}$*Mb1-Cre*$^{+}$ and control mice. **G.** Immunofluorescence staining on spleen section of *Gclc*$^{fl/fl}$*Mb1-Cre*$^{+}$ and control mice with IgD (green) and IgM (red). Scale bars: 50 µm. For all applicable figure panels, data are mean ± SD and each dot represents one single mouse. Data shown are representative of ≥3 independent experiments with 3-5 mice/group. Significance (P) was calculated with unpaired t-test or two-way ANOVA (C and E). **: $P \leq 0.01$; ***: $P \leq 0.001$; ****: $P \leq 0.0001$.

3.3.2 The lack of MZB in *Gclc*$^{fl/fl}$ *Mb1-Cre*$^{+}$ does not originate from altered microenvironmental cues and it is *Cre*-independent

Other reports have shown that the control of lymphoid tissue compartments and MZB localization in the spleen depends on signals delivered by integrins and chemokines (Ansel et al., 2000; Lu and Cyster, 2002). In particular, ICAM-1 and VCAM-1 expressed by splenic stromal cells and MZ macrophages are critical for the MZB lodging in the MZ (Lu and Cyster, 2002; Karlsson et al., 2003). Moreover, MZB entry and retention in the MZ are tightly regulated by chemotactic molecules, such as CXCL13 and sphingsoine-1-phosphate (S1P) (Cinamon et al., 2004). The loss of MZB in *Gclc*$^{fl/fl}$ *Mb1-Cre*$^{+}$ mice led us to investigate the possibility of flaws in the cellular migration properties. The expression level of the integrins ICAM-1 and VCAM-1 in total splenocytes and seric levels of chemotactic factors were unchanged between *Gclc*-deficient and control littermates (Figure 12 A, B).

Literature reports have also connected MZB localization and/or function to an extrinsic defect in the MZ microenvironment. In particular, it has been shown that trafficking and retention of MZB require specific macrophage–B cell interactions (Karlsson et al., 2003; Chen et al., 2005b; You et al., 2009; You et al., 2011). Two major macrophage populations can be discerned in the MZ: marginal metallophilic macrophages (MMM) and marginal zone macrophages (MZM) (Borges da Silva et al., 2015). The MZM typically express the surface C-type lectin SIGN-related 1 (SIGNR1) and a type I scavenger receptor called Macrophage Receptor with Collagenous structure (MARCO), which recognize blood-borne antigens. Furthermore, MMM are defined by the expression of Sialic acid-binding Ig-like Lectin-1 (Siglec-1 or CD169) and MOMA-1.

To investigate if *Gclc*-deficient mice had impaired cross-talk in the MZ microenvironment, which could justify the lack of MZB, we stained spleen section for

MARCO and Siglec-1 to discriminate between MZM and MMM. As shown in Figure 12 C, both populations of MZ macrophages were unchanged in the spleen of *Gclc*$^{fl/fl}$ *Mb1-Cre*$^{+}$ mice. These results suggested that migratory inputs are not affected by the absence of *Gclc* in B cells, and that the MZB loss in the spleen is B cell intrinsic. Importantly, flow cytometric analysis of heterozygous and homozygous *Gclc* expression in B cell-specific mutant mice excluded any gene-dosage effect of *Gclc* expression and confirmed that the drastic loss of MZB was independent of any *Cre*-associated toxicity (Figure 13A, B), a concern raised in a previous study (Schmidt-Supprian and Rajewsky, 2007).

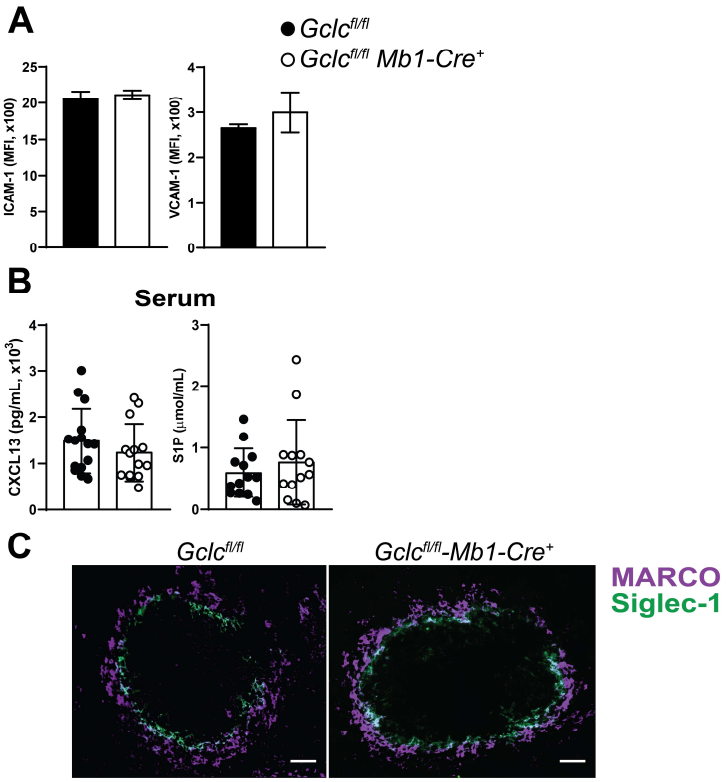

Figure 12: The effect of Gclc deficiency on MZB is independent of environmental cues.

A. Levels of ICAM-1 and VCAM-1 as measured by FACS on total splenocytes from *Gclc$^{fl/fl}$ Mb1-Cre^{+}* and control mice. **B.** Quantitative measure of CXCL13 and S1P by ELISA from serum of *Gclc$^{fl/fl}$ Mb1-Cre^{+}* and control mice. **C.** Representative immunofluorescence of one follicle from *Gclc$^{fl/fl}$ Mb1-Cre^{+}* and control mice showing the disposition of MMM (Siglec-1^{+}, green) and MZM (MARCO^{+}, purple) in the marginal zone area. Scale bars: 50 µm. For all applicable figure panels, data are mean ± SD and each dot represents one single mouse. Data shown are representative of ≥3 independent experiments with 3-5 mice/group, except for B where data are pooled from 4 independent assays. Significance (P) was calculated with unpaired t-test.

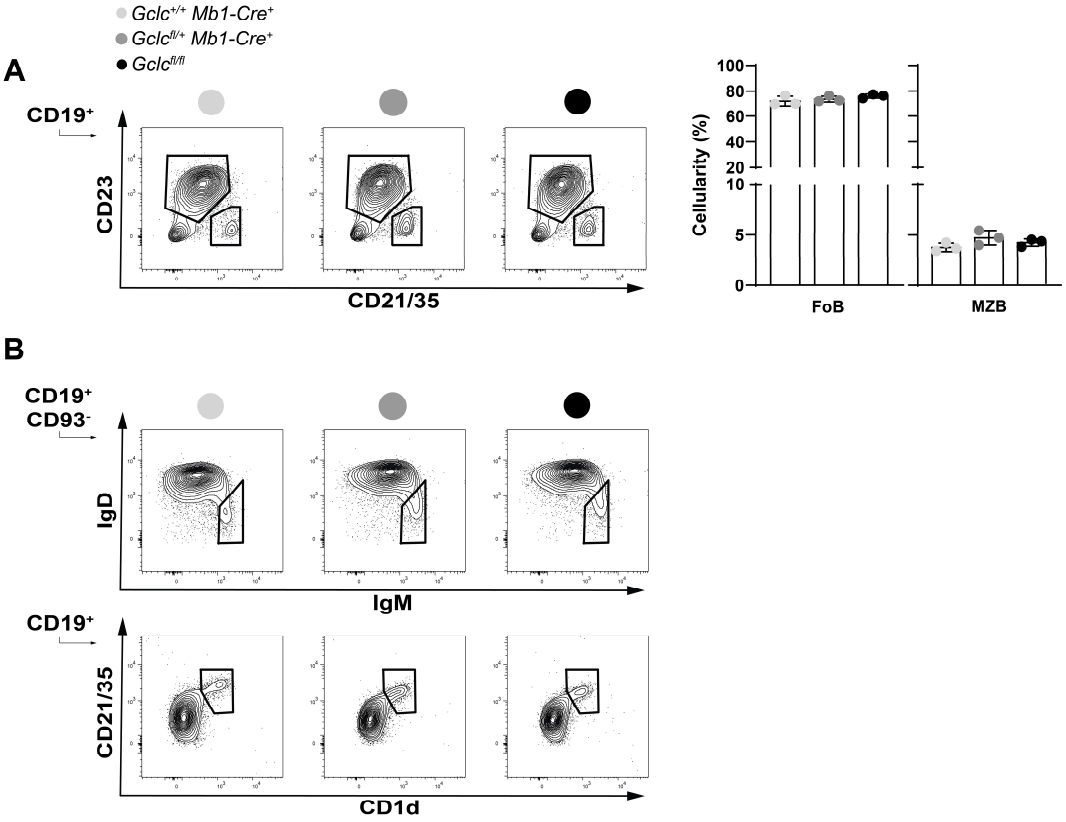

Figure 13: MZB loss is independent of Cre.

A. Representative FACS contour plot (left) and quantitation (right) of splenic FoB and MZB from *Gclc*$^{+/+}$ *Mb1-Cre*$^{+}$, *Gclc*$^{fl/+}$ *Mb1-Cre*$^{+}$ and *Gclc*$^{fl/fl}$ mice. **B.** Representative contour plots of the indicated MZB markers expressed by total the sub-gated cells indicated on the upper left corner from *Gclc*$^{+/+}$ *Mb1-Cre*$^{+}$, *Gclc*$^{fl/+}$ *Mb1-Cre*$^{+}$ and *Gclc*$^{fl/fl}$ mice. Data are the mean ± SD. Each dot represents one mouse. Data shown are representative of ≥2 independent experiments with 2-3 mice/group. Significance (P) was calculated with one-way ANOVA.

Lastly, to assess whether *Gclc* is necessary for the development of MZB rather than their homeostatic persistence at steady state, we investigated the developmental stages of B cell maturation in the spleen of young mice, based on the fact that MZB generally develop at 2-3 weeks after birth (Pillai and Cariappa, 2009). We studied B cell development and identified the three different stages in the spleen by flow cytometry: T1, T2 and mature (M) (Figure 14 A) (Loder et al., 1999; Srivastava et al., 2005; Allman and Pillai, 2008). As shown, the absence of *Gclc* influenced T1 B cells by 2 weeks of age, indicating that a block in the B cell differentiation process occurred at the very early stage in the spleen (Figure 14 B). In 8 weeks old mice, mature B cells (M) dropped as well, indicating that *Gclc* is needed for the proper differentiation of B cells. Although we cannot exclude that the tonicity of BCR signaling could influence developing *Gclc*-deficient B cells (Loder et al., 1999), these results support the notion that *Gclc* plays a role in MZB ontology.

Taken together, these data indicate that the *Gclc* system is nonessential for the early B cell development in the BM and mildly affect the persistence of FoB in the spleen, but it is crucial for MZB ontology.

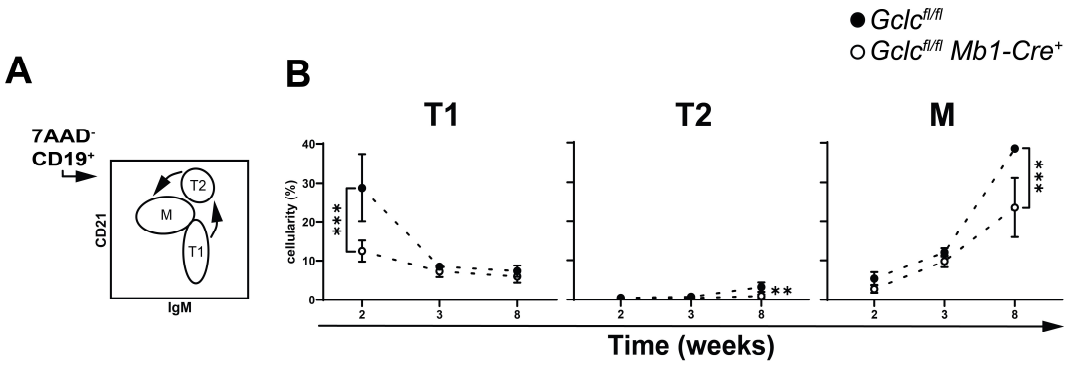

Figure 14: Development of MZB is disturbed in Gclc-deficient mice.

A. Representative gating model to identify splenic T1, T2 and M stages of splenic B cells via FACS. **B.** Summary statistics of T1, T2 and M subsets in *Gclc$^{fl/fl}$ Mb1-Cre^{+}* and control mice are plotted over time (2, 3 and 8 weeks old mice were used). For all applicable figure panels, data are mean ± SD and each dot represents the mean of triplicates. Data shown are representative of ≥2 independent experiments with 3-4 mice/group. Significance (P) was calculated with one-way ANOVA. **: $P \leq 0.01$; ***: $P \leq 0.001$.

3.3.3 Deletion of *Gclc* in B cells causes loss of peritoneal B1 cells

B lymphocytes bearing receptors for Ags generally recognized by innate receptors often possess characteristics that distinguish them from the bulk of B cells. Published studies have shown a number of converging observations related to B1 and MZB functions (Yancopoulos et al., 1984; Martin and Kearney, 2000b; Won and Kearney, 2002; Kretschmer et al., 2003; Carey et al., 2008). Furthermore, B1 cells are also able to produce Abs against TI Ags (Martin et al., 2001; Haas et al., 2005; Kearney, 2005).

Based on these analogies, we sought to determine whether the role of *Gclc* is confined to splenic MZB by analyzing B1 cells in the peritoneal cavity (PEC), which represents their major reservoir (Hardy and Hayakawa, 1986; Herzenberg et al., 1986), and spleen (Wells et al., 1994). We found reduced frequencies and numbers of B1 cells in the PEC (Figure 15 A) and spleen (Figure 15 B) of $Gclc^{fl/fl}$ *Mb1-Cre*$^{+}$ compared to control animals. Seminal studies have shown that B1 cells are positively selected and maintained by the self-Ag Thy-1 (CD90.1) that is expressed mostly on thymocytes (Hayakawa et al., 1999; Hayakawa et al., 2003). Therefore, to exclude the influence of extrinsic factors and confirm the B cell-autonomous effect of *Gclc*, we measured seric Thy-1 by ELISA and detected no significant difference between mutant and control sera (Figure 15 C). This corroborates the notion that the contraction of peritoneal B1 cells is not caused by diminished or altered level of seric Thy-1.

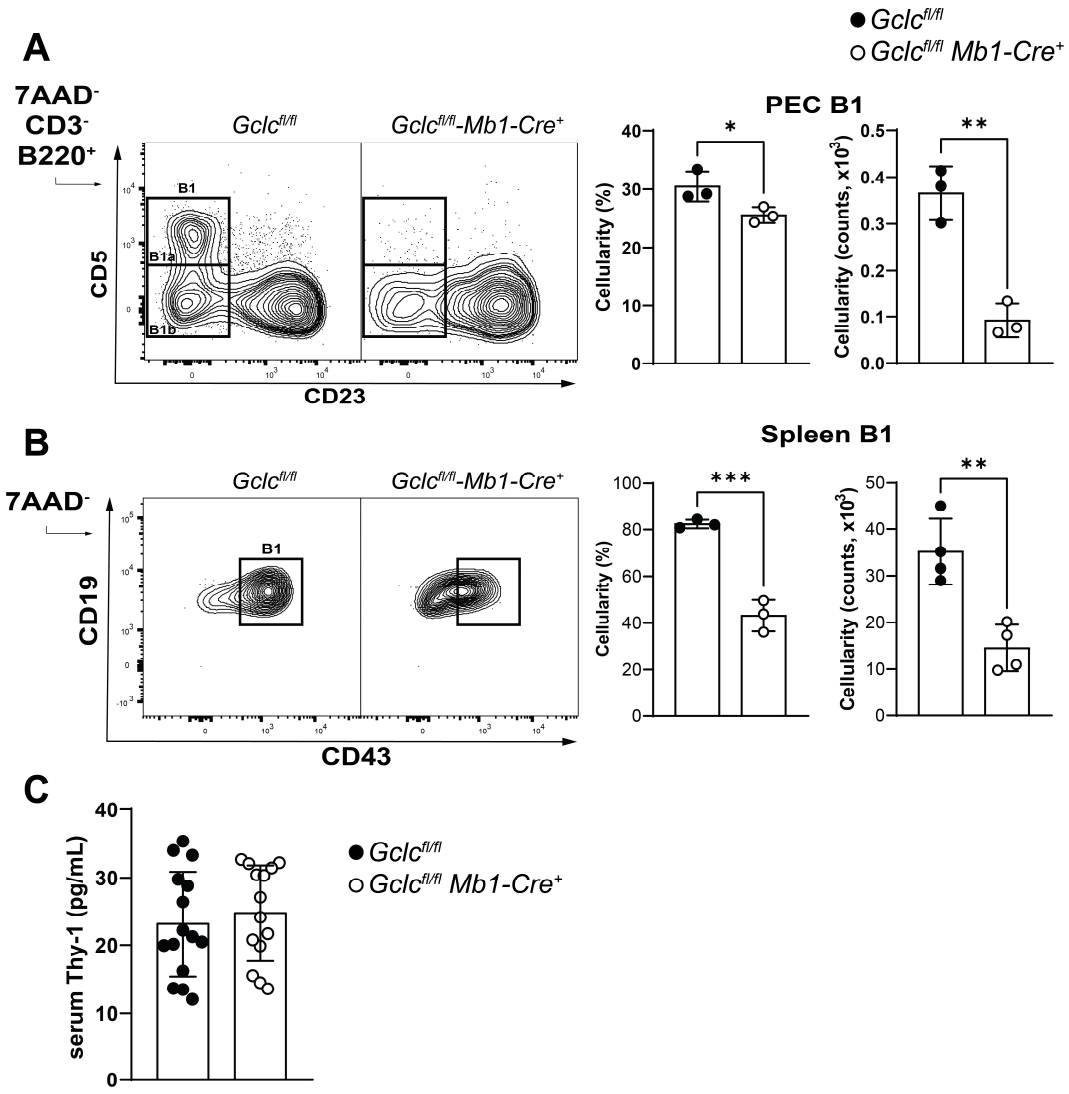

Figure 15: Gclc-deficient mice lack B1 cells in the peritoneal cavity and spleen.

A. Representative contour plot used to identify peritoneal B cells B1, B1a and B1b with FACS. Right: summary statistics of percentages and counts of PEC B1 cells in *Gclc$^{fl/fl}$ Mb1-Cre^{+}* and control mice. **B.** Representative contour plot used to identify splenic B cells B1 with FACS. Right: summary statistics of percentages and counts of splenic B1 cells in *Gclc$^{fl/fl}$ Mb1-Cre^{+}* and control mice. **C.** Level of Thy-1 measured with ELISA from serum of *Gclc-Mb1-Cre^{+}* and control mice. For all applicable figure panels, data are mean ± SD and each dot represents one single mouse. Data shown are representative of ≥4 independent experiments with 3-4 mice/group, except in C where data are pooled from 4 independent assays. Significance (P) was calculated with unpaired t-test. *: $P \leq 0.05$; **: $P \leq 0.01$; ***: $P \leq 0.001$.

3.3.4 Absence of innate-like B cells induces reduction of induced and natural humoral immune protection

Although both FoB and MZB belong to the mature B2 subset, they are topographically, phenotypically and functionally distinct (Oliver et al., 1997; Oliver et al., 1999). Indeed, due to their strategic positioning, MZB are able to rapidly activate against thymus-independent (TI) blood borne Ags (Pillai and Cariappa, 2009). Since the absence of *Gclc* appears to be critical for MZB development (Figure 14), we used an established TI type II immunization model to confirm the absence of MZB-related functions *in vivo* (Guinamard et al., 2000; Cariappa et al., 2000; Girkontaite et al., 2001). To this purpose, $Gclc^{fl/fl}$ *Mb1-*Cre^{+} and control animals were i.v. injected with the polyclonal Ag TNP-Ficoll. 30 minutes later, we measured the TNP bound on the surface of FoB and MZB with flow cytometry. The amount of Ag bound to MZB of mutant animals was negligible, close to FoB levels, which possess less binding capacity (Figure 16 A, left), as confirmed by IF microscopy (Figure 16 A, right). Moreover, by injecting TNP-Ficoll i.p., we monitored the early MZB-specific immunoglobulin M (IgM) response against the TNP moiety over 7 days (Guinamard et al., 2000; Haas et al., 2018). We measured TNP-specific IgM antibodies in the serum of immunized animals at various time points pre- and post-immunization. As shown in Figure 16 B, the $Gclc^{fl/fl}$ *Mb1-*Cre^{+} animals were inefficient in producing anti-TNP IgM. These results are congruent with those shown in Figure 11, and confirm the functional absence of MZB in B cell-specific *Gclc*-deficient animals.

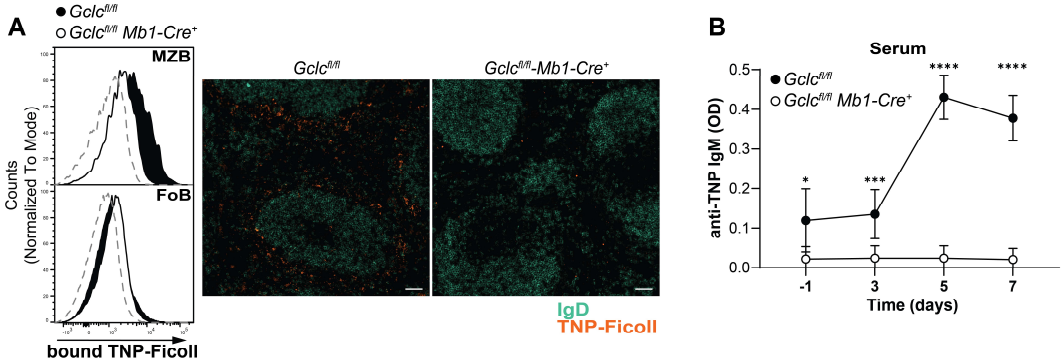

Figure 16: The immune response to T cell independent antigen is impaired following the absence of MZB in Gclc-depleted mice.

A. Representative FACS histogram of TNP binding to MZB and FoB in *Gclc$^{fl/fl}$ Mb1-Cre^{+}* and control mice is shown on the left. Gray dotted line: PBS-treated control. Right: representative immunofluorescence staining of spleen cryosections after 30min injection of TNP-Ficoll (orange). FoB are stained for reference with IgD (green). Scale bars: 100 µm. **B.** Each dot represents the mean of antibody (IgM) level measured by ELISA from 3-4 mice and it is plotted over a 7 days timeframe after i.p. injection of TNP-Ficoll in *Gclc$^{fl/fl}$ Mb1-Cre^{+}* mice and controls. For all applicable figure panels, data are mean ± SD and each dot represents the mean of triplicates. Data shown are representative of ≥2 independent experiments with 3-4 mice/group. Significance (P) was calculated with one-way ANOVA. *: $P \leq 0.05$; ***: $P \leq 0.001$; ****: $P \leq 0.0001$.

Notably, the sera of *Gclc*-deficient animals did not produce as much background signal to be detected by the ELISA assay, even before injection of the Ag, (Figure 16 B, day -1). This observation led us to further investigate the Ab composition in the serum of unimmunized *Gclc*$^{fl/fl}$ *Mb1-Cre*$^{+}$ animals. As anticipated, we detected a sharp absence of IgM compared to the control group (Figure 17 A). Moreover, levels of seric IgGs where all underrepresented in the serum of B cell-specific *Gclc*-deficient mice (Figure 17 A).

Primarily found as IgM or IgG3 isotypes, NAs are produced mainly by B1 cells (Lalor et al., 1989; Baumgarth et al., 1999; Durand et al., 2009; Choi et al., 2012) or, to a lesser extent by MZB (Ichikawa et al., 2015). NAs are found in the serum of unimmunized animals and humans and they are spontaneously produced before Ag exposure (Ehrlich and Morgenroth, 1902). Due to their flexible Ag-pocket binding site (Notkins, 2004; Zhou et al., 2007), NAs are capable of binding diverse microbial determinants, autoantigens, and tumor Ags (Vollmers and Brandlein, 2009). Therefore, NAs protect the host by favoring early opsonization of pathogens and cellular debris (Casali and Schettino, 1996; Baumgarth et al., 2005). Since *Gclc*-deficient mice do not have MZB nor peritoneal B1 cells (Figures 11 and 15), we assessed the ability of *Gclc*$^{fl/fl}$ *Mb1-Cre*$^{+}$ and control animals to produce specific NAs in the BM and spleen, which are the main sites of spontaneous production (Choi et al., 2012; Savage et al., 2017). As expected, *Gclc*$^{fl/fl}$ *Mb1-Cre*$^{+}$ animals secreted lower IgM in both compartments (Figure 17 B).

Previous studies have concluded that B1 cells represent a heterogeneous population (Kantor et al., 1992; Baumgarth, 2016). Indeed, B1 cells can be generally subdivided into B1a and B1b subsets on the basis of the expression of CD5 (Hayakawa et al., 1983; Berland and Wortis, 2002). This distinction seems to be related to a division of labor where CD5^{+} B1a cells are responsible for NAs secretion and CD5^{-} B1b for IgM production upon TI Ag encounter (Martin et al., 2001; Haas et al., 2005; Haas et al., 2018). In our case, both B1

subpopulations were reduced in the absence of *Gclc* in the spleen and PEC (Figure 17 C). Accordingly, the absence of B1a cells correlate with a the decrease in serum NAs against PC (Figure 17 D, left), lower binding of PtC-containing liposomes (Figure 17 D, right) and natural polyreactive antibodies against double-strand (ds) DNA and Thy1 (ATA) (Figure 17 E); while the loss of B1b cells is linked to the inability to mount an anti-TNP-ficoll response (Figure 16 B).

The diminished seric titers where further investigated in relation to renal damage. Indeed, age-related renal deterioration is known to occur in mice and is characterized by sclerosis and albuminuria (Yumura et al., 1989). Furthermore, one sign of renal disease is the marked deposition of immunoglobulins and/or immunocomplexes in the glomeruli. *Gclc*$^{fl/fl}$ *Mb1-Cre*$^{+}$ mice showed low levels of seric immunoglobulins compared to control animals. Thus, we reasoned that mutant mice would not accumulated immunoglobulins upon aging. Threfore, in order to evaluate antibody-mediated damage of the kidney glomeruli, we stained kidneys sections of one year old mice for total IgG detection. As expected, the glomeruli of *Gclc*$^{fl/fl}$ *Mb1-Cre*$^{+}$ mice showed less antibody deposition as shown in Figure 17 A, in alignment with the our previous tests.

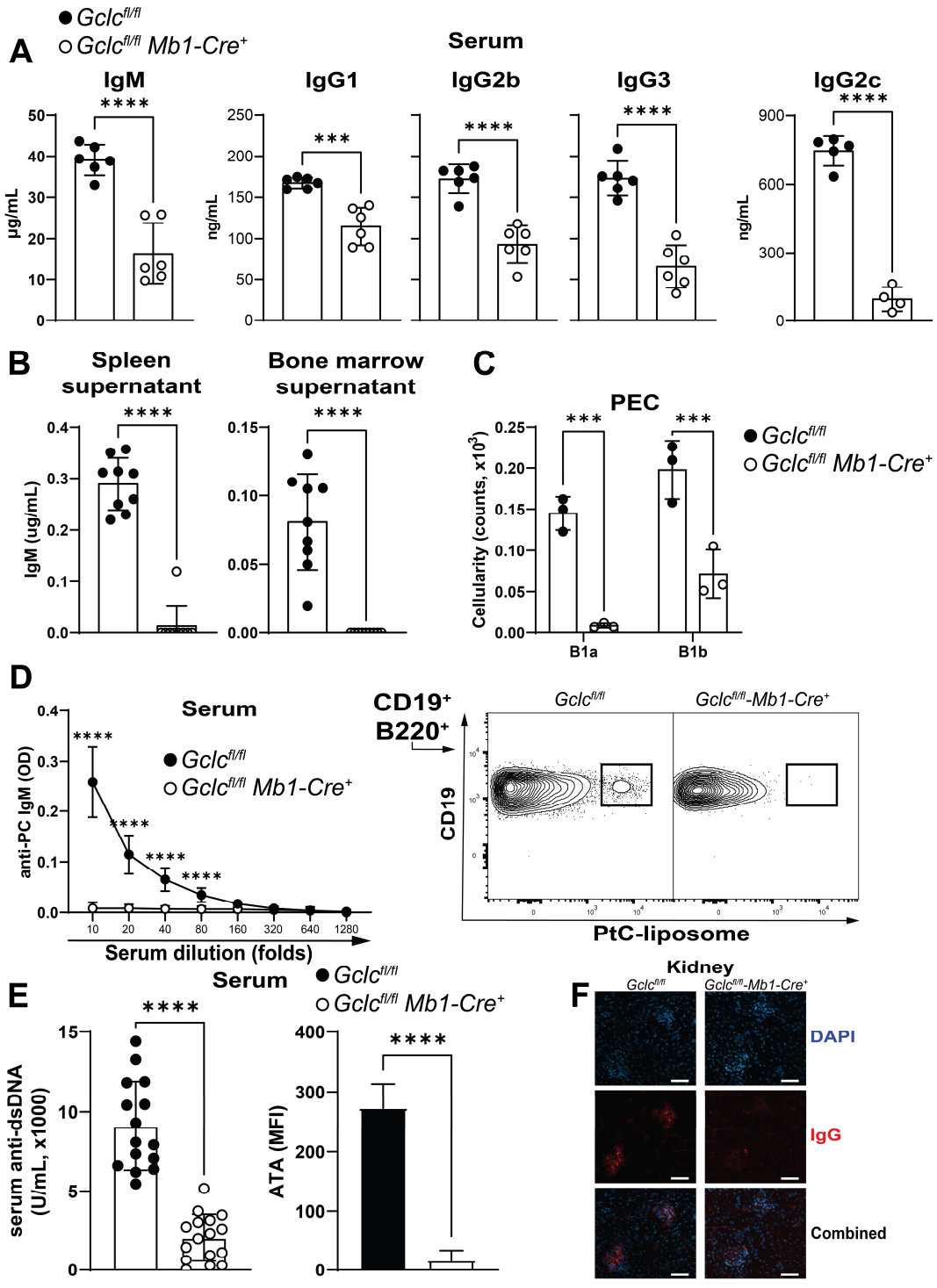

(Legend on next page)

Figure 17: Gclc-deficient mice are defective in Ab-mediated humoral immunity and autoreactive Abs.

A. Serum Ig measured by quantitative ELISA in *Gclc*$^{fl/fl}$ *Mb1-Cre*$^{+}$ and control mice. **B.** Spontaneous IgM production from spleen or BM quantified in the supernatants after 12h culture. **C.** Counts of PEC B1a and B1b cells from gates shown in Figure 15 A. **D.** Seric anti-PC IgM level measured by ELISA. Right: FACS plot of PtC-liposome binding on PEC B cells in *Gclc*$^{fl/fl}$ *Mb1-Cre*$^{+}$ and control mice. **E.** Serum levels of anti-dsDNA total Ig. Right: Anti-Thy-1 IgM detected with FACS on thymic cells, after incubation with serum from *Gclc*$^{fl/fl}$ *Mb1-Cre*$^{+}$ and control mice. **F.** Representative immunofluorescence staining of two renal glomeruli of 1 year old *Gclc*$^{fl/fl}$ *Mb1-Cre*$^{+}$ and control mice stained for total IgG deposition (red). Nuclei are stained for reference with DAPI (blue). Scale bars: 500 µm. For all applicable figure panels, data are mean ± SD and each dot represents one single mouse, except for C and E where each dot represents the mean of triplicates. Data shown in B and E are pooled from 3 independent experiments. Data shown are representative of ≥3 independent experiments with 3-4 mice/group. Significance (P) was calculated with unpaired t-test or one-way ANOVA (C and D). ***: $P \leq 0.001$; ****: $P \leq 0.0001$.

Chapter 4: Investigating the role of *Gclc* in the antibody response

4.1 Introduction

As discussed above, mature B cells either circulate through the bloodstream or reside in B cell follicles of secondary lymphoid organs, such as the spleen (Pieper et al., 2013). Here, B2 cells - and FoB in particular - reside in a naïve state until they encounter the Ag, and after receiving help by activated cognate T cells, they undergo GC reactions (Berek et al., 1991; MacLennan, 1994; Mesin et al., 2016).

Our analysis has shown that MZB and B1 cells were scarce upon *Gclc* deletion (Figure 11 and 15) and, therefore, their antibody-mediated immunity was non-functional (Figure 16 and 17). However, FoB were only mildly affected by the deletion of *Gclc* (Figure 11 D and E). Therefore, we conducted a series of experiments aiming at the analysis of B cell activation during and after the GC reaction. In particular, we deployed established *in vivo* models that mimic TD responses (Hangartner et al., 2006; Burbage et al., 2018) to study GC dynamics, PC generation, Ab production and Ag persistence over time.

This chapter describes the effect of *Gclc* deletion upon T-cell mediated activation of B cells in response to chronic and acute activation models. The data presented here indicate that the absence of *Gclc* causes inefficient GC formation, leading to a lack of Ab production in B cell-specific *Gclc*-depleted mice and impaired humoral immunity.

4.2 Objective

To investigate how *Gclc*-deficient FoB react against TD stimulation *in vivo*. Particularly, we investigated the GC formation, monitored PC formation and Ab production.

4.3 Results

4.3.1 *Gclc* is required for the germinal center reaction in TD responses

We have shown that the absence of *Gclc* in B cells caused a drastic perturbation in innate-like B cell homeostasis and functions. We first measured the levels of *Gclc* transcripts in C57BL/6 (B6) FoB activated *in vitro* with anti-IgM, CD40 ligand and IL-4. We observed a sharp increase in *Gclc* mRNA after 24 hr (Figure 18 A), indicating that FoB activation is associated with *Gclc* upregulation. Concurrently, *in vitro* activated B6 FoB increased intracellular thiols (of which the most abundant is represented by GSH) as shown by monochlorobimane (MBB) staining (Cossarizza et al., 2009), but also total and mitochondrial ROS (Figure 18 A). These data suggest that activation of FoB upregulated GSH expression and it is associated to a ROS burst. To further dissect immune responses in *Gclc*-deficient B cells, we immunized $Gclc^{fl/fl}$ $Mb1\text{-}Cre^{+}$ and control mice with the hapten TNP conjugated to the keyhole limpet hemocyanin (KLH) in alum, a model of T cell-dependent (TD) antigenic stimulation. We then measured the titers of TNP-specific antibodies in the serum and found that titer kinetics of the early (IgM) and late (IgGs) isotypes were reduced in $Gclc^{fl/fl}$ $Mb1\text{-}Cre^{+}$ mice (Figure 18 B).

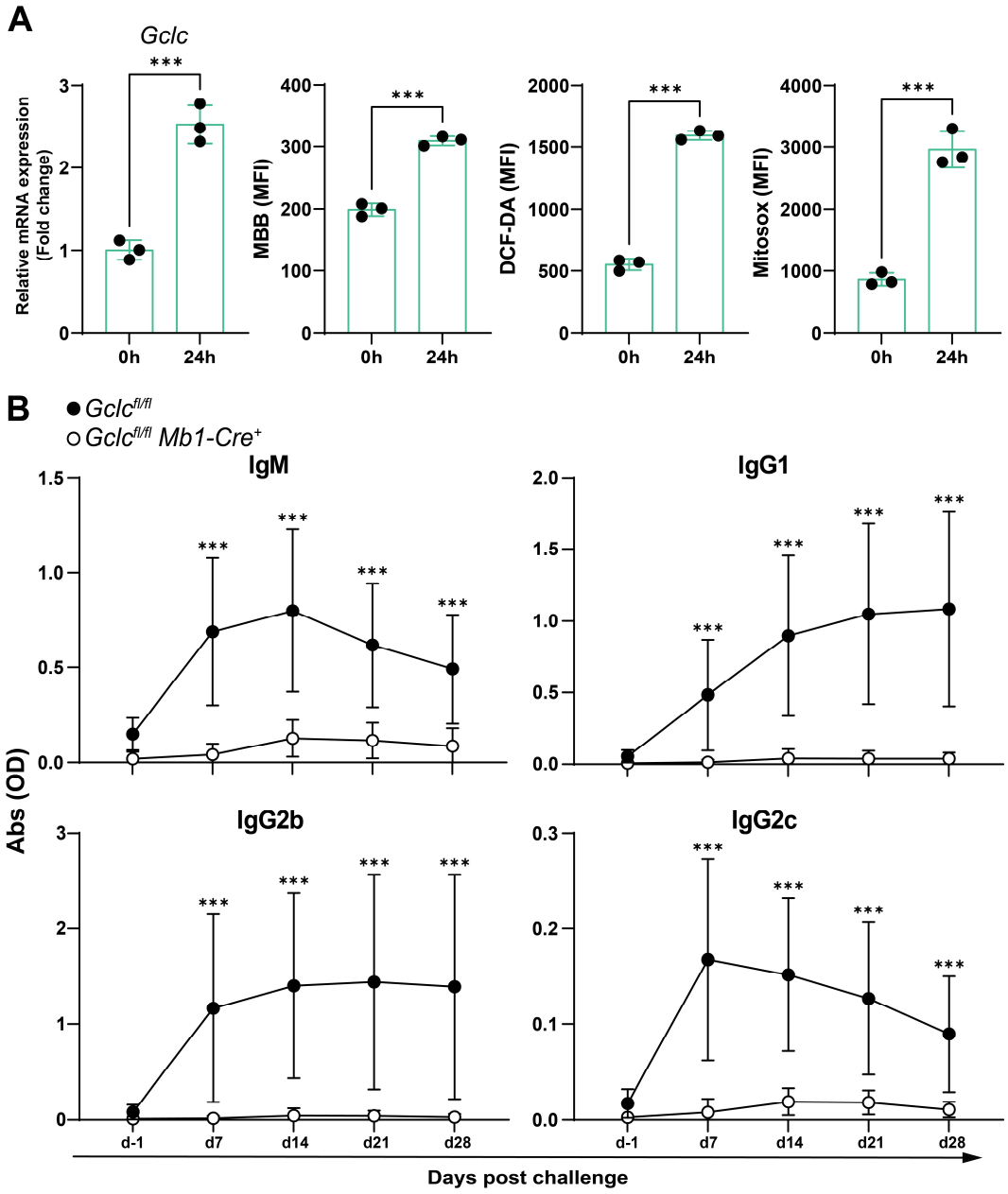

Figure 18: Gclc-deficient mice show a defective humoral response to TNP-KLH immunization.

A. mRNA levels measured by RT-qPCR of *Gclc* mRNA, MFI of MBB, DC-FDA, MitoSOX of B6 FoB at 0 or 24h after activation *in vitro* with anti-IgM, CD40 ligand and IL-4. **B.** Levels of NP-specific IgM, IgG1, IgG2b and IgG2c measured by ELISA from serum collected at the indicated time points from *Gclc*$^{fl/fl}$ *Mb1-Cre*$^{+}$ and control mice that were immunized with TNP-KLH. Data are mean ± SD and each dot represents one single mouse in A. In B, each dot represents the mean of 3-6 mice. Data shown are representative of ≥2 independent experiments with 3-6 mice/group. Significance (P) was calculated with unpaired t-test or one-way ANOVA (B). ***: $P \leq 0.001$.

To further dissect the B cell response in the *Gclc*-deficient context, we used a more physiological model of persistent viral infection and immunized *Gclc*$^{fl/fl}$ *Mb1-Cre*$^{+}$ and control animals with lymphocytic choriomeningitis virus Clone 13 (LCMV Cl13) (Matloubian et al., 1990; Matloubian et al., 1993; Sullivan et al., 2011; McIlwain et al., 2015). We monitored LCMV Cl13-specific Abs against Gp1 by ELISA over time (Recher et al., 2004) and confirmed that both the early IgM and late IgG responses were not detected in the serum of infected *Gclc*-deficient mice compared to control (Figure 19 A). Sustained IgG production is facilitated by long-lived IgG-producing plasma cells typically residing in the BM (Slifka et al., 1998). Therefore, we measured the quantity of LCMV-specific IgG antibody-secreting cells (ASCs) present in both the spleen and BM at 12 and 50 days post infection (p.i.). As shown in Figure 19 B, *Gclc*-deficient mice possessed only minimal quantities of LCMV-specific IgG ASCs in the spleen and BM compared to control mice, consistent with the inability to sustain antibody production upon viral infection (Figure 19 A). Accordingly, the viremia in *Gclc*$^{fl/fl}$ *Mb1-Cre*$^{+}$ animals was still elevated at later time points in the liver and all the organs sampled (Figure 19 C), suggesting that *Gclc*$^{fl/fl}$ *Mb1-Cre*$^{+}$ animals could not efficiently control the viral infection through the Ab response.

The lack of LCMV-specific Abs could be due to either a failure of the GC reaction or a defect in Ab production. Even though LCMV infections induce GC reactions, the immune response to LCMV Cl13 is uniquely associated to rapid clonal exhaustion of the T cell response and viral persistence (Ahmed et al., 1984; Borrow et al., 1995; Sullivan et al., 2011). However, when we compared B cells in the GC by flow cytometry 12 days p.i., we found decreased CD95^{+}GL-7^{+} GC B cells in *Gclc*$^{fl/fl}$ *Mb1-Cre*$^{+}$ animals (Figure 19 D). These data imply that the absence of *Gclc* prevent B cells to establish GC reactions.

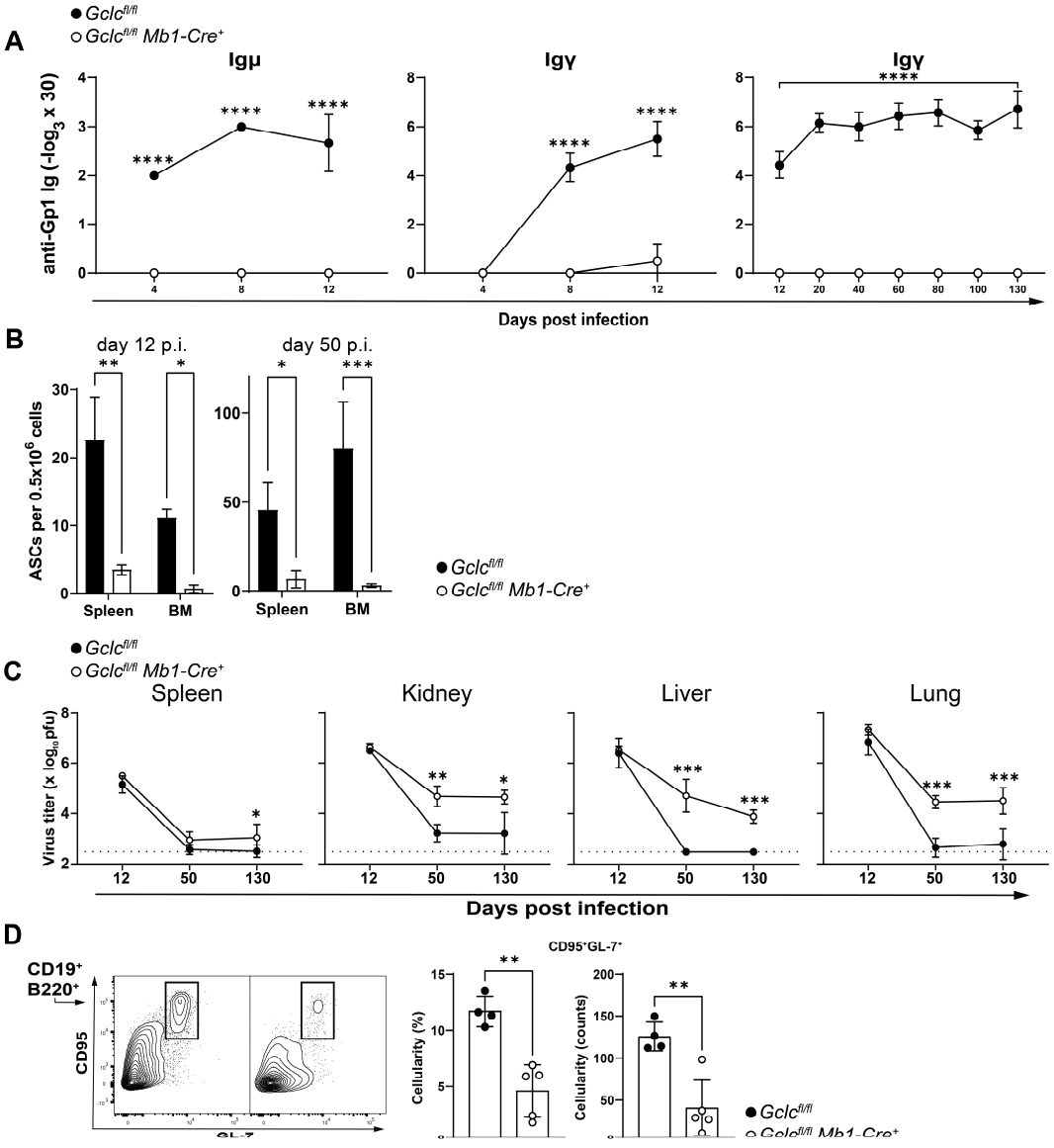

Figure 19: Gclc-deficient mice do not mount an effective antiviral immune response.

A. Serum anti-LCMV GP1 IgM (μ) or G (γ) measured at early and late time points by qualitative ELISA in *Gclc$^{fl/fl}$ Mb1-Cre^{+}* and control mice in response to LCMV Cl13 infection. **B.** LCMV-specific antibody secreting cells (ASCs) in spleen or BM were counted on day 12 and 50 post infection (p.i.) by ELISPOT. **C.** LCMV Cl13 viral titers measured by plaque assay on the indicated organs at the indicated time points. **D.** FACS plot and summary statistics of percentages and counts of GC B cells in the spleen at 12 days post LCMV Cl13 infection. For all applicable figure panels, data are mean ± SD and each dot represents one single mouse, except for A and C where each dot represents the mean of 3-6 mice. Data shown are representative of ≥3 independent experiments with 3-6 mice/group. Significance (P) was calculated with one-way ANOVA or unpaired t-test (D). *: P ≤ 0.05; **: P ≤ 0.01***: P ≤ 0.001; ****: P ≤ 0.0001.

LCMV is a non- cytopathic virus and it is characterized by slow replication, which favors its persistence in the host due to an inefficient cytotoxic T cell response (Borrow et al., 1995; Sullivan et al., 2011). We further investigated the TD response of *Gclc*-depleted B cells in the context of an acute, T cell-driven model of cytopathic infection. Thus, we infected $Gclc^{fl/fl}$ $Mb1\text{-}Cre^{+}$ and control animals with vesicular stomatitis virus (VSV), which predominantly involves the antiviral activity of endogenously produced interferon and, subsequently, the generation of neutralizing IgG antibody to the VSV-G glycoprotein (Lefrancois, 1984; Vandepol et al., 1986). Survival was assessed and $Gclc^{fl/fl}$ $Mb1\text{-}Cre^{+}$ mice succumbed to the infection earlier compared to control animals (Figure 20 A). This effect was most likely due to the lack of neutralizing IgG Abs against VSV-G in *Gclc*-deficient hosts (Figure 20 B), which have been shown to be critical for the control of VSV infection (Lefrancois, 1984) and is consistent with the general lack of antibody response shown in Figures 18 and 19.

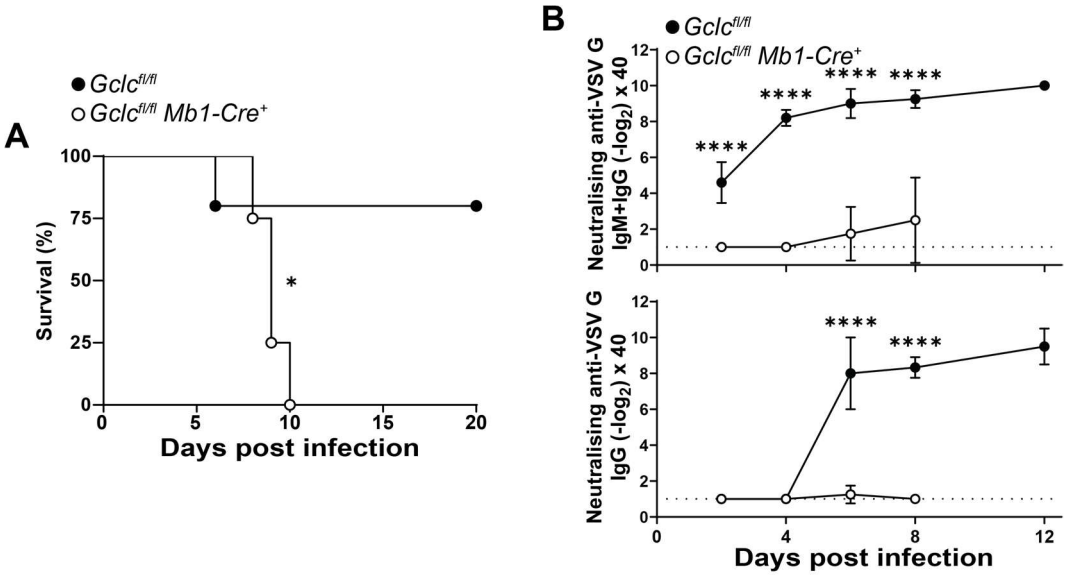

Figure 20: VSV infection is lethal for B cell-specific Gclc-deficient mice.

A. Survival plot of *Gclc*$^{fl/fl}$ *Mb1-Cre*$^{+}$ and control mice upon VSV infection. **B.** Neutralizing titers of total (top) and IgG (bottom) anti VSV G protein in the serum of VSV infected *Gclc*$^{fl/fl}$ *Mb1-Cre*$^{+}$ and control mice. Dotted line represent the lower limit of detection of the assay. For all applicable figure panels, data are mean ± SD and each dot represents the mean of 5-8 mice. Data shown are representative of ≥2 independent experiments with 3-6 mice/group.

Taken together, these results indicate that the expression of *Gclc* in B cells is crucial for their development and activation *in vivo*. Our data shows that innate-like B cell development is impaired in mice lacking *Gclc*, and so is the natural immune protection related to NAs production. Additionally, upon TD immunization, the absence of *Gclc* in FoB cells disrupts cell activation and GC reactions. Consequently, antibody production is not achieved and this causes the inability of $Gclc^{fl/fl}$ *Mb1-*Cre^{+} to control viral infections.

Chapter 5: Investigating the metabolic dependencies of Follicular B cells in relation to *Gclc*

5.1 Introduction

From a bioenergetic point of view, maintenance of immune cells carries a basal energetic consumption quota (Raberg et al., 2002). Clearly, the immune response to a pathogen would result in an increase of the net energetic cost (Kominsky et al., 2010). In the case of B cells, changes initiated by antigen recognition such as proliferation and differentiation, followed by population contraction and eventually the generation of memory, require a sustained energy supply that matches the fluctuating cellular needs at the different stages (Franchina et al., 2018b) (Figure 9). Furthermore, several studies showed that, rather than simply being involved in biosynthesis, metabolic regulators such as the myelocytomatosis virus oncogene cellular homolog (Myc), hypoxia-inducible factor 1-a (HIF-1a), mechanistic target of rapamycin (mTOR), and the glycogen synthase kinase 3 (Gsk3) can regulate the immune response (Wahl et al., 2012; O'Neill and Pearce, 2016; Jellusova et al., 2017).

We have only recently begun to appreciate the extent to which immune cell activation requires metabolic reprogramming. In particular, intrinsic metabolic pathways self-regulate the supply of energy for every immune function (O'Neill et al., 2016). The scope of these cellular processes is to catalyze the synthesis of adenosine triphosphate (ATP), which represents the energy-carrying molecule (Bonora et al., 2012). Glucose and O_2 take part in a chemical reaction chain, which eventually leads to ATP. This reaction is called aerobic respiration and includes glycolysis, the tricarboxylic acid (TCA) cycle and electron transport chain/oxidative phosphorylation (ETC/OXPHOS) relay (Bonora et al., 2012).

Aerobic respiration has a theoretical yield of 36 ATP molecules per molecule of glucose. In particular, glycolysis (which takes place in the cytosol) and the TCA cycle contributes 2 molecules of ATP each. Both TCA and ETC/OXPHOS are confined to the mitochondria and latter make up most of the remaining ATP. Here, high-energy electrons traverse downhill the ETC in a series of exergonic redox reactions, which create the chemiosmotic proton gradient that ultimately produces ATP in the OXPHOS reaction catalyzed by the ATP synthase (Morelli et al., 2019).

This whole process capitalizes on the strong driving force for O_2 reduction (Babcock, 1999). However, O_2 reduction is imperfect and often leads to the incomplete reduction of O_2 molecules, which are collectively termed ROS (Sena and Chandel, 2012). Physiological ROS have a central role in redox signaling via different post-translational modifications, denoted as ‘oxidative eustress’, yet elevated ROS lead to molecular damage or ‘oxidative distress’ (Reczek and Chandel, 2015; Sies and Jones, 2020).

Whilst it has been reported that GSH controls ROS-dependent engagement of metabolic signaling pathways that lead to protective T cell responses (Mak et al., 2017), it has not been established whether the GSH/ROS balance influences the metabolic reprogramming of B cells. Given the pleiotropic function of metabolic ROS in the cell, we sought to analyse the metabolic capacity of FoB in relation to the absence of the GSH. We determined intracellular ROS composition in FoB and studied how the GSH/ROS imbalance affects glycolysis, the ETC, OXPHOS and other metabolic properties.

5.2 Objective

To determine how the absence of GSH contributes to the metabolic dependencies of FoB.

5.3 Results

5.3.1 Wild type Follicular and Marginal Zone B cells show distinct GSH-dependent redox characteristics

B cell distribution in *Gclc*$^{fl/fl}$ *Mb1-Cre*$^{+}$ mice spleen has shown a drastic decrease in MZB compared to FoB (Figure 11). In a similar fashion, we found limited frequencies of B1 cells in the PEC (Figure 15). Given that GSH production is bound to *Gclc*-dependent catalysis, and that GSH is the master intracellular ROS antagonist, we reasoned that ROS contribution could play a distinct role in different B cell subsets. Then, we characterized ROS in FoB, MZB and peritoneal B1 cells from wild type mice with flow cytometry. Generally, in flow cytometry we can approximate a linear relationship between number of fluorochrome-conjugated antibodies or fluorescent dies on a cell and the calculated fluorescence value for that cell (Cossarizza et al., 2019). It is well known that MZB are larger in size than FoB (Oliver et al., 1997), as also confirmed in Figure 21 A. Therefore, in order to exclude the autofluorescence signal derived from the increased volume of MZB, and therefore control for the size bias of MZB, we performed a pre-gating in all the flow cytometric analyses based on the forward scatter signal area (FSC-A) of FoB to as indicated in Figure 21 A.

To measure cellular ROS, we used MitoSOX and DCFDA. Both signals derived from the MitoSOX dye, which stains the most proximal mitochondrial ROS superoxide ($O_2^{\cdot -}$) (Murphy, 2009) and DCFDA (which is an indicator of H_2O_2) were significantly higher in MZB than FoB cells (Figure 21 B). Interestingly, MZB have a significantly lower GSH/GSSH ratio (Figure 21 C, left) and express higher levels of the *Gclc* transcript at the steady state compared to FoB (Figure 21 C, right). When we compared peritoneal B1 vs. B2 cells, we found a similar trend (Figure 21 D). The higher amount of ROS of MZB and

B1 cells can be owed to their constitutive partial activation and, therefore signaling through their BCR signaling, which is inherently coupled to ROS generation (Tsubata, 2020).

In MZB, the lower GSH/GSSG ratio might indicate that GSH may be used to counteract the higher $O_2^{\cdot -}$ generation within mitochondria. These differences highlight the differential requirements for *Gclc* expression in MZB vs. FoB and might explain the phenotype of *Gclc*$^{fl/fl}$ *Mb1-Cre*$^{+}$ mice at the steady state (Figure 11 and 15).

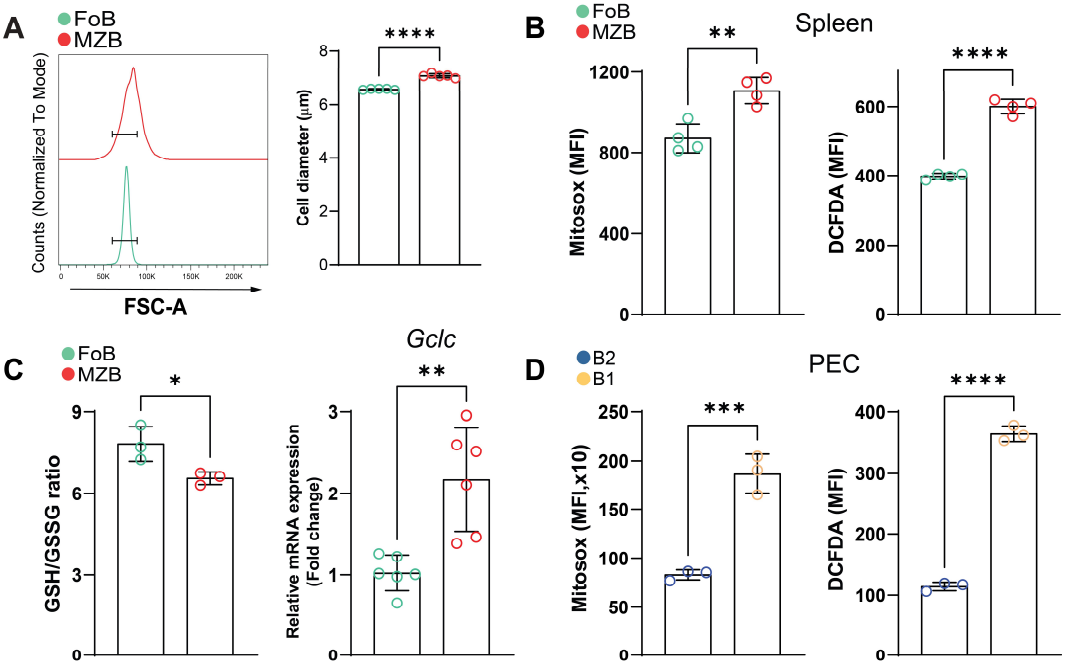

Figure 21: Wild type MZB express higher basal level of Gclc compared to FoB and show distinct ROS levels together with B1 cells.

A. Left: representative histogram of forward scatter area (FSC-A) signal of B6 FoB and MZB (gated as in Figure 11 D). Right: mean diameter (µM) of enriched B6 FoB and MZB using the CASY cell counter. **B.** MFI of ROS indicator dyes on FoB and MZB (gated as in Figure 11 D) in the spleen of B6 mice. **C.** GSH/GSSG ratio measured in sorted wild-type FoB and MZB (left) and fold change mRNA level of *Gclc* in sorted B6 FoB and MZB (right). **D.** MFI of ROS indicator dyes on B1 cells from in the PEC of B6 mice. For all applicable figure panels, data are mean ± SD and each dot represents one single mouse. Data shown are representative of ≥2 independent experiments with 3-6 mice/group. Significance (P) was calculated with unpaired t-test. *: $P \leq 0.05$; **: $P \leq 0.01$; ***: $P \leq 0.001$; ****: $P \leq 0.0001$.

5.3.2 GSH-deficient Follicular B cells upregulate glycolysis

The production of the proximal mitochondrial ROS, $O_2^{\cdot-}$, in the mitochondrial matrix derives from the core metabolic machinery present in the mitochondrial inner membrane and matrix during electron transfer (*i.e.* ETC). Since *Gclc*$^{fl/fl}$ *Mb1-Cre*$^{+}$ mice lack MZB, we reasoned that GSH might exert a protective role in the mitochondria, or that the antioxidant properties of GSH regulate mitochondrial functions in MZB. Since the ETC is directly coupled to OXPHOS for the production of ATP in the mitochondria (Hatefi, 1985), we measured total ATP levels in sorted *Gclc*-deficient FoB and detected higher ATP in the mutant cells (Figure 22 A).

Accumulation of ATP is linked with apoptotic cell death (Zamaraeva et al., 2005) and, in our case, the rise in ATP could be an indicator of death in *Gclc*-deficient FoB. However, we detected no changes in the binding of annexin V in total splenic B cells (Figure 22 B) nor in the activation of Caspase 3 in splenic FoB (Figure 22 C), which can be used as indicator of apoptosis. A second possibility is that the increase in the ATP pool is caused by augmented metabolic output and could be due to higher rates of glycolysis, TCA cycle and/or OXPHOS.

To investigate this further, we evaluated glucose uptake and detected a higher glucose uptake with the glucose analog (2-(N-(7-Nitrobenz-2-oxa-1,3-diazol-4-yl)Amino)-2-Deoxyglucose) (2-NBDG) (Zou et al., 2005) (Figure 22 D), along with a small but significant increase of the high-affinity surface glucose transporter Glut-1 (Figure 22 E) in *Gclc*-deficient FoB compared to control cells, which also accumulated intracellularly (Figure 22 F). Furthermore, by feeding FoB with 11mM ^{13}C-glucose we quantified the remaining labelled glucose in the medium after 5h of activation with anti-IgM, CD40

ligand and IL-4. As shown in Figure 22 G, *Gclc*-deficient FoB took up more glucose upon activation *in vitro*.

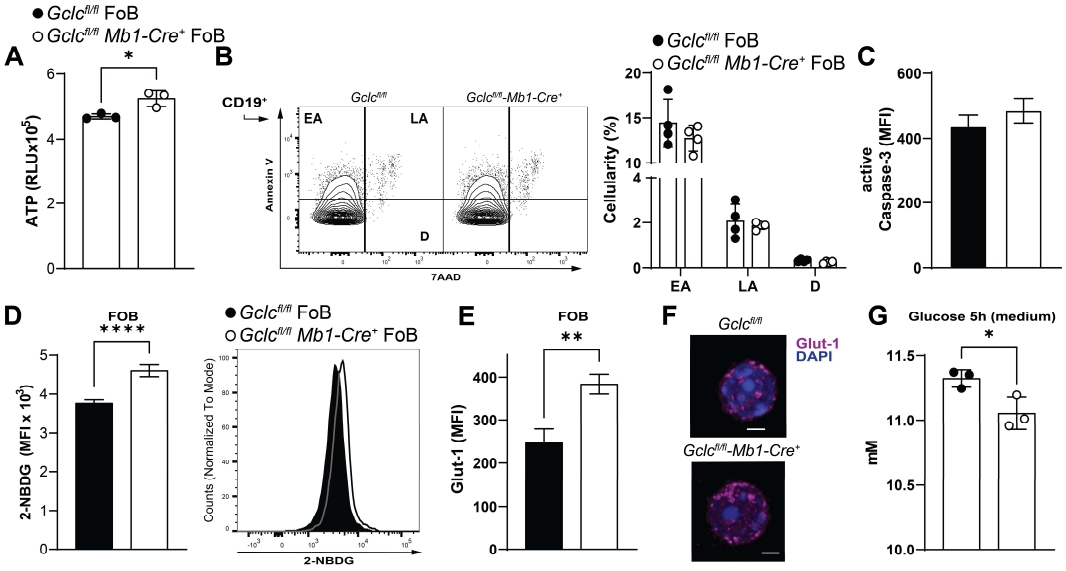

Figure 22: Gclc-deficient FoB accumulate more ATP and increase the uptake of glucose.

A. ATP levels measured in sorted FoB from *Gclc*$^{fl/fl}$ *Mb1-Cre*$^{+}$ and control mice. **B.** Gating strategy for the apoptotic test of B cells at the steady state in the spleen. Left: summary statistics of percentages of early apoptotic (EA), late apoptotic (LA) and dead (D) splenic B cells. **C.** Expression level (MFI) of active Caspase3 in splenic FoB (gated as in Figure 11 D). **D.** Glucose analogue (2-NBDG) uptake assay in FoB cells from *Gclc*$^{fl/fl}$ *Mb1-Cre*$^{+}$ and control mice (left) and a representative FACS histogram (right). **E.** Glucose transporter (Glut-1) surface expression (MFI) in splenic FoB (gated as in Figure 11 D). **F.** Representative confocal microscopy image of one cell from *Gclc*$^{fl/fl}$ *Mb1-Cre*$^{+}$ and control mice showing intracellular Glut-1 (purple). Scale bars: 2 µm. **G.** Quantification (mM) of labelled ^{13}C-glucose from the medium of 5h activated FoB. For all applicable figure panels, data are mean ± SD and each dot represents one single mouse. Data shown are representative of ≥2 independent experiments with 3-6 mice/group. Significance (P) was calculated with unpaired t-test or one-way ANOVA (B). *: $P \leq 0.05$; **: $P \leq 0.01$; ****: $P \leq 0.0001$.

Once glucose is internalized, it feeds into catabolic pathways to produce ATP (Locasale and Cantley, 2011). Therefore, we sought to determine the fate of glucose (*i.e.* glycolysis and TCA) in FoB from *Gclc*$^{fl/fl}$ *Mb1-Cre*$^{+}$ mice. To this extent, we *in vitro* activated FoB cells for short time (5h) to avoid bias due to proliferation and cell cycle, and incubated the cells with ^{13}C-labeled glucose concomitantly (Figure 23 A). As shown in Figure 23, glucose tracing revealed that the internalized glucose funnels into glycolytic intermediates. Indeed, we detected higher M3-3-Phosphoglyceric acid (3PG) flux (Figure 23 B) and M3-lactate (Figure 23 C, left). Moreover, lactate accumulation was also confirmed by direct measurement from the supernatant after 5h stimulation (Figure 23 C, right). This finding is in line with our previous quantification of total glucose in the supernatant of 5h activated FoB, which decreased in the medium of *Gclc*-deficient cells (i.e. increased cellular uptake) (Figure 22 G). Given the higher fluxes into glycolytic intermediates and the increased secretion of lactate upon activation, we sought to determine whether the glycolytic-derived ATP would be increased in *Gclc*-deficient FoB. Seahorse-based analysis showed that mutant FoB produce more glycolysis-linked ATP (Figure 23 D). Overall, these results indicate that the absence of *Gclc* upregulates glucose uptake in FoB, which is used in the glycolytic pathway to produce ATP.

Once glucose is metabolized through the glycolytic pathway, 2 molecules of pyruvate are produced and converted into Acetyl CoA, which feeds the enzyme citrate synthase together with oxaloacetate (Lunt and Vander Heiden, 2011) (Figure 23 A). This enzyme catalyzes the first step of the TCA cycle to form citrate. Glucose contribution to M2-citrate was decreased in *Gclc*-deficient FoB compared to control cells (Figure 23 E). Accordingly, this suggests that most of the glucose is used up during glycolysis and does not enter the TCA, as shown by the ratio M3-lactate/M2-citrate (Figure 23 F).

In line, we found that ATP levels in *Gclc*-deficient FoB dropped in a dose-dependent fashion in response to the addition of the glycolysis inhibitor 2-deoxy-D-glucose (2-DG), which was less pronounced in *Gclc*-sufficient FoB (Figure 23 G). In parallel, 2-DG increased cell death in *Gclc*-deficient FoB cultures compared to controls (Figure 23 H), confirming the dependency of GSH-deficient FoB on glycolysis.

Taken together, our data indicate that the altered ROS balance triggered by *Gclc* deletion induces upregulation of and dependency on glycolytic metabolism. This observation implies the existence of a regulatory function for GSH in the context of energy metabolism shifts in B cells.

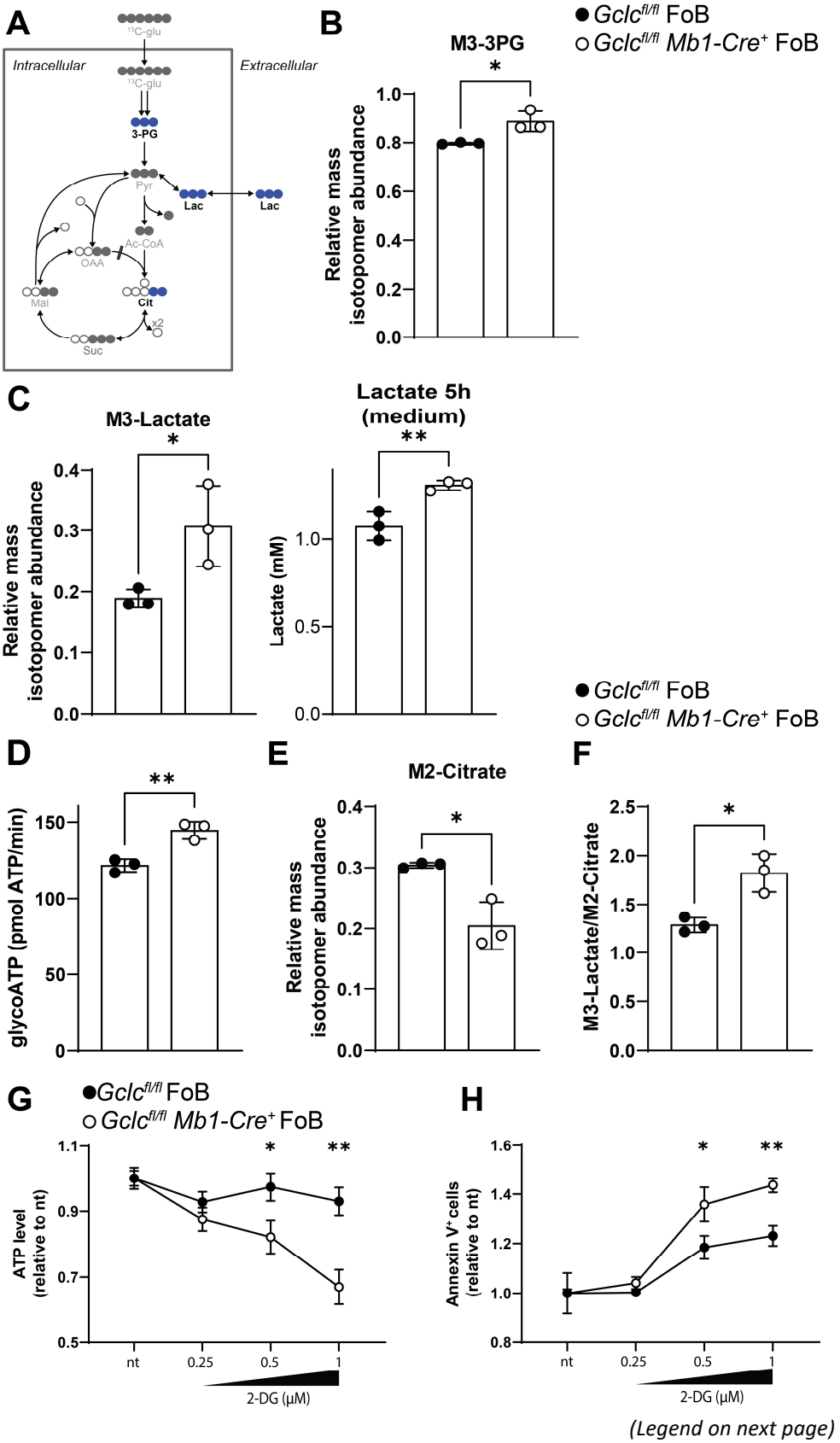

(Legend on next page)

Figure 23: Gclc-deficient FoB have higher basal glycolysis and leads to increased ATP production.

A. Carbon racing map of ^{13}C-glucose metabolism. Blue: metabolites measured in panels B, C, D. **B.** MIDs plots of ^{13}C-glucose-derived M3-3PG upon 5h activation of FoB with anti-IgM, CD40 ligand and IL-4. **C.** Glucose-derived M3-lactate (left) and total lactate quantification (right) from 5h activated FoB cells and medium respectively. **D.** Seahorse quantification of glycolysis-derived ATP in resting *Gclc$^{fl/fl}$* and *Gclc$^{fl/fl}$ Mb1-Cre^{+}* FoB. **E.** ^{13}C-glucose-derived M2-citrate contribution in *Gclc$^{fl/fl}$* and *Gclc$^{fl/fl}$ Mb1-Cre^{+}* FoB that were incubated with ^{13}C-glucose and assayed at 5h post-activation. **F.** Ratio of M3-lactate/M2-citrate in *Gclc$^{fl/fl}$* and *Gclc$^{fl/fl}$ Mb1-Cre^{+}* FoB that were incubated with ^{13}C-glucose and assayed at 5h post-activation. **G.** ATP levels (RLU, normalized to nt), and **H.** percentage of Annexin V-expressing cells, in *Gclc$^{fl/fl}$* and *Gclc$^{fl/fl}$ Mb1-Cre^{+}* FoB after 5h incubation with the indicated concentrations of 2-DG. For all applicable figure panels, data are mean ± SD and each dot represents one single mouse except for G and H where data are mean of 3-6 measurements. Data shown are representative of ≥2 independent experiments with 3-6 mice/group. Significance (P) was calculated with unpaired t-test or one-way ANOVA (G, H). *: $P \leq 0.05$; **: $P \leq 0.01$. 3-PG, 3-phospohglyceric acid; Lac, lactate; Pyr, pyruvate; AcCoA, acetyl-CoA; Cit, citrate; Suc, succinate; Mal, malate; OAA, oxaloacetate; nt, non-treated.

5.3.3 Absence of *Gclc* alters the mitochondrial morphology and ATP production in Follicular B cells

Deficiency in the antioxidant capacity led to an alteration of the glucose fluxes in FoB. In particular, we detected higher basal glycolytic ATP and contribution of glucose to glycolytic intermediates (Figure 23). Therefore, we suspected an alteration of the processes downstream glycolysis, such as the TCA cycle, which takes place in the matrix of the mitochondria.

Mitochondria are double-membrane organelles that possess their own double-stranded DNA genome. The outer membrane covers the organelle and contains pore with generally high permeability while the inner membrane hosts the respiratory chain (ETC) and a plethora of protein carriers specialized in the transport of anionic intermediates of metabolism (Ernster and Schatz, 1981). These two membranes create two distinct mitochondrial regions: the matrix and the intermembrane space. The former is surrounded by the inner membrane and represents the major active compartment of mitochondria. The latter is small interstice between the mitochondrial membranes and communicates with the cytosol (Friedman and Nunnari, 2014).

To investigate the effect of the absence of GSH and its effect on the metabolism of FoB cells downstream the glycolytic pathway, we assessed mitochondria size and conformation. Staining for the mitochondrial import receptor Tom20 in sorted FoB showed an increased area of mitochondria per cell in FoB cells lacking *Gclc* (Figure 24 A). As briefly mentioned, mitochondria possess their own DNA (mtDNA), which encodes genes mainly related to the ETC and OXPHOS systems (Bibb et al., 1981). Quantification of the mtDNA is a good marker of the amount of mitochondrial mass, relative to the abundance of nuclear DNA (nDNA) (Quiros et al., 2017). Lower mtDNA/nDNA ratio in *Gclc*-deficient FoB (Figure

24 B) suggest that the absence of GSH induced an increase in mitochondrial mass without influencing mtDNA replication, a property of activated B cells (Waters et al., 2018).

To gain more resolution and information on the mitochondrial inner space, we analyzed FoB with transmission electron microscopy (TEM). These images confirmed the accumulation of mitochondria in the cytoplasm of *Gclc*-deficient FoB (Figure 24 C). Moreover, *Gclc*-deficient mitochondria were characterized by disorganized intercristal space (Figure 24 C, insert). These data imply that loss of *Gclc* alters mitochondrial structure and metabolism.

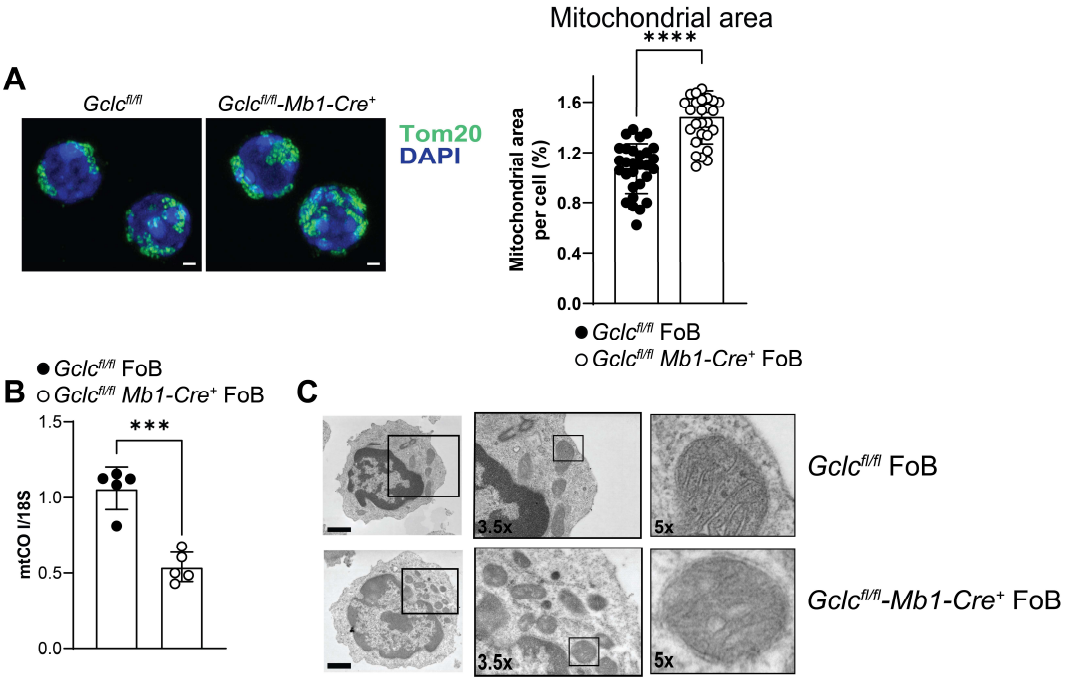

Figure 24: Gclc-deficient FoB accumulate mitochondria with loose cristae.

A. Representative confocal microscopy images of two FoB from *Gclc*$^{fl/fl}$ *Mb1-Cre*$^{+}$ and control mice. Mitochondria are detected with Tom20 (green) and nuclei with DAPI (blue). Scale bars: 1µm. Right: quantification of mitochondrial area percentage of Tom20 signal compared to DAPI. **B.** Mitochondrial-to-nuclear DNA ratio derived from the expression of mtCOI and the ribosomal RNA 18S. **C.** Representative TEM image of ultrastructural mitochondrial morphology in *Gclc*$^{fl/fl}$ and *Gclc*$^{fl/fl}$ *Mb1-Cre*$^{+}$ FoB. Scale bars: 700nm. Insert digital magnification, 3.5 and 5x. For all applicable figure panels, data are mean ± SD and each dot represents one single mouse. Data shown are representative of ≥2 independent experiments with 3-5 mice/group. Significance (P) was calculated with unpaired t-test. *: $P \leq 0.05$; **: $P \leq 0.01$.

To gain more insight into the effect of GSH paucity on mitochondria, we used MitoTracker (MT) green and MT deep red FM staining to assess mitochondrial membrane potential ($\Delta\Psi_m$) with flow cytometry (Monteiro et al., 2020; Di Gioia et al., 2020). We found that *Gclc* deficiency increased $\Delta\Psi_m$ in mutant FoB compared to controls (Figure 25 A). Of note, loose mitochondrial cristae have been associated with poor electron transport chain (ETC) efficiency in T cells (Buck et al., 2016). ATP production and TCA cycle are dependent on the ETC machinery, which accounts for the $\Delta\Psi_m$. Moreover, the $\Delta\Psi_m$ is the motive force necessary to fuel OXPHOS in the process of ATP generation and O_2 consumption. In line, we found that mitochondria-derived ATP production was decreased in *Gclc*-deficient FoB (Figure 25 B).

Therefore, we speculated that the impairment of mitochondrial metabolism in FoB might be the cause of increased glycolysis for ATP production. Indeed, the data presented here indicate that the altered ROS balance triggered by *Gclc* deletion induces mitochondrial fragmentation in FoB and impaired supply of ATP, which leads to compensation through upregulation of glycolytic metabolism. This observation implies the existence of a regulatory function for GSH in the context of metabolic pathway usage in B cells.

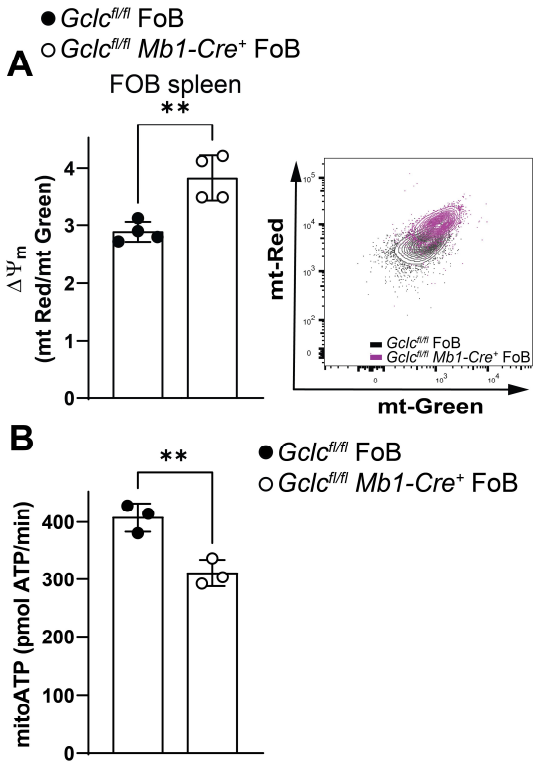

Figure 25: Mitochondrial metabolic function and potential in FoB are altered in the absence of Gclc.

A. Mitochondrial membrane potential ($\Delta\Psi_m$) calculated from the mitotracker Red/ mitotracker Green MFI ratio in splenic FoB (gated as in Figure 11 D). Right: representative contour plot of the mitotracker Red/ mitotracker Green signal in splenic FoB. **B.** Quantification of mitochondria-derived ATP (Seahorse assay) from freshly enriched and resting *Gclc*$^{fl/fl}$ and *Gclc*$^{fl/fl}$ *Mb1-Cre*$^{+}$ FoB. For all applicable figure panels, data are mean ± SD and each dot represents one single mouse. Data shown are representative of ≥3 independent experiments with 3-4 mice/group. Significance (P) was calculated with unpaired t-test. **: $P \leq 0.01$.

5.3.4 Mitochondrial respiratory parameters are compromised in GSH-deficient Follicular B cells

Our preliminary analysis showed that lack of GSH caused a general dysfunction of FoB metabolism, with a specific increase in glycolysis (Figure 23), and alteration of mitochondrial function (Figure 24 and 25). In particular, we detected a higher flux of glucose into the glycolytic pathway rather than the TCA cycle upon *in vitro* activation (Figure 23 F). The mitochondrial matrix hosts the TCA cycle, which consists of a series of iterative reactions catalyzed by several enzymes (Krebs, 1936; Krebs et al., 1938). Importantly, some of the TCA enzymes are components of the ETC and are embedded in the inner mitochondrial matrix (Hatefi, 1985) (Figure 26 A).

Interestingly, in our tracing results, we found that labelled M2-succinate accumulated to much higher levels in mutant cells than in $Gclc^{fl/fl}$ FoB (Figure 26 B). Within the TCA cycle, succinate is converted into fumarate by the succinate dehydrogenase (SDH), which represents the respiratory complex II (CII) of the ETC (Martinez-Reyes and Chandel, 2020) (Figure 26 A). Because SDH is the only enzyme that participates in both the TCA cycle and the ETC, we speculated that the ETC might be compromised in *Gclc*-deficient FoB. Indeed, the basal oxygen consumption rate (OCR) of *Gclc*-deficient FoB measured by extracellular flux analysis was significantly reduced compared to $Gclc^{fl/fl}$ FoB (Figure 26 C and D), indicating that loss of GSH results in dysfunctional mitochondrial respiration in FoB at steady-state. However, no difference in the OCR profiles of mutant and control FoB was detected upon treatment with oligomycin A (Oligo) (Figure 26 C and E) which inhibits the ATP synthase, and thus, indicate that ADP phosphorylation capacity in the absence of GSH is unchanged. Interestingly, the most striking respiratory difference attributable to loss of GSH emerged upon treatment of $Gclc^{fl/fl}$ and $Gclc^{fl/fl}$ *Mb1-Cre*$^{+}$ FoB with the mitochondrial ionophore FCCP (Figure 26 C and F), which increases the OCR to the

maximal respiration (*i.e.* reserve capacity) that the cells can sustain (Little et al., 2020). Upon FCCP treatment, the ETC activity rate increases in the attempt to restore the proton gradient and re-couples it to OXPHOS. We found that an absence of *Gclc* in FoB prevented this FCCP-mediated uncoupling (Figure 26 C and F), suggesting that GSH promotes electron transport through the ETC in FoB.

Previous work has established that any residual OCR detected after Oligo treatment is due to non-respiratory oxygen consumption, which is usually ascribed to proton leakage through the mitochondrial inner membrane (Brand, 1990). We found that, despite the similar Oligo-dependent OCR profiles in $Gclc^{fl/fl}$ and $Gclc^{fl/fl}$ *Mb1-Cre*$^{+}$ FoB (Figure 26 C and E), the contributions to the maximal OCR value in each case by ATP-linked OCR**,** proton leakage, reserve capacity, and non-mitochondrial OCR were tremendously altered by *Gclc* deficiency (Figure 26 G). In particular, *Gclc*-deficient FoB experienced greater proton leakage (Figure 26 G and H) and accumulated higher mtROS (Figure 26 I). These findings suggest that GSH deficiency leads to damage of the mitochondrial membrane and/or ETC malfunction. In this regard, it is tempting to speculate that the accumulation of glucose-derived M2-succinate (the CII substrate in the TCA cycle) in GSH-deficient FoB (Figure 26 B) might be associated with the observed ETC insensitivity to FCCP treatment (Figure 26 C and F).

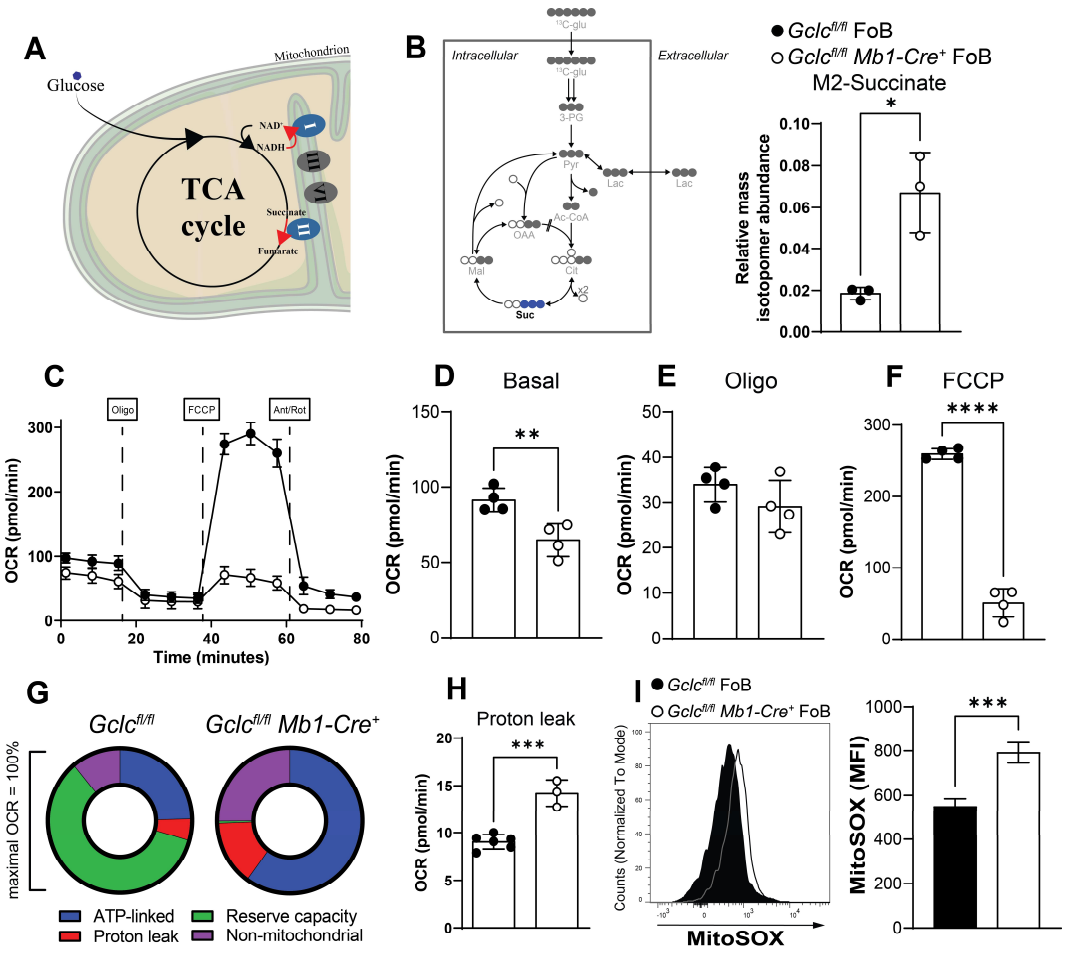

Figure 26: Gclc-deficient FoB show altered respiratory profile due to mitochondrial ROS accumulation.

A. Complex I and II (CI and CII) reactions (red arrows) contribute to the enzymatic series of the TCA cycle within the mitochondria. **B.** Left: carbon racing map of ^{13}C-glucose metabolism highlighting in blue succinate (Suc). Right: MID of M2-succinate in *Gclc*$^{fl/fl}$ and *Gclc*$^{fl/fl}$ *Mb1-Cre*$^{+}$ FoB at 5h post-activation determined as in Figure 23 A. **C.** Seahorse quantitation of OCR of resting *Gclc*$^{fl/fl}$ and *Gclc*$^{fl/fl}$ *Mb1-Cre*$^{+}$ FoB at the indicated time points. **D-F.** Quantitation of the OCR data from panel C at baseline (D) and upon treatment with Oligo (E) or FCCP (F). **G.** OCR components from panel C plotted as proportions of maximal OCR after FCCP treatment. **H.** Quantitation of the contribution of proton leakage from panel C as determined by Ant/Rot treatment. **I.** Representative histogram (left) and quantitation (right) of MitoSOX staining in resting *Gclc*$^{fl/fl}$ and *Gclc*$^{fl/fl}$ *Mb1-Cre*$^{+}$ FoB (gated as in Figure 21 A). For all applicable figure panels, data are mean ± SD and each dot represents one single mouse except in C where dots are mean of 3-6 measurements. Data shown are representative of ≥3 independent experiments with 3-6 mice/group. Significance (P) was calculated with unpaired t-test. *: $P \leq 0.05$; **: $P \leq 0.01$; ***: $P \leq 0.001$; ****: $P \leq 0.0001$.

Mitochondrial damage is often defined as a deviation of respiratory parameters, which were originally defined *in vitro* using isolated mitochondria (Chance and Williams, 1955a, b; Chance and Williams, 1956). However, these measurements can also be derived from whole cells (Figure 27 A). In particular, state 3 respiration is equivalent to the OCR after FCCP treatment (*i.e.* maximal respiration induced by the substrate + ADP), and state 4 corresponds to the rate upon Oligo addition (*i.e.* absence of substrate-dependent respiration) (Brown et al., 1990). These assumptions allow for the calculation of the intermediate respiratory state or $state_{apparent}$ (Choi et al., 2009; Salabei et al., 2014), which is an indicator of mitochondrial workload (Figure 27 B). We determined a $state_{apparent}$ value of 2.94 ± 0.15 in *Gclc*-deficient FoB (Figure 27 C), suggesting that mitochondria of FoB with *Gclc* deficiency are running at higher rate compared to those of control cells. This higher activity results from the insensitivity of ETC to FCCP treatment in the absence of GSH and is consistent with the limited reserve capacity of *Gclc*-deficient FoB (Figure 26 C). In other words, the $state_{apparent}$ derived in Figure 27 C confirms that the mitochondria of *Gclc*-deficient FoB have impaired ETC, which cannot support steady state mitochondrial respiration and, therefore, appear "exhausted". Taken together, these results establish that loss of GSH in FoB profoundly impairs mitochondrial respiration.

To determine whether the accumulation of ^{13}C-glucose-derived M2-succinate in *Gclc*-deficient FoB was caused by a dysfunctional ETC, we assessed the respiratory parameters of each ETC complex. First, we performed extracellular flux analysis to assay the mitochondrial OCR profile of each complex in saponin-permeabilized $Gclc^{fl/fl}$ and $Gclc^{fl/fl}$ *Mb1-Cre*$^{+}$ FoB. In *Gclc*-deficient FoB, CI delivers reducing equivalents (NAD^{+}) to the ETC (Figure 26 A) and showed no activation upon substrate injection (pyruvate + malate) (Figure 27 D, CI). Similarly, CII activation (measured as increase in OCR) upon addition of Succinate was also negligible in $Gclc^{fl/fl}$ *Mb1-Cre*$^{+}$ FoB compared to control

cells (Figure 27 D, CII). Therefore, both CI and CII exhibited a lower $state_{apparent}$ (Figure 27 E). However, substrate-dependent CIII and CIV OCR tended to be increased in GSH-deficient FoB cells compared to control FoB (Figure 27 D, CIII and E, CIV), suggesting the possibility of a mild compensatory activation that may also contribute to the high $\Delta\Psi_m$ in mutant FoB (Figure 25 A). These data indicate that GSH-dependent ETC dysfunction mostly affected the activity of CI and CII. In line with these results, we detected lower CI activity in total lysates of *Gclc*-deficient FoB compared to control FoB (Figure 27 F). Consequently, NADH levels were increased in the mutant cells (Figure 27 G), which resulted in a lower NAD^+/NADH ratio (Figure 27 H). Moreover, the expression level of the main subunit of CII (succinate dehydrogenase A; Sdha) was decreased in *Gclc*-deficient FoB (Figure 27 I). Accordingly, protein levels of CI-IV were reduced in mutant FoB compared to controls (Figure 27 J).

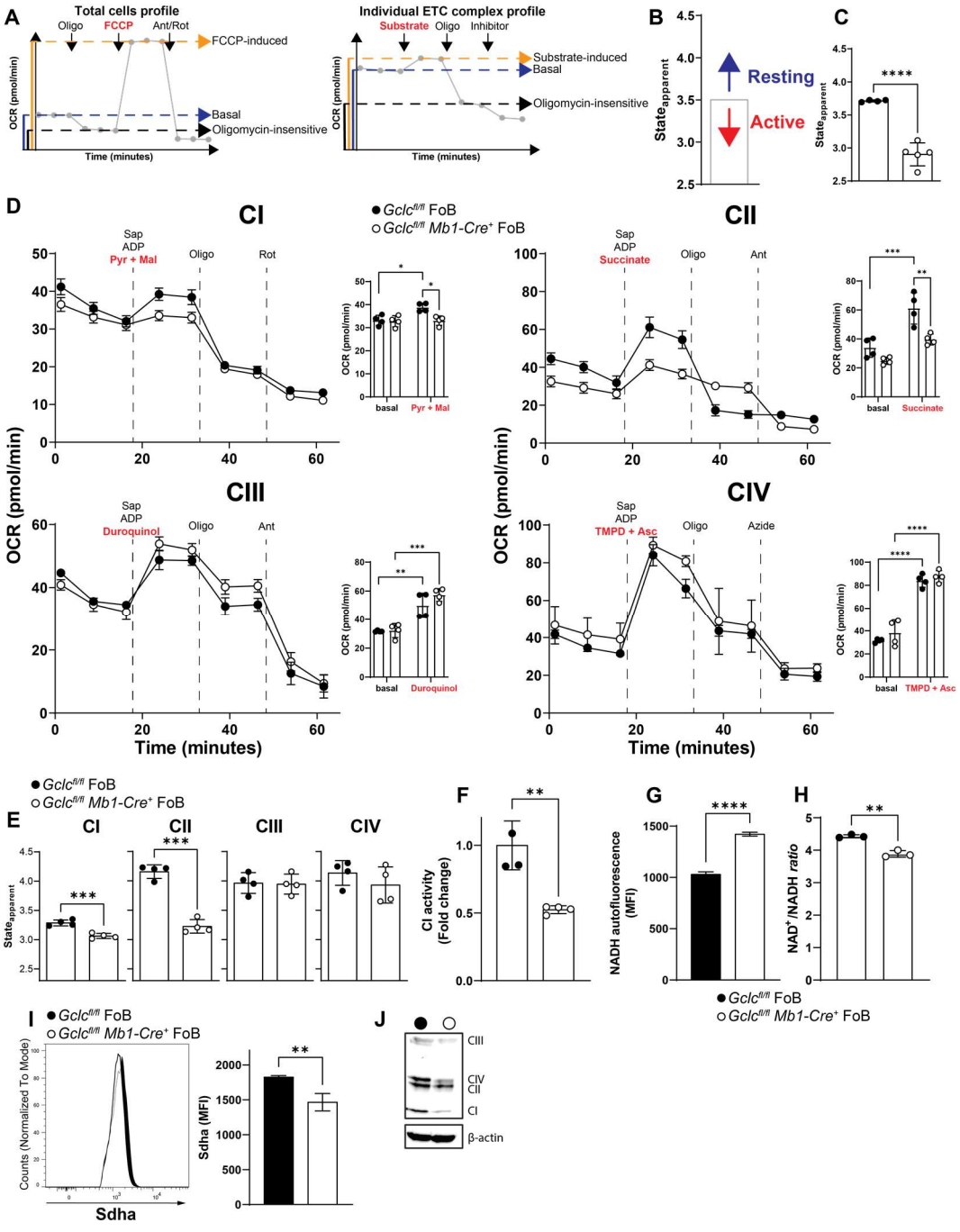

(Legend on next page)

Figure 27: TCA cycle is halted at CII and CI intersection in Gclc-defcient FoB.

A. To derive the apparent respiratory state ($state_{apparent}$), we assumed that State 3 respiration was equivalent to the OCR measured after addition of FCCP (orange bar) for total FoB (top) and Complex-specific substrate (bottom). Similarly, we assumed that State 4 corresponded to the rate measured after addition of Oligo (black bar), when OXPHOS is unable of utilizing the proton gradient to generate ATP because of the presence of the Complex V inhibitor. These assumptions allow for calculation of the $state_{apparent}$ under basal conditions, which were corrected to the basal OCR (blue bar). Top: OCR profile of a standard mitochondria stress test (Seahorse) using intact FoB cells. Bottom: OCR profile of saponin-permeabilized FoB cells to determine mitochondrial ETC complex activity. Dashed lines represent the indicated OCR values (left) used for the derivation of the $state_{apparent}$, calculated as $4 - \frac{(\text{Basal OCR}) - (\text{Oligo-insen OCR})}{(\text{FCCP- or Substrate-i OCR}) - (\text{Oligo-insensi OCR})}$ (Hill et al., 2012). **B.** Representative $state_{apparent}$ respiration for total FoB or ETC complex as calculated from Figure 26 C and E. Blue and red arrows indicate a more resting or active respiratory state respectively. **C.** Respiratory status of *Gclc*$^{fl/fl}$ and *Gclc*$^{fl/fl}$ *Mb1-Cre*$^{+}$ FoB in (B) displayed as $state_{apparent}$. **D.** OCR of *Gclc*$^{fl/fl}$ and *Gclc*$^{fl/fl}$ *Mb1-Cre*$^{+}$ FoB sequentially treated with saponin (Sap), adenosine diphosphate (ADP), and the indicated substrates for ETC complexes CI to CIV (red), as indicated. For each assay the the comparison of OCR before (basal) and after substrate injection (in red) in in *Gclc*$^{fl/fl}$ and *Gclc*$^{fl/fl}$ *Mb1-Cre*$^{+}$ FoB is plotted next to the OCR profile. **E.** Energetic status calculated as in C. for the ETC complexes CI to CIV in E. **F.** Quantitation of relative activity of CI in *Gclc*$^{fl/fl}$ and *Gclc*$^{fl/fl}$ *Mb1-Cre*$^{+}$ FoB as measured by a colorimetric assay. **G.** Quantitation of NADH autofluorescence in *Gclc*$^{fl/fl}$ and *Gclc*$^{fl/fl}$ *Mb1-Cre*$^{+}$ FoB (gated as in 11 D) as measured by FACS. **H.** CI activity in *Gclc*$^{fl/fl}$ and *Gclc*$^{fl/fl}$ *Mb1-Cre*$^{+}$ FoB expressed as the ratio of NAD^{+} (CI substrate) to NADH (CI product), as measured by colorimetric assay. **I.** Representative histogram (left) and quantitation (right) of immunostaining to detect the expression of succinate dehydrogenase a (Sdha, the major subunit of CII) in *Gclc*$^{fl/fl}$ and *Gclc*$^{fl/fl}$ *Mb1-Cre*$^{+}$ FoB (gated as in 11 D). **J.** Representative immunoblot to detect the indicated ETC complex proteins in total lysates of *Gclc*$^{fl/fl}$ and *Gclc*$^{fl/fl}$ *Mb1-Cre*$^{+}$ FoB. β-actin, loading control. For all applicable figure panels, data are mean ± SD and each dot represents one single mouse except in D where dots are mean of triplicates. Data shown are representative of ≥2 independent experiments with 3-6 mice/group. Significance (P) was calculated with unpaired t-test or one-way ANOVA (panel D). *: $P \leq 0.05$; **: $P \leq 0.01$; ***: $P \leq 0.001$; ****: $P \leq 0.0001$.

These data indicate that GSH plays a role in sustaining the activities of CI and CII, and thus the ETC function in general. In particular, our energetic steady-state analyses (Figure 27 D, E) show that loss of GSH induces a partial uncoupling of ETC from OXPHOS, suggesting that *Gclc* function has a direct effect on the metabolic dependencies of FoB. GSH deficiency has a negative impact on the mitochondrial respiration machinery, halting the TCA cycle at the ETC branch point (*i.e.* CII). Thus, compared to T cells (Mak et al., 2017; Kurniawan et al., 2020), we have identified a heretofore-unappreciated role for GSH in B cells: that of sustaining the activity of mitochondrial ETC by preventing ROS accumulation.

Chapter 6: Single cell analysis confirms the change in metabolic pathways in *Gclc*-deficient Follicular B cells, which show Marginal Zone B cells attributes

6.1 Introduction

Assessments of gene expression or protein expression are often used to understand the complex cellular diversity. For protein expression studies, the application of multi-color flow or mass cytometry is commonly used to simultaneously assess protein levels (Spitzer and Nolan, 2016). However, it remains challenging to examine the plethora of proteins expressed by the genome that exists in a single cell. Often used as a proxy for studying the proteome, the expression of protein-encoding mRNA molecules (collectively termed the transcriptome) is used to correlate with cellular traits and changes to specific treatments (*i.e.* activation). This approach is usually referred as to RNA sequencing (RNA-seq) and allows for the detection and quantitative analysis of mRNA molecules in a biological sample (Haque et al., 2017) that has been used to study the heterogeneity of B cells (Mabbott and Gray, 2014; Shi et al., 2015; Kleiman et al., 2015; Haines et al., 2019).

As discussed in the previous chapters, the B cell compartment includes various subsets with defined properties. Therefore, performing RNA-seq on the bulk B cell population (bulk RNA-seq), assuming homogeneity of transcriptomes, would hinder the assessment of the distinct cell populations. This problem was originally overcame by purifying the subsets of interest based on selected surface markers via flow cytometry-based sorting, and performing bulk RNA-seq in the distinct fractions. However, bulk RNA-seq does not allow detailed assessment of the fundamental biological unit (the cell). The rapid progress in the development of sequencing technologies allows the characterization of single cell

transcriptomes (Hwang et al., 2018). More recently, single cell RNA sequencing (scRNA-seq) methods have been integrated with single cell protein measurements. This method, known as cellular indexing of transcriptomes and epitopes by sequencing (CITE-seq) (Stoeckius et al., 2017) simultaneously detects transcripts and proteins in single cells and it is suitable for detailed characterization of cellular phenotypes (Figure 28). Additionally, it is possible to multiplex CITE-seq experiments by using a series of oligo-tagged antibodies against ubiquitously expressed surface proteins (*i.e.* CD45) with different barcodes to uniquely label cells from distinct samples (hereafter "hashtags") (Stoeckius et al., 2018). By including these hashtags alongside the cellular transcriptome, we can assign each cell to its sample of origin.

CITE-seq includes antibodies directed against cellular proteins which are conjugated to oligonucleotides that can be captured by primers and amplified, and contain a barcode for antibody identification during the analysis. The signal detected and amplified by the protein marker is referred as to antibody-derived tag (ADT) and can be analyzed independently of the transcriptomic library (Figure 28). The ability to layer additional protein measurements on top of scRNA-seq data represents the perfect method for the analysis of complex cell populations, such as the B cell lineage. Indeed, in a similar fashion to flow cytometry gating, it is possible to classify or cluster the single cell transcriptomes based on the ADT protein signals, and then perform downstream computational analyses (such as differential expression, gene ontology and Gene Set Enrichment Analysis (GSEA)) on the specified groups.

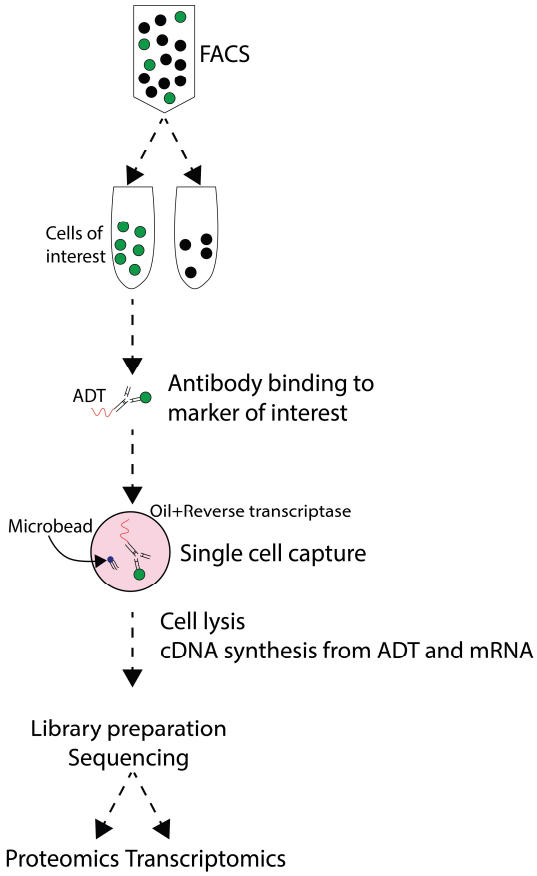

Figure 28: Schematic view of the workflow for single cell Cellular Indexing of Transcriptomes and Epitopes by Sequencing (CITE-Seq).

A simplified example of droplet-based library generation. Cells are FACS-sorted and incubated with antibody-derived tags (ADT) to detect protein of interests. Then, libraries for scRNA-seq are generated via cell lysis, reverse transcription into complementary DNA (cDNA) using uniquely barcoded microbeads, second-strand synthesis, and cDNA amplification. cDNA is prepared from both ADTs and cellular mRNAs. The independent libraries are pooled, sequenced and analyzed. Thus, proteomics and transcriptomics data can be obtained from a single sequencing run.

GSH is a key intracellular antioxidant that scavenges excess ROS (Meister and Anderson, 1983; Wu et al., 2004; Deponte, 2013), and it is an extremely important molecule for the regulation of lymphocytes activation (Hamilos and Wedner, 1985; Fidelus and Tsan, 1986; Droge et al., 1986). In B cells, ROS are instrumental in regulating activation (Vene et al., 2010; Franchina et al., 2018b), but the contribution to B cell subsets and functions of metabolic ROS, is poorly understood. Given the binary effect of GSH deletion in FoB and MZB, it is therefore possible to postulate the existence of subset-specific redox thresholds, and that these thresholds mediate homeostatic functions that could account for the differing properties of MZB and FoB.

ROS balance can be regulated by plenty of intracellular reactions. Of these, upstream the mitochondrial metabolism, is the mechanistic target of rapamycin (mTOR), whose signaling is a key modulator of anabolic and catabolic reactions (Saxton and Sabatini, 2017). mTOR has emerged as a crucial control point for B cell functions (Limon and Fruman, 2012). Previous reports have shown that relatively high levels of mTOR complex 1 (mTORC1) signaling prevail in MZB (Donahue and Fruman, 2007; Gaudette et al., 2020), but that the maturation of FoB downregulates the mTORC1/Akt pathway (Farmer et al., 2019). However, other groups have shown that efficient mTORC1 suppression is necessary to avoid MZB loss (Benhamron and Tirosh, 2011). Because mTORC1 is a well-known regulator of metabolic functions, these findings imply that specific metabolic programs may underlie the unique characteristics of B cell subsets in relation to ROS signaling.

Cellular metabolism has emerged as a key regulator of immune functions and responses (O'Neill et al., 2016; Voss et al., 2021). However, the characterization of cellular metabolic programs was performed on bulk cellular populations (Artyomov and Van den Bossche, 2020) and share the same limitations of bulk RNA-seq. Indeed, as every cell resides in a

unique microenvironment, no single cell within our body is completely identical metabolically (nor transcriptomically). Recent advances in single cell profiling technologies have highlighted the power to investigate metabolic properties (Artyomov and Van den Bossche, 2020). Particularly, scRNA-seq data can be used to make *in silico* predictions on metabolic fluxes with Compass, a flux-balanced analysis which characterizes the metabolic heterogeneity among cells by integrating publicly available metabolic pathways in conjunction with scRNA expression of metabolic enzymes (Wang et al., 2020; Wagner et al., 2021).

In conclusion, current state-of-the-art single cell technologies contribute to our understanding of both transcriptomic and metabolic regulation of immunity and can be exploited to better characterize the molecular heterogeneity of distinct cell populations. In our case, CITE-seq analyses coupled with the Compass algorithm allowed for the metabolic characterization of specific B cell subsets and, in particular, the identification of unexpected similarities between *Gclc*-sufficient MZB and *Gclc*-deficient FoB.

6.2 Objective

To investigate the transcriptional changes and infer the metabolic state induced by the deletion of *Gclc* in FoB.

6.3 Results

6.3.1 FoB and MZB can be identified by CITE-seq proteomics

To investigate the function of GSH in the FoB subset, we performed single cell CITE-seq on FACS sorted splenic B cells from four $Gclc^{fl/fl}$ and four $Gclc^{fl/fl}$ $Mb1\text{-}Cre^{+}$ mice (Figure 29 A). T-distributed stochastic neighbor embedding (tSNE) visualization of the B

cells transcriptomic landscape did show minor changes in the distribution of single cell transcriptomes between the two conditions across the hashtags (Figure 29 B and C, and 30 A). We also detected significantly lower signal for *Gclc* expression in sequenced B cells from *Gclc*$^{fl/fl}$ *Mb1-Cre*$^{+}$ compared to control mice (Figure 30 B). By using CD23, IgD, CD21/CD35 and CD1d antibody-derived tag (ADT) signals, we identified FoB and MZB and assigned each cell type using SCINA (Figure 30 C) (Zhang et al., 2019). Mirroring the results previously shown by FACS analysis (Figure 11 D, G), loss of MZB in *Gclc*$^{fl/fl}$ *Mb1-Cre*$^{+}$ mice was confirmed by the ADT signals from the CITE-seq analysis (Figure 30 C and D). In line, FoB were detectable in *Gclc*$^{fl/fl}$ *Mb1-Cre*$^{+}$ mice by the expression of ADT-CD23 and ADT-IgD (Figure 30 C).

In order to study the transcriptomic changes induced by the deletion of *Gclc*, we performed downstream analyses of FoB (Figure 30 E). As shown in Figure 30 F, the PCA analysis indicated that the principal component 1 (PC1) covers most of the variation in gene expression (58% of total variance). This suggested that the PC1 captured the effect caused by the genetic deletion of *Gclc*. Thus, the deletion of *Gclc*, and therefore the absence of GSH, influences gene expression levels in FoB, as shown by the total gene transcripts per cell (Figure 30 G).

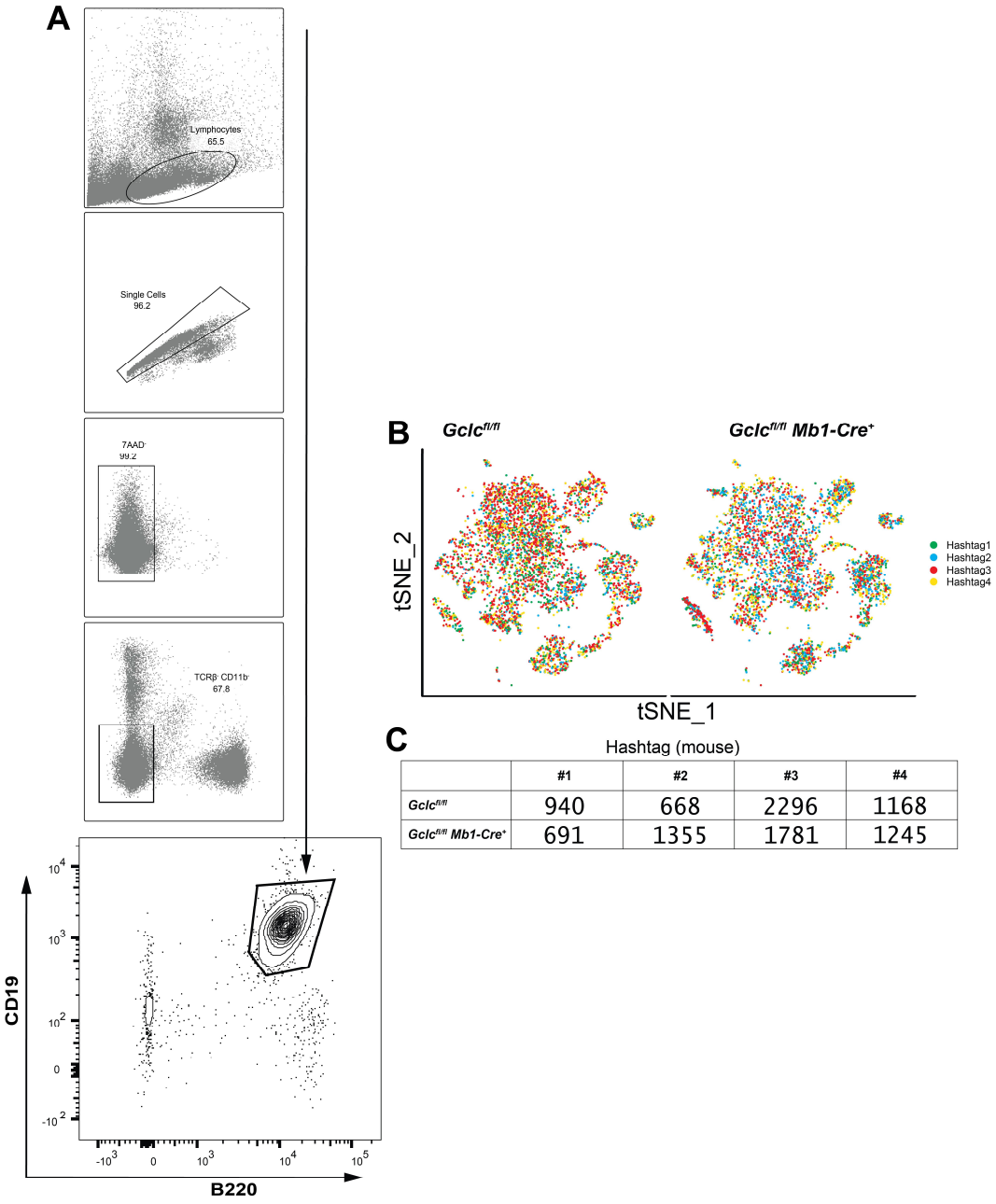

C

Hashtag (mouse)

	#1	#2	#3	#4
Gclc$^{fl/fl}$	940	668	2296	1168
Gclc$^{fl/fl}$ Mb1-Cre^{+}	691	1355	1781	1245

(Legend on next page)

Figure 29: Sample multiplexing using DNA-barcoded antibodies allows cell labeling from individual samples.

A. Dot plots show the back-gating of the sorting strategy (top to bottom) used to purify total splenic B cells from *Gclc*$^{fl/fl}$ and *Gclc*$^{fl/fl}$ *Mb1-Cre*$^{+}$ mice that were used for sequencing. **B.** tSNE transcriptome-based clustering of single cell expression profiles shows relatively homogeneous distribution of cells derived from each mouse (hashtag) across genotypes (*Gclc*$^{fl/fl}$ and *Gclc*$^{fl/fl}$ *Mb1-Cre*$^{+}$). Each single cell expression profile is arbitrarily colored based on the hashtag classification. **C.** Summary table of number of cells for each hashtag label in four *Gclc*$^{fl/fl}$ and four *Gclc*$^{fl/fl}$ *Mb1-Cre*$^{+}$ mice.

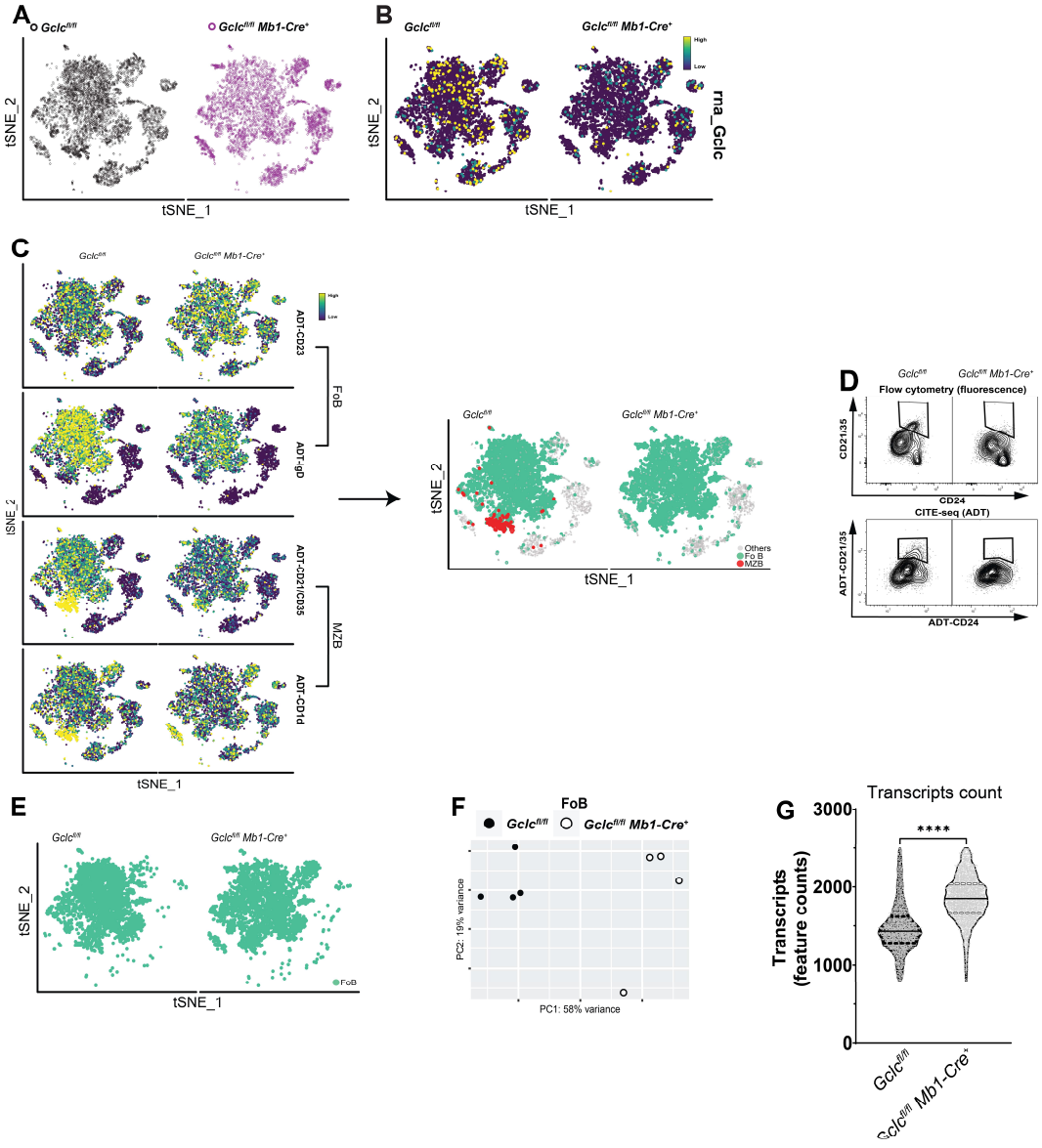

(Legend on next page)

Figure 30: FoB and MZB can be identified with CITE-seq proteomics for downstream analyses.

A. tSNE distribution of single cell transcriptomes of FACS sorted splenic B cells from of *Gclc*$^{fl/fl}$ and *Gclc*$^{fl/fl}$ *Mb1-Cre*$^{+}$ mice. **B.** Expression of *Gclc* in sequenced B cells from *Gclc*$^{fl/fl}$ and *Gclc*$^{fl/fl}$ *Mb1-Cre*$^{+}$ mice presented in a tSNE plot. **C.** Left: tSNE plots comparing ADT signals for FoB (top) and MZB (bottom) markers among splenic B cells from *Gclc*$^{fl/fl}$ and *Gclc*$^{fl/fl}$ *Mb1-Cre*$^{+}$ mice. Right: SCINA assignments of FoB (green) and MZB (red) from *Gclc*$^{fl/fl}$ and *Gclc*$^{fl/fl}$ *Mb1-Cre*$^{+}$ mice. **D.** Comparison of FACS (fluorescence) and CITE-seq signal (ADT) for the detection of MZB in *Gclc*$^{fl/fl}$ and *Gclc*$^{fl/fl}$ *Mb1-Cre*$^{+}$ mice. **E.** SCINA assignments of FoB from *Gclc*$^{fl/fl}$ and *Gclc*$^{fl/fl}$ *Mb1-Cre*$^{+}$ mice used for downstream analyses. **F.** PCA plot showing distinct patterns of *Gclc*$^{fl/fl}$ and *Gclc*$^{fl/fl}$ *Mb1-Cre*$^{+}$ FoB transcriptomes. Each dot represents a single mouse. **G.** Number of detected gene transcripts per cell in *Gclc*$^{fl/fl}$ and *Gclc*$^{fl/fl}$ *Mb1-Cre*$^{+}$ FoB. Each dot represents a single cell and data are pooled from 4 mice/genotype. Solid line, median; dashed lines, 1st and 3rd quartiles. Data are the mean ± SD. Significance (P) was calculated with unpaired t-test. ****$P \leq 0.0001$.

6.3.2 The mTOR pathway confers Marginal Zone B cell-like properties to GSH-deficient Follicular B cells

As noted above, mTOR signaling has emerged as a key control point for B cell functions (Limon and Fruman, 2012). Given that *Gclc*$^{fl/fl}$ *Mb1-Cre*$^{+}$ mice had few MZB compared to FoB (Figure 11 D-F), we performed gene set enrichment analysis (GSEA) on differentially expressed genes of *Gclc*$^{fl/fl}$ MZB versus FoB to investigate whether mTOR signaling might be involved in the effects seen in the GSH-deficient cells. In accordance with previous reports, our GSEA analysis revealed positive enrichment for genes of the mTORC1 signaling pathway in *Gclc*-sufficient MZB compared to FoB (Figure 31 A).

Flow cytometric evaluation of resting B6 MZB confirmed increased phosphorylation of both mTOR and its canonical target S6 (Figure 31 B and C). Strikingly, our GSEA analysis also showed that *Gclc*$^{fl/fl}$ *Mb1-Cre*$^{+}$ FoB displayed increased mTORC1 signaling genes compared to *Gclc*$^{fl/fl}$ FoB (Figure 31 D). Corresponding increase in phosphorylated mTOR and S6 were detected in mutant FoB compared to control FoB (Figure 31 E and F). These data pointed to an unexpected similarity between *Gclc*-deficient FoB and *Gclc*-sufficient MZB. Importantly, mutant FoB showed no changes in size (Figure 31 G), which excluded any autofluorescence bias and indicated that *Gclc* deficiency does not alter the cell volume of FoB.

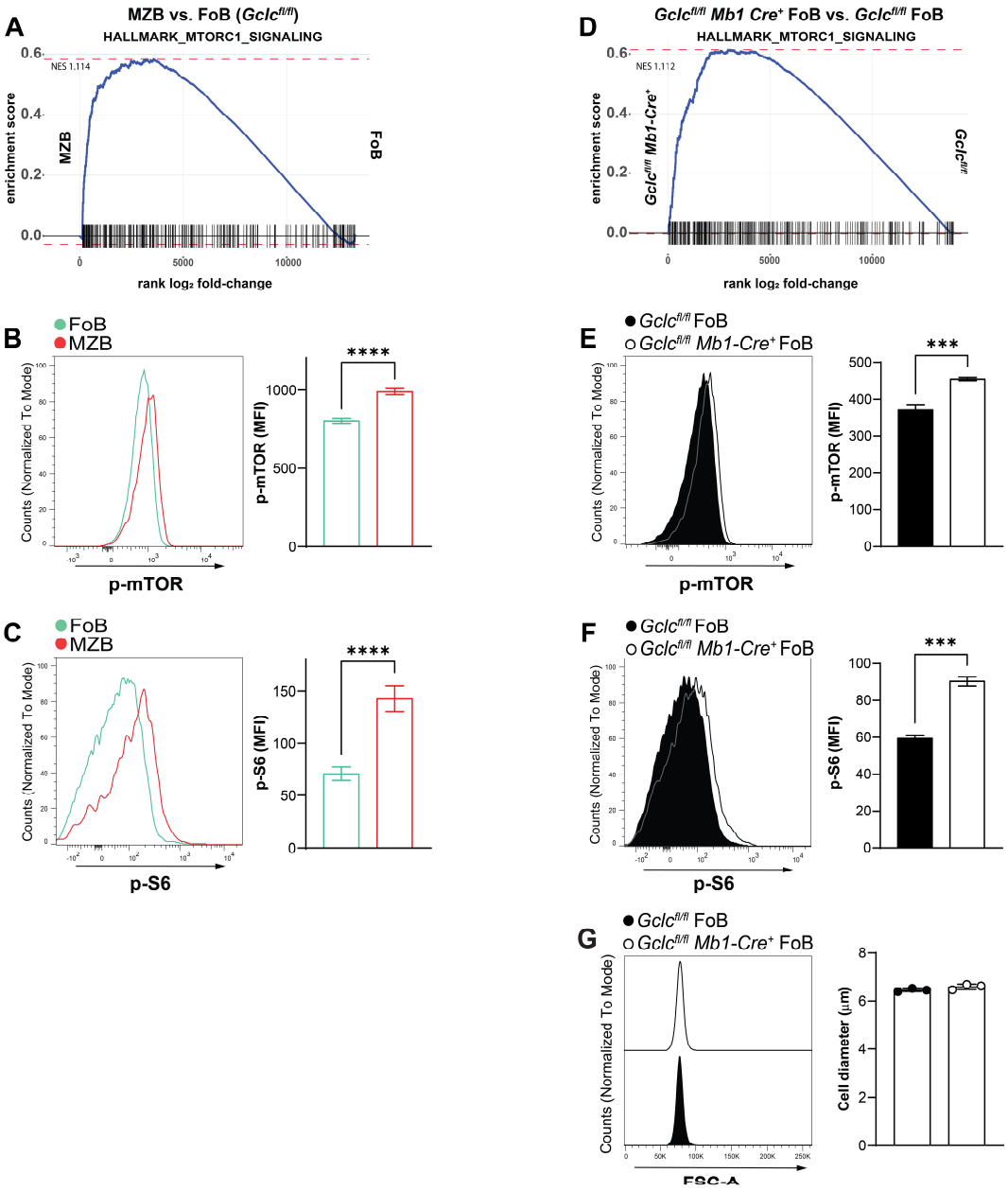

(Legend on next page)

Figure 31: mTORC1 is comparably elevated in Gclc-sufficient MZB and Gclc-deficient FoB.

A. GSEA plot comparing expression of mTORC1 signaling hallmark gene sets between *Gclc*$^{fl/fl}$ FoB and *Gclc*$^{fl/fl}$ MZB. **B, C.** Representative histogram (left) and quantitation (right) of immunostaining to detect p-mTOR and p-S6 staining in B6 FoB and MZB (gated as in Figure 21 A). **D.** GSEA plot comparing the expression of mTORC1 signaling hallmark gene sets between *Gclc*$^{fl/fl}$ and *Gclc*$^{fl/fl}$ *Mb1-Cre*$^{+}$ FoB. **E, F.** Representative histogram (left) and quantitation (right) of immunostaining to detect p-mTOR and p-S6 in *Gclc*$^{fl/fl}$ and *Gclc*$^{fl/fl}$ *Mb1-Cre*$^{+}$ FoB (gated as in Figure 11 D). **G.** Left: representative histogram of forward scatter area (FSC-A) signal of *Gclc*$^{fl/fl}$ and *Gclc*$^{fl/fl}$ *Mb1-Cre*$^{+}$ FoB (gated as in Figure 11 D). Mean diameter (µM) of enriched *Gclc*$^{fl/fl}$ and *Gclc*$^{fl/fl}$ *Mb1-Cre*$^{+}$ FoB using the CASY cell counter. For all applicable figure panels, data are mean ± SD and each dot represents measruments from one single mouse. Data are representative of ≥3 independent experiments with 3-4 mice/group. Significance (P) was calculated with unpaired t-test. ***: $P \leq 0.001$; ****: $P \leq 0.0001$.

mTOR is also an important regulator of translation (Ma and Blenis, 2009), and supports the enhanced secretory apparatus and superior secretory activity of MZB compared to FoB (Oliver et al., 1997; Gunn and Brewer, 2006). Accordingly, we found that B6 MZB had a higher endoplasmic reticulum (ER)/Golgi ratio than B6 FoB as measured by their greater staining intensity of ER-tracker and α-giantin (Figure 32 A), as well as by their increased phosphorylation of the translation initiation factor eIF4E (Figure 32 B). In addition, our differential gene expression analysis identified upregulation of a considerable number of transcripts related to ribosomal proteins in *Gclc*$^{fl/fl}$ MZB compared to *Gclc*$^{fl/fl}$ FoB (Figure 32 C). Additionally, gene ontology analysis detected accumulation of transcripts related to the three steps of protein synthesis (initiation, elongation, termination) in *Gclc*$^{fl/fl}$ MZB compared to *Gclc*$^{fl/fl}$ FoB (Figure 32 D). To confirm this heightened protein translation *in vitro*, B6 FoB and B6 MZB were activated with anti-IgM, CD40 ligand and IL-4 or LPS, pulsed with puromycin, and chased for up to 6h (Schmidt et al., 2009). As shown in Figure 32 E, B6 MZB indeed showed greater protein synthesis compared to B6 FoB. Strikingly, an absence of *Gclc* in FoB resulted in secretory properties that recapitulated those of *Gclc*-sufficient MZB at both the transcriptional and protein levels (Figure 32 F-J).

Collectively, these data suggest that the absence of GSH in FoB diminishes their ability to buffer ROS, therefore promoting activation of the mTOR pathway and conferring MZB-like properties. Moreover, mitochondrial ROS are higher in wild-type MZB compared to FoB (Figure 21 B), further indicating that *Gclc*-deficient FoB might acquire wild-type MZB redox characteristics. Thus we explored the intriguing hypothesis that GSH-dependent control of ROS could play a role in defining the distinctive metabolic signaling of MZB and FoB.

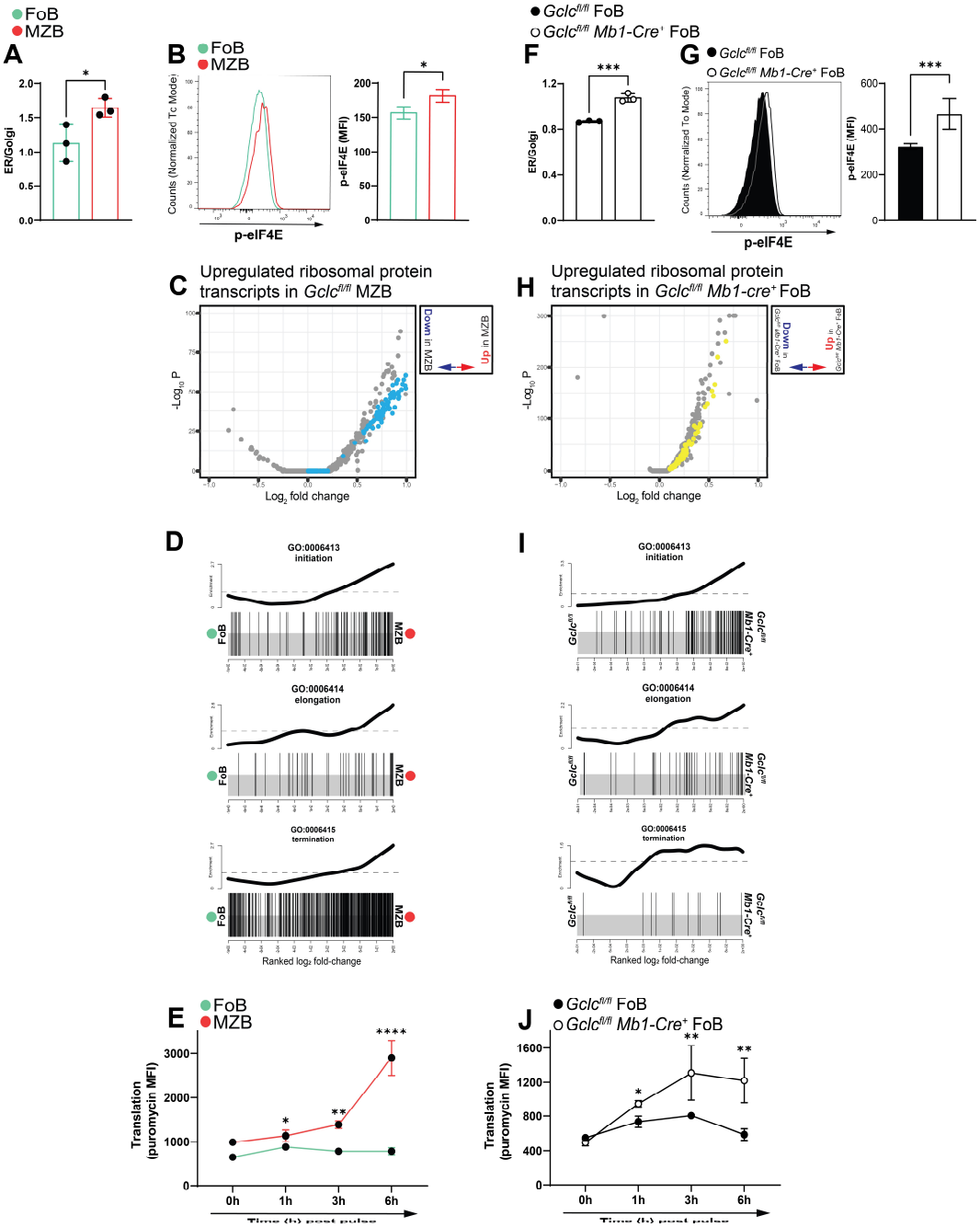

(Legend on next page)

Figure 32: Protein synthesis is enhanced in Gclc-sufficient MZB and Gclc-deficient FoB.

A. ER/Golgi ratio derived from the mean fluorescence signal (MFI) of ER-tracker and α-giantin measured in splenic B6 FoB and MZB (gated as in Figure 21 A). **B.** Representative histogram (left) and quantitation (right) of p-eIF4E MFI measured in B6 FoB and MZB (gated as in Figure 21 A). **C.** Volcano plot of differentially expressed genes in *Gclc*$^{fl/fl}$ FoB and MZB. Light blue dots indicate ribosomal-related transcripts. Data represent up- and downregulation of MZB vs. FoB transcripts among total transcripts pooled from 4 *Gclc*$^{fl/fl}$ mice. **D.** Barcode plots showing transcripts from the GO:0006413, GO:0006414 and GO:0006415 gene lists that were enriched in *Gclc*$^{fl/fl}$ MZB vs. FoB. **E.** Protein translation at the indicated times measured as puromycin MFI after puromycin pulse-chase of B6 FoB and MZB upon stimulation with anti-IgM, CD40 ligand and IL-4 or LPS. **F-J.** Same analyses as shown in A-E but comparing *Gclc*$^{fl/fl}$ versus *Gclc*$^{fl/fl}$ *Mb1-Cre*$^{+}$ FoB. Data are the mean ± SD. Each dot represents one mouse in A and F, one transcript C and H, mean of duplicates from 2-3 mice in E and J. Data shown are representative of ≥2 independent experiments with 2-4 mice/group. Significance (P) was calculated with unpaired t-test or one-way ANOVA (E and J). *P ≤ 0.05; **P ≤ 0.01; ***P ≤ 0.001; ****P ≤ 0.0001.

6.3.3 Compass analysis reveals increased glycolysis in *Gclc*-deficient Follicular B cells

mTORC1 signaling plays a role in both MZB and FoB (Donahue and Fruman, 2007; Benhamron and Tirosh, 2011; Farmer et al., 2019; Gaudette et al., 2020), and is key for the regulation of various metabolic pathways (Saxton and Sabatini, 2017). Broadly speaking, metabolism is an established regulator of immune cell function, but it remains difficult to study in individual cells. Moreover, the metabolic network includes a plethora of pathways which increases its scale and complexity, making hard the interpretation of data. With the advent of the single cell -omics technologies, there is increasing need to investigate metabolic observations and perturbations at the single cell level. Therefore, in order to contextualize the complexity of the metabolic network and the impact of *Gclc* on it, we analyzed our transcriptomic data using Compass, a flux balance analysis-based approach that allows the characterization and interpretation of metabolic diversity at the single cell level (Wang et al., 2020; Wagner et al., 2021). In order to study and compare the metabolic changes in different B cell subsets, we made use of the SCINA assignments (Figure 30 C and E) to group and extrapolate the gene expression matrices of each subsets (MZB vs. FoB for $Gclc^{fl/fl}$, and $Gclc^{fl/fl}$ FoB vs. $Gclc^{fl/fl}$ *Mb1*-Cre^{+} FoB). Each matrix group was then fed into the Compass analysis pipeline. Essentially, for each cell transcriptome Compass builds numeric scores based on murine metabolic reactions from RECON2 (Thiele et al., 2013; Penalver Bernabe et al., 2019), and ultimately reflects how the cell transcriptome is capable of maintaining a particular reaction flux (Wagner et al., 2021).

Using this computational prediction, we found that $Gclc^{fl/fl}$ MZB exhibited increased glucose catabolism compared to $Gclc^{fl/fl}$ FoB (Figure 33 A, top). Glucose can be catabolized to lactate during glycolysis or glucose-derived carbons can enter the TCA. We therefore sorted the metabolic reactions identified by the Compass algorithm into two groups:

glycolysis and TCA. This analysis showed that glycolysis was upregulated in *Gclc*$^{fl/fl}$ MZB compared to *Gclc*$^{fl/fl}$ FoB (Figure 33 A, bottom), suggesting that MZB rely on glycolysis rather than oxidative metabolism when at steady-state. To confirm these predictions, we measured the uptake of 2-NBDG to monitor glucose uptake by B6 MZB and FoB. In line with our Compass results, B6 MZB at steady-state showed increased 2-NBDG uptake compared to B6 FoB (Figure 33 B) as well as higher expression of the glucose transporter Glut-1 as measured by flow cytometry (Figure 33 C). Moreover, total intracellular glucose was elevated in freshly isolated B6 MZB compared to B6 FoB as measured by mass spectrometry (Figure 33 D).

Our data above indicated that GSH deficiency upregulated mTORC1 signaling in mutant FoB. Therefore, we sought to determine whether this heightened mTORC1 skewed FoB metabolism towards glycolysis. Indeed, our Compass analysis reflected a global increase in glucose catabolism in FoB when *Gclc* was ablated (Figure 33 E), just as occurred in *Gclc*-sufficient MZB (Figure 33 A). As previously shown, mutant FoB also showed increased 2-NBDG uptake at steady-state (Figure 22 D), higher Glut-1 expression (Figure 22 E and F), and elevated accumulation of glucose (Figure 33 F) compared to control FoB. These data indicate that mutant FoB in the absence of GSH undergo an increase in oxidative state that induces a metabolic shift similar to that observed in *Gclc*-sufficient MZB.

In conclusion, the metabolic analysis performed on our transcriptome data set represents a powerful tool that corroborate our findings in two ways. First, the Compass predictions reiterate the *in vitro* assays shown in Figure 22 and 23. Second, the result of this algorithm, whose computations are based on gene expression data, indicates that *Gclc* deletion (and its perturbation of cell transcription) poises FoB transcriptome towards glycolysis.

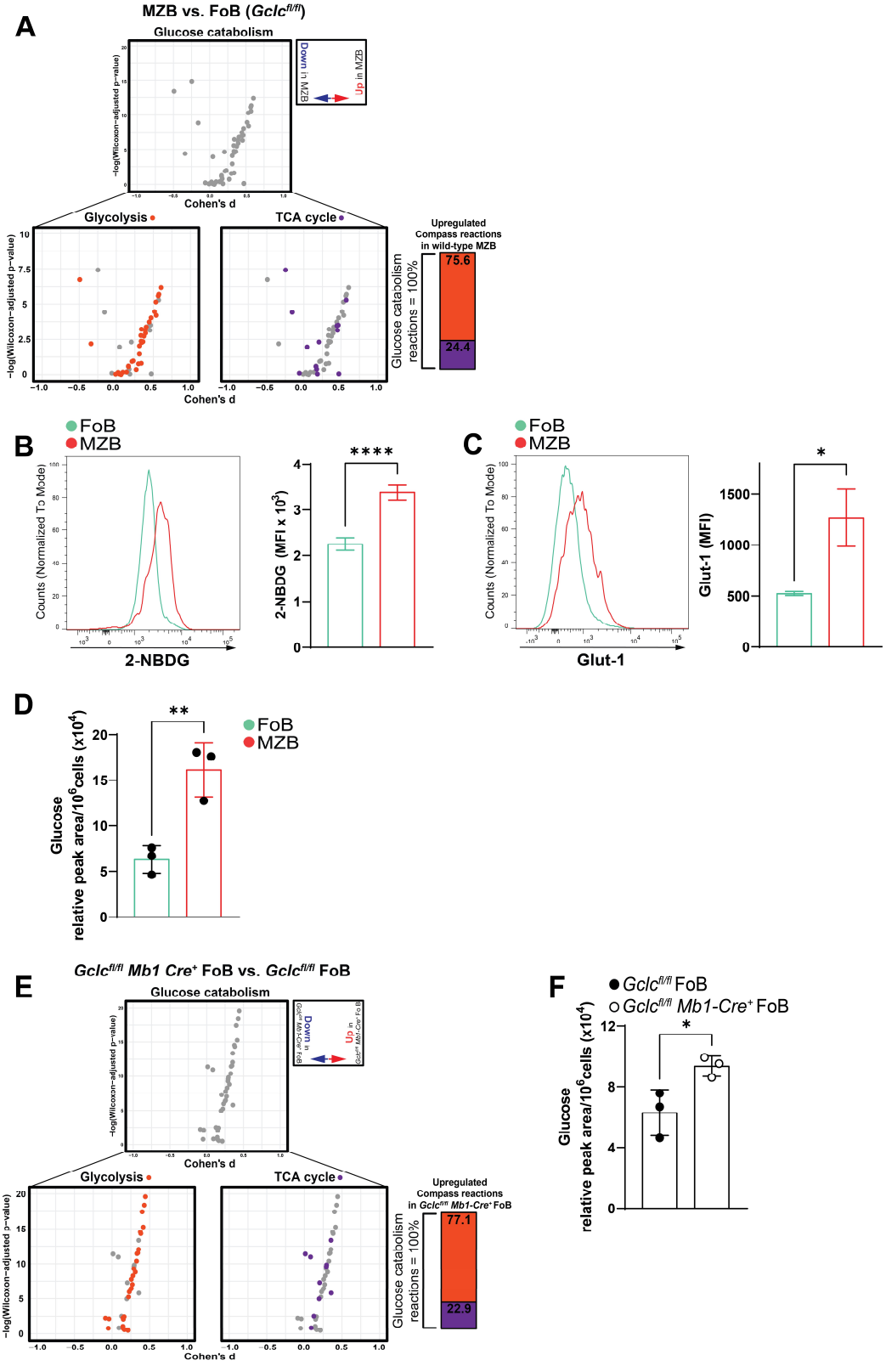

(Legend on next page)

Figure 33: Gclc-deficient FoB show increased glycolytic reactions and glucose uptake, mirroring Gclc-sufficient MZB.

A. Compass analysis comparing glucose catabolism (top) and its constituent components (glycolysis and TCA cycle) (bottom) in *Gclc*$^{fl/fl}$ MZB vs. FoB. Each dot represents a single biochemical reaction. Means difference (Cohen's d) and Wilcoxon rank sum p values were computed as described in (Wang et al., 2020; Wagner et al., 2021). Vertical bar on the right shows relative contributions (percentage) of upregulated glycolytic reactions and TCA reactions to total glucose catabolism computed from glycolysis and TCA cycle reactions in *Gclc*$^{fl/fl}$ MZB vs. FoB. **B, C.** Representative histogram (left) and quantitation (right) of 2-NBDG and Glut-1 staining in resting splenic B6 FoB and MZB (gated as in Figure 21 A). **D.** Quantitation of intracellular glucose level measured by LC-MS in resting *Gclc*-sufficient FoB and MZB. **E, F.** Same analyses as shown in A and D, but comparing *Gclc*$^{fl/fl}$ versus *Gclc*$^{fl/fl}$ *Mb1-Cre*$^{+}$ FoB. For all applicable Figure panels, data are mean ± SD and each dot represents one single metabolic reaction or mouse. Data shown are representative of ≥2 independent experiments with 3-4 mice/group. Significance (P) was calculated with unpaired t-test. *: $P \leq 0.05$; **: $P \leq 0.01$; ****: $P \leq 0.0001$.

Chapter 7: Results summaries and discussion

7.1 Results Summaries

7.1.1 Chapter 3

The initial goal of the study detailed in Chapter 3 was to dissect the main stages of B cell development in the absence of *Gclc* expression. We examined the early B cell development in the BM via flow cytometry following Hardy's classification. We found that the most mature population, namely fraction F, which includes blood-recirculating mature B cells, was lower in B cell-specific *Gclc*-depleted animals. These results suggested that *Gclc* is dispensable for the early development of B cells (Figure 10). Following the natural course of B cell development, we analyzed the major resident mature B cell populations in the spleen. *Gclc* deficiency led to a drastic decrease in the MZB compartment, which was also confirmed by immunofluorescence microscopy (Figure 11). Importantly, we excluded that MZB loss in *Gclc*-depleted animals was caused by alteration of the MZ microenvironment, such as altered expression of integrins, chemokines and variation in MZ-resident macrophages (Figure 12). Furthermore, based on the analogies between MZB and B1 cells, which together are referred to as "innate-like" B cells, we showed that lack of *Gclc* induces a stark reduction of both splenic and peritoneal B1 cells (Figure 15). Finally, due to the decrease of innate-like B cells in *Gclc*-depleted animals, we explored natural and induced humoral immune protection. In line, these experiments showed null response to antigen-induced early antibody immunization (Figure 16) and decreased levels of natural antibodies (Figure 17) in the absence of *Gclc*.

7.1.2 Chapter 4

In Chapter 4, we demonstrated that, despite the negligible effect of *Gclc* deficiency on FoB at steady state, *Gclc* expression is required to ensure efficient GC reaction and antibody immunity upon T-dependent B cell activation. To study antigen specific antibodies, we used models of T-cell dependent B cell activation (TNP-KLH, LCMV Cl13 and VSV) to immunize $Gclc^{fl/fl}$ *Mb1-Cre*$^{+}$ and control mice. By measuring antibody levels in the serum of immunized mice, we showed that absence of *Gclc* diminished antibody production (IgM and IgG) (Figure 18 B and 19). This resulted in higher viral titers in the organs of *Gclc*-depleted mice and limited survival upon acute viral infection (Figure 20). Overall, the results shown in Figure 18-20 indicate that the expression of *Gclc* in FoB cells is necessary for activation *in vivo*, allowing the success of the GC response.

7.1.3 Chapter 5

Having implicated *Gclc* in MZB development and function of FoB-mediated immunity, and being *Gclc* important in the maintenance of cellular redox homeostasis, in chapter 5 we investigated how the metabolic properties of MZB and FoB would differ in the context of ROS metabolism. We found that MZB produce more GSH, which is used up (*i.e.* low GSH/GSSG ratio) to counteract higher mitochondrial ROS at steady state (Figure 21), suggesting that GSH is indeed a critical determinant for the distinct properties of MZB and FoB. Similarly, *Gclc*-deficient FoB showed increased mitochondrial ROS. Because of the central role of mitochondria in energy metabolism, we studied glucose catabolism in detail and found that mutant FoB have increased glycolysis and, therefore increased glycolytic-dependent ATP generation (Figure 22 and 23), but showed a profound alteration of mitochondrial metabolic properties (Figure 24 and 25). In particular, glucose flux into the tri-carboxylic acid (TCA) cycle was halted (Figure 25). We found increase labeling into

succinate (Figure 26), which is metabolized to fumarate by the succinate dehydrogenase complex (complex II or CII). We also found decreased activity of CI, which is crucial for the correct cycling of the TCA cycle. These findings were confirmed by flux analysis and indicated that GSH plays a role in sustaining the activities of CI and CII, and so of the overall ETC fitness. In particular, our energetic steady-state analyses (Figure 27) showed that loss of GSH induces a partial uncoupling of ETC from OXPHOS, suggesting that *Gclc* function has a direct effect on the metabolic dependencies of FoB. We described that GSH deficiency had a large negative impact on the mitochondrial respiration machinery, halting the TCA cycle at the ETC branch point (*i.e.* CII).

7.1.4 Chapter 6

In order to contextualize the complexity of the metabolic network and the impact of *Gclc* on it, we analyzed FoB transcriptomes with CITE-seq in chapter 6. GSEA analysis highlighted upregulated mTORC1 signaling in *Gclc*-deficient FoB, which is strikingly similar to wild-type MZB (Figure 30). In line, absence of *Gclc* increased protein synthesis in mutant FoB, substantiating the analogy with MZB (Figure 31). Given that mTOR is an important regulator of cellular metabolism, we analyzed our transcriptomic data using Compass, a flux balance analysis-based approach that allows the characterization and interpretation of metabolic diversity at the single cell level. This analysis showed that when *Gclc* was ablated, FoB increased in glucose catabolism, just as occurred in *Gclc*-sufficient MZB (Figure 32). These data confirmed the *in vitro* experiments (chapter 5) and indicated that FoB in the absence of GSH undergo an increase in oxidative state that induces a metabolic shift similar to that observed in *Gclc*-sufficient MZB.

7.2 Discussion

ROS-induced signals regulate B cell activation and early metabolic reprogramming (Wheeler and Defranco, 2012; Akkaya et al., 2018), and a flexible redox system controls B cell differentiation (van Anken et al., 2003; Bertolotti et al., 2010; Vene et al., 2010). The present study has uncovered the previously unrecognized contribution of GSH to B cell homeostasis and function. We have shown that genetic deletion of *Gclc*, and therefore loss of GSH, in B cells has important and subset-specific effects in terminally differentiated B cells. Our data further indicate that GSH acts as a rheostat to regulate mitochondrial function and ETC activity in B cells and determines the metabolic properties of MZB vs. FoB.

Postnatal B cell development occurs in the BM. Here, the differentiation pathway from hematopoietic progenitors to mature B cells can be divided into discrete stages (Hardy et al., 1991; Hardy and Hayakawa, 2001). Previous analysis has shown that B cells progression through the different maturation stages is regulated by pre-BCR and BCR signals (Loffert et al., 1994). Our analysis has shown that deletion of *Gclc* upon expression of *Mb1*, which occurs before the B cell's commitment decision (at the CLP stage), did not alter BM development. This finding raises the question about how antioxidants function during B cell development, and which antioxidant is active during cell proliferation in B cells, since differentiation is inherently linked to proliferation and increased metabolic demands. In particular, large pre-B cells proliferate and, although data is currently unavailable, they may increase glycolysis and OXPHOS (Urbanczyk et al., 2018). However, the microenvironment in the BM also plays a fundamental role in supporting B cell transition to the naïve stage (Carsetti, 2000). Therefore, it is possible that the plasticity of the BM microenvironment regulates the function or number of stromal cells, which are

able to produce survival factors, such as IL-7, and, eventually, allow a normal progression of B cell differentiation in the absence of GSH. Alternatively, other antioxidants systems might be as well able to exert compensatory mechanisms allowing the normal B cell development in the BM of *Gclc*$^{fl/fl}$ *Mb1-Cre*$^{+}$ mice.

B cells leave the BM at the transitional B cell stage and complete their final development into mature B cells in the periphery (Loder et al., 1999). In the spleen, *Gclc*$^{fl/fl}$ *Mb1-Cre*$^{+}$ lack MZB, which are necessary for the early humoral response to blood borne pathogens. On the other hand, FoB were only mildly affected by the absence of GSH at the steady state.

The intracellular environment of MZB operates at a higher oxidative level compared to that in FoB. GSH is essential to sustain MZB homeostasis, and these cells are more sensitive to any uncontrolled increase in intracellular ROS. This effect might also be linked to the peculiar positioning of MZB in the spleen marginal zone compared to FoB. Indeed, the marginal zone receives blood from the terminal arterioles (Kraal, 1992), thus exposing MZB to the higher O_2 blood tension. In contrast, FoB are segregated into the follicle and exhibit lower intracellular ROS, maintaining a metabolic setup that is clearly distinct from that in MZB. Notably, *Gclc* ablation increased mtROS in FoB, which then adopted characteristics of *Gclc*-sufficient MZB. This finding indicates that redox-dependent regulation of metabolic activities can occur by B cell subset-specific mechanisms. These differences in metabolism appear to be related to the divergent functions of FoB and MZB, which have been documented in numerous studies (Oliver et al., 1997; Oliver et al., 1999; Martin et al., 2001; Gunn and Brewer, 2006; Mabbott and Gray, 2014; Kleiman et al., 2015; Shi et al., 2015; Haines et al., 2019). In particular, the differences between FoB and MZB in recirculation properties when at rest (Arnon et al., 2013), and in degree of activation upon stimulation (Martin and Kearney, 2002), have raised interest in their differential

metabolic dependencies. MZB have the potential to self-renew (Hao and Rajewsky, 2001) and are activated more quickly than FoB (Oliver et al., 1997; Oliver et al., 1999), properties consistent with a requirement for glycolytic reprogramming in activated B cells (Caro-Maldonado et al., 2014). In accordance with this observation, we demonstrated that resting MZB show increased glucose uptake and glycolysis compared to resting FoB. Resting FoB are instead characterized by down-regulation of mTORC1 and its downstream targets (Benhamron and Tirosh, 2011; Farmer et al., 2019; Gaudette et al., 2020), which is indicative of metabolic quiescence. Strikingly, *Gclc* ablation increased mTORC1 activation in FoB to a level similar to that found in MZB.

Moreover, by injecting TNP-Ficoll i.p., $Gclc^{fl/fl}$ $Mb1\text{-}Cre^{+}$ animals were inefficient at producing an IgM response confirming the functional absence of MZB. Intriguingly, the sera of *Gclc*-deficient animals did not produce sufficient background signal to be detected by the ELISA assay, even before encountering the Ag. This observation led us to further investigate the Ab composition in the serum of $Gclc^{fl/fl}$ $Mb1\text{-}Cre^{+}$ animals at the steady state. As anticipated, we detected lower seric antibodies, which are normally produced as a natural defense mechanism in unimmunized animals (Ehrlich and Morgenroth, 1902). These NAs are primarily found as IgM or IgG3 isotypes, and are produced mainly by B1 cells (Lalor et al., 1989; Baumgarth et al., 1999; Durand et al., 2009; Choi et al., 2012) or, to a lesser extent by MZB (Ichikawa et al., 2015). Due to their flexible Ag-pocket binding site (Notkins, 2004; Zhou et al., 2007), NAs are capable of binding diverse microbial determinants, autoantigens, and tumor Ags (Casali and Schettino, 1996; Baumgarth et al., 2005; Vollmers and Brandlein, 2009). Published studies have shown a number of converging observations related to B1 and MZB functions (Yancopoulos et al., 1984; Martin and Kearney, 2000b; Won and Kearney, 2002; Kretschmer et al., 2003; Carey et al., 2008). Furthermore, B1 cells are also able to produce Abs against TI Ags (Martin et al.,

2001; Haas et al., 2005) and are indeed included in the innate B cell pool together with MZB. Accordingly, we found reduced B1 cells in the PEC and spleen of *Gclc*$^{fl/fl}$ *Mb1-Cre*$^{+}$ animals compared to controls, and less total NAs in the serum. Moreover, B1 cells showed comparably higher levels of mtROS when compared to B2 cells in the PEC, which recall the differences between MZB and FoB in the spleen. Similarly, total ROS were higher in MZB and B1 cells compared to FoB and PEC B2 cells. This disparity sets a definitive distinction between innate-like B cells and B2 cells in relation to ROS signaling. This might be explained by the differential activation status and BCR engagement of differentiated MZB and B1 cells (Tsubata, 2020). In summary, the deletion of *Gclc* mostly affected MZB and B1 cells, which are characterized by either lower activation threshold or constant activation associated to Ab production. Thus, the function of GSH is specifically segregated to innate-like B cells at the steady state, and appears to be correlated with the activation status of the cell. Furthermore, activation of FoB drove increased production of ROS and upregulation of *Gclc*, which indicates that GSH as a modulator of B cell activation in general.

Upregulation of metabolic pathways upon activation is necessary to generate ATP to support functions such as antibody production (Caro-Maldonado et al., 2014). This increase in metabolic activity is also associated with elevated ROS, which are also known modulators of the functions of immune cells (Mak et al., 2017; Franchina et al., 2018b; Franchina et al., 2018a; Muri and Kopf, 2020; Kurniawan et al., 2020). Metabolic ROS are generated in the mitochondria by inefficient electron transfer through the ETC (Boveris et al., 1972), and defects in the ETC have been shown to increase mtROS even further (Sena et al., 2013). Although cells benefit from low ROS levels, high ROS impose irreversible oxidative damage and so efficient ROS removal is necessary to maintain homeostasis (Finkel, 2011; Sies and Jones, 2020).

Balanced mtROS are critical for the correct function of the redox-sensitive ETC proteins, which are susceptible to inactivation by these reactive molecules (Zhang et al., 1990; Brand, 2010; Garcia et al., 2010; Wang et al., 2013; Mailloux et al., 2013). In our study, we found that activities of ETC CI and CII were reduced in GSH-deficient FoB. CI activity in particular requires adequate levels of reduced GSH in the mitochondria for its function (Balijepalli et al., 1999; Beer et al., 2004). GSH-dependent mitochondrial functions are influenced by changes in levels of cytosolic GSH because GSH is synthesized in the cytosol and must be imported into the mitochondria to exert its function as antioxidant (Martensson et al., 1990; Masini et al., 1992). In addition to decreased CI, we found compromised CII activity in *Gclc*-deficient FoB cells. Reduced CII activity has consequences for central carbon metabolism because CII is involved in the conversion of succinate to fumarate within the TCA cycle (Martinez-Reyes and Chandel, 2020). Our glucose carbon tracing experiments showed that *Gclc* deficiency led to an accumulation of M2-succinate, indicating a block in the TCA cycle. Interestingly, M2-succinate appears to accumulate only in *Gclc*-deficient B cells and not in *Gclc*-deficient effector T cells nor Tregs (Mak et al., 2017; Kurniawan et al., 2020). This result identifies an unexpected B cell-specific function of GSH in the regulation of the TCA cycle and the ETC.

Based on the results above, we theorize that GSH preserves basal ETC functionality in MZB but not in FoB at steady state (Figure 34). Alterations of redox metabolism have been previously shown to have deleterious effects on MZB but not on FoB (Muri et al., 2019; Muri and Kopf, 2020). These findings support the notion that differential redox capacity exists in different B cell subsets, and suggest that steady-state MZB require greater redox buffering capacity. Our data have revealed that MZB and FoB rely on activities that differ in their dependence on GSH. Accordingly, deletion of *Gclc* in B cells leads to a specific loss of MZB but not FoB. We have shown that GSH modulates redox functions in steady-

state B cells in a subset-specific manner, adding a new element of complexity to the distinct homeostatic properties of FoB and MZB (Martin and Kearney, 2002; Pillai et al., 2005; Cerutti et al., 2013). Given that B1 cells share common features with MZB, it is reasonable to postulate that *Gclc* deficiency has a similar impact on the metabolism of B1 cells. However, this mechanistic analogy is speculative and cannot be concluded by the results presented here.

In support of the binary function of GSH depending on the activation status, we have also found that activated FoB upregulate *Gclc* and their demand for GSH increases to cope with accumulating ROS. BCR engagement is often associated with non-metabolic ROS signaling (Tsubata, 2020). ROS scavenging upon BCR ligation was shown to dampen B cell activation and proliferation (Wheeler and Defranco, 2012; Tsubata, 2020), indicating that BCR-induced ROS regulates BCR signaling and cellular activation. In $Gclc^{fl/fl}$ *Mb1-*Cre^{+} mice, GSH was also required for the *in vivo* activation of FoB in T cell-dependent infection models. Indeed, our data clearly showed that FoB of $Gclc^{fl/fl}$ *Mb1-*Cre^{+} mice could not ensure GC formation and antibody-mediated protection following Ag challenge *in vivo*. Contrary to BCR-induced ROS, these data suggest that increased or accumulated mtROS do not promote B cell activation.

The deleterious effect of GSH deletion on the humoral immune response was exacerbated upon VSV infection, resulting in the reduced survival of infected $Gclc^{fl/fl}$ *Mb1-*Cre^{+} mice. In this case, the more acute inflammation induced by the T cell response during VSV infection disproved the possibility of increased activation threshold induced by *Gclc* deletion in FoB. Concomitantly, impaired activation was followed by the inability to produce antibodies upon VSV infection. Importantly, the lower survival of $Gclc^{fl/fl}$ *Mb1-*Cre^{+} mice highlights the crucial role of innate-like B cells (MZB and B1 cells) during the early phases of the viral infection. The lack of rapid Abs response and low-affinity Abs in

Gclc$^{fl/fl}$ *Mb1-Cre*$^{+}$ mice made them more vulnerable to VSV compared to controls. These results suggest that GSH is not only necessary for MZB homeostasis, but it has a pivotal role for FoB cell activation.

It is important to note that despite the higher mTORC1 signaling in *Gclc*-deficient FoB cells, *Gclc*$^{fl/fl}$ *Mb1-Cre*$^{+}$ mice did not mount efficient Ab responses against LCMV nor VSV. On the contrary, mTORC1 signaling upregulation was found to be dispensable for GC formation and serum antibody responses (Ci et al., 2015). Thus, these findings further indicate that mTORC1 signaling upregulation is a consequence of GSH depletion and does not promote humoral immunity, as a reflection of the FoB ability to metabolically adapt to oxidative stress.

Despite the crucial role of GSH in murine B cell biology, the contribution of GSH in human B cells is not well characterized. However, previous research have shown that intracellular GSH levels of B cells of HIV-1-infected individuals showed a tendency to be decreased compared to uninfected donors (Staal et al., 1992c; Staal et al., 1992a). These results highlight the important and non-redundant role of GSH in B cell functions *in vivo* and correlates with decreased GSH levels and the impairment of B cell functions during HIV-1 infection (Moir and Fauci, 2009).

In conclusion, we have shown that GSH is critical for B cell homeostasis and orchestrates the metabolism of MZB and FoB (Figure 34). GSH regulates the TCA cycle and ETC activity in a B cell-specific manner that stands in stark contrast to its function in T cells. Our work highlights B cell-specific alterations that offer novel insights for the understanding of the role of GSH in the regulation of B cell functions and defects during disease, such as viral infections.

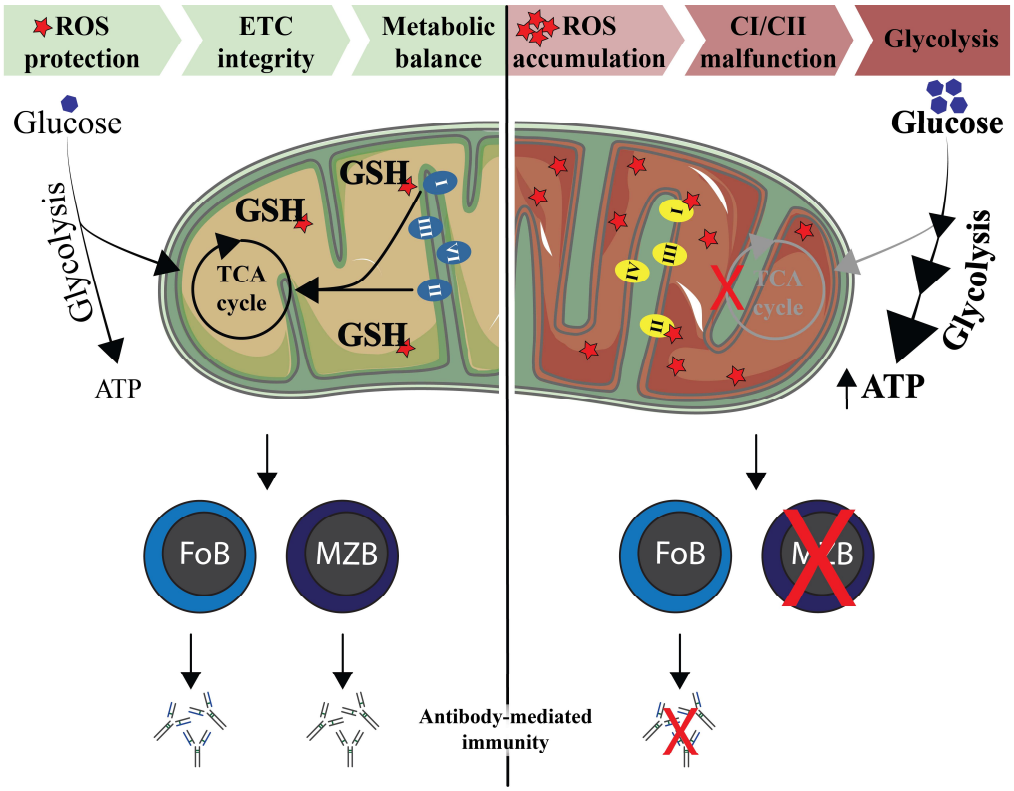

Figure 34: Glutathione-dependent redox balance defines the distinct metabolic properties of FoB and MZB.

Control of mitochondrial reactive oxygen species by the antioxidant glutathione (GSH) has a subset-specific role in murine B cells. GSH is identified as non-redundant antioxidant for the correct function of the electron transport chain (ETC), and it is required for antibody-mediated humoral immunity. In particular, Marginal Zone B cells (MZB) rely on GSH to ensure redox balance at rest. GSH is required for the ETC to work, and sustain the tricarboxylic acid (TCA) cycle. GSH-deficient Follicular B cells (FoB) show curtailed activity of complex I and II and divert glucose to glycolysis to produce ATP. Moreover, *Gclc*-deficient FoB acquire metabolic properties of wild-type MZB.

7.3 Future directions and limitations

(1) We observed that *Gclc* regulates B cell metabolism in a subset-specific manner that is clearly distinct from its function in T cells. However, it is difficult to postulate a mechanistic explanation. Notably, due to the similarity between MZB and B1, the metabolism of B1 cells deserves further efforts to investigate the role of GSH in the mitochondrial respiration. Moreover, this study focused on the main B cell subsets, and further studies on tissue-specific or rare B cell populations might lead to promising results (*i.e.* mucosal B cells, regulatory B cells).

(2) We did not validate our mouse data in human B cell subsets. It will be important to investigate whether and how GSH affects the metabolism and function of the diverse human B cell subsets. Literature reports have shown that human MZB cells possess a memory phenotype and can be found in the spleen and blood (Weill et al., 2009). Human MZB possess the ability to respond rapidly when challenged with blood borne T cell-independent antigens (Kruetzmann et al., 2003; Weller et al., 2004). These similar characteristics between mouse and human MZB potentially indicate that GSH might support human MZB metabolism in a distinct way compared to the human FOB.

(3) Our study depends on GSH depletion achieved using *in vivo* mouse models. We show that GSH depletion interferes with FoB metabolism and increases ROS and that ROS accumulation alters the electron transport chain and mitochondrial metabolism. However, we cannot exclude the possibility that other GSH-dependent, but ROS-independent, mechanisms might contribute to our findings. Moreover, deletion of *Gclc* in B cells was achieved with the constitutive *Cre* system, which does not exclude systemic compensatory adaptation, which can influence *Gclc*-deficient B cells.

(4) Although GSH is the main intracellular antioxidant, several other types of antioxidants exist. Therefore, a possibility is that FoB preferentially use or adapt to use distinct antioxidant defense mechanism throughout their development in the absence of *Gclc*.

(5) Given the important subset-specific effect of *Gclc*-ablation on splenic B cells, almost all the assays were carried out in non-activated FoB in order to decipher the steady state metabolic dependencies of FOB versus MZB. Similarly to van Anken *et al.*, a more dynamic approach could be applied on activated wild-type FOB and MZB to better understand the metabolic and antioxidant capacity during *in vitro* activation.

(6) The main function of B cells is to provide protection through the production of antibodies. For this reason we have used models that mimic the activation of specific B cell subsets. Thus, we have shown that antigen-specific activation of MZB (TNP-Ficoll) or FoB (TNP-KLH, LCMV Cl13 and VSV) in the contest of *Gclc* ablation results in a loss of function in regards to germinal center expansion and antibody production. However, other models could be used to assess the functionality of *Gclc*-deficient B cells. In particular pristane-induced lupus could be used as a model of induced systemic lupus erythematosus, a complex autoimmune disease characterized by autoantibody production and immune complex deposition followed by damage to tissues (*i.e.* kidneys). Therefore, the role of *Gclc* in the development and expansion of auto-reactive B cells as well as the production of autoantibodies can be assessed. We speculate that this experimental application may confer protection to B cell-specific *Gclc*-deficient mice against autoimmune damage (such as body weight loss and kidney lesions).

(7) In order to comprehensively address the influence of the lack of GSH on the metabolism of B cells we used the Compass algorithm, which has certain limitations. The

algorithm makes the simplifying assumption of metabolic steady state and heuristically aggregates expression of multiple genes that are linked to a reaction. Therefore, post-transcriptional and post-translational regulation are not taken into account in the analysis. Moreover, the metabolic state of a cell depends on the nutrients available in its environment, which are often poorly characterized. These computations assume a nutrient-rich environment, which may differ for MZB and FoB as they sit in distinct areas within the mouse spleen.

(8) Transcriptomic analysis using single cell resolution allowed us to distinguish different B cell subset and perform downstream analyses. However, recent advances in the field have made possible the analysis of transcriptome dynamics of cell subsets at different stage of maturation. Such unsupervised algorithms could be used to infer pseudotime trajectories and study dynamic changes in gene expression of transitional B cells versus MZB and/or FoB in the context of *Gclc* deficiency.

Publications

- Franchina, D. G., Dostert, C., Brenner, D. (2018). "Reactive Oxygen Species: Involvement in T Cell Signaling and Metabolism." *Trends in Immunology.*
- Franchina, D. G., Grusdat M., Brenner, D. (2018). "B-Cell Metabolic Remodeling and Cancer." *Trends in Cancer.*
- Franchina, D. G., He, F., Brenner, D. (2018). "Survival of the fittest: Cancer challenges T cell metabolism." *Cancer Letters.*
- Kurniawan, H., Franchina, D. G., Guerra, L., Bonetti, L., Baguet, L. S., Grusdat, M., Schlicker, L., Hunewald, O., Dostert, C., Merz, M. P., Binsfeld, C., Duncan, G. S., Farinelle, S., Nonnenmacher, Y., Haight, J., Das Gupta, D., Ewen, A., Taskesen, R., Halder, R., Chen, Y., Jager, C., Ollert, M., Wilmes, P., Vasiliou, V., Harris, I. S., Knobbe-Thomsen, C. B., Turner, J. D., Mak, T. W., Lohoff, M., Meiser, J., Hiller, K., Brenner, D. (2020). "Glutathione Restricts Serine Metabolism to Preserve Regulatory T Cell Function." *Cell Metabolism.*
- Sipol, A., Hameister, E., Xue, B., Hofstetter, J., Barenboim, M., Ollinger, R., Jain, G., Prexler, C., Rubio, R. A., Baldauf, M. C., Franchina, D. G., Petry, A., Schmah, J., Thiel, U., Gorlach, A., Cario, G., Brenner, D., Richter, G., Grunewald, T. G. P., Rad, R., Wolf, E., Ruland, J., Sorensen, P. H., Burdach, S. E. G. (2021). "MondoA Drives B-ALL Malignancy through Enhanced Adaptation to Metabolic Stress." *Blood.*

References

- Aguzzi, A., Kranich, J., and Krautler, N.J. (2014). Follicular dendritic cells: origin, phenotype, and function in health and disease. Trends Immunol *35*, 105-113.
- Ahmed, R., and Gray, D. (1996). Immunological memory and protective immunity: understanding their relation. Science *272*, 54-60.
- Ahmed, R., Salmi, A., Butler, L.D., Chiller, J.M., and Oldstone, M.B. (1984). Selection of genetic variants of lymphocytic choriomeningitis virus in spleens of persistently infected mice. Role in suppression of cytotoxic T lymphocyte response and viral persistence. J Exp Med *160*, 521-540.
- Akira, S., Uematsu, S., and Takeuchi, O. (2006). Pathogen recognition and innate immunity. Cell *124*, 783-801.
- Akkaya, M., Traba, J., Roesler, A.S., Miozzo, P., Akkaya, B., Theall, B.P., Sohn, H., Pena, M., Smelkinson, M., Kabat, J.*, et al.* (2018). Second signals rescue B cells from activation-induced mitochondrial dysfunction and death. Nat Immunol *19*, 871-884.
- Allen, C.D., Ansel, K.M., Low, C., Lesley, R., Tamamura, H., Fujii, N., and Cyster, J.G. (2004). Germinal center dark and light zone organization is mediated by CXCR4 and CXCR5. Nat Immunol *5*, 943-952.
- Allende, M.L., Tuymetova, G., Lee, B.G., Bonifacino, E., Wu, Y.P., and Proia, R.L. (2010). S1P1 receptor directs the release of immature B cells from bone marrow into blood. J Exp Med *207*, 1113-1124.
- Allman, D., and Pillai, S. (2008). Peripheral B cell subsets. Curr Opin Immunol *20*, 149-157.

- Allman, D., Lindsley, R.C., DeMuth, W., Rudd, K., Shinton, S.A., and Hardy, R.R. (2001). Resolution of three nonproliferative immature splenic B cell subsets reveals multiple selection points during peripheral B cell maturation. J Immunol *167*, 6834-6840.
- Amulic, B., Cazalet, C., Hayes, G.L., Metzler, K.D., and Zychlinsky, A. (2012). Neutrophil function: from mechanisms to disease. Annu Rev Immunol *30*, 459-489.
- Ansel, K.M., Ngo, V.N., Hyman, P.L., Luther, S.A., Forster, R., Sedgwick, J.D., Browning, J.L., Lipp, M., and Cyster, J.G. (2000). A chemokine-driven positive feedback loop organizes lymphoid follicles. Nature *406*, 309-314.
- Arnold, L.W., Pennell, C.A., McCray, S.K., and Clarke, S.H. (1994). Development of B-1 cells: segregation of phosphatidyl choline-specific B cells to the B-1 population occurs after immunoglobulin gene expression. J Exp Med *179*, 1585-1595.
- Arnon, T.I., and Cyster, J.G. (2014). Blood, sphingosine-1-phosphate and lymphocyte migration dynamics in the spleen. Curr Top Microbiol Immunol *378*, 107-128.
- Arnon, T.I., Horton, R.M., Grigorova, I.L., and Cyster, J.G. (2013). Visualization of splenic marginal zone B-cell shuttling and follicular B-cell egress. Nature *493*, 684-688.
- Artyomov, M.N., and Van den Bossche, J. (2020). Immunometabolism in the Single-Cell Era. Cell Metab *32*, 710-725.
- Avrameas, S. (1991). Natural autoantibodies: from 'horror autotoxicus' to 'gnothi seauton'. Immunology Today *12*, 154-159.
- Babcock, G.T. (1999). How oxygen is activated and reduced in respiration. Proc Natl Acad Sci U S A *96*, 12971-12973.
- Baccala, R., Gonzalez-Quintial, R., Lawson, B.R., Stern, M.E., Kono, D.H., Beutler, B., and Theofilopoulos, A.N. (2009). Sensors of the innate immune system: their mode of action. Nat Rev Rheumatol *5*, 448-456.

- Balijepalli, S., Annepu, J., Boyd, M.R., and Ravindranath, V. (1999). Effect of thiol modification on brain mitochondrial complex I activity. Neuroscience Letters *272*, 203-206.
- Bannai, S., and Tateishi, N. (1986). Role of membrane transport in metabolism and function of glutathione in mammals. J Membr Biol *89*, 1-8.
- Batista, F.D., and Harwood, N.E. (2009). The who, how and where of antigen presentation to B cells. Nat Rev Immunol *9*, 15-27.
- Battegay, M., Cooper, S., Althage, A., Banziger, J., Hengartner, H., and Zinkernagel, R.M. (1991a). Quantification of lymphocytic choriomeningitis virus with an immunological focus assay in 24- or 96-well plates. J Virol Methods *33*, 191-198.
- Battegay, M., Cooper, S., Althage, A., Bänziger, J., Hengartner, H., and Zinkernagel, R.M. (1991b). Quantification of lymphocytic choriomeningitis virus with an immunological focus assay in 24- or 96-well plates. Journal of Virological Methods *33*, 191-198.
- Baumgarth, N. (2016). B-1 Cell Heterogeneity and the Regulation of Natural and Antigen-Induced IgM Production. Front Immunol *7*, 324.
- Baumgarth, N., Tung, J.W., and Herzenberg, L.A. (2005). Inherent specificities in natural antibodies: a key to immune defense against pathogen invasion. Springer Semin Immunopathol *26*, 347-362.
- Baumgarth, N., Herman, O.C., Jager, G.C., Brown, L., Herzenberg, L.A., and Herzenberg, L.A. (1999). Innate and acquired humoral immunities to influenza virus are mediated by distinct arms of the immune system. Proc Natl Acad Sci U S A *96*, 2250-2255.

- Beer, S.M., Taylor, E.R., Brown, S.E., Dahm, C.C., Costa, N.J., Runswick, M.J., and Murphy, M.P. (2004). Glutaredoxin 2 catalyzes the reversible oxidation and glutathionylation of mitochondrial membrane thiol proteins: implications for mitochondrial redox regulation and antioxidant DEFENSE. J Biol Chem *279*, 47939-47951.
- Benhamron, S., and Tirosh, B. (2011). Direct activation of mTOR in B lymphocytes confers impairment in B-cell maturation and loss of marginal zone B cells. Eur J Immunol *41*, 2390-2396.
- Berek, C., Berger, A., and Apel, M. (1991). Maturation of the immune response in germinal centers. Cell *67*, 1121-1129.
- Berland, R., and Wortis, H.H. (2002). Origins and functions of B-1 cells with notes on the role of CD5. Annu Rev Immunol *20*, 253-300.
- Bertolotti, M., Yim, S.H., Garcia-Manteiga, J.M., Masciarelli, S., Kim, Y.J., Kang, M.H., Iuchi, Y., Fujii, J., Vene, R., Rubartelli, A*., et al.* (2010). B- to plasma-cell terminal differentiation entails oxidative stress and profound reshaping of the antioxidant responses. Antioxid Redox Signal *13*, 1133-1144.
- Beumer, J. (1962). Jules Bordet 1870-1961. Journal of General Microbiology *29*, 1-13.
- Beutler, B.A. (2009). TLRs and innate immunity. Blood *113*, 1399-1407.
- Bibb, M.J., Van Etten, R.A., Wright, C.T., Walberg, M.W., and Clayton, D.A. (1981). Sequence and gene organization of mouse mitochondrial DNA. Cell *26*, 167-180.
- Binder, C.J., and Silverman, G.J. (2005). Natural antibodies and the autoimmunity of atherosclerosis. Springer Semin Immunopathol *26*, 385-404.
- Birben, E., Sahiner, U.M., Sackesen, C., Erzurum, S., and Kalayci, O. (2012). Oxidative stress and antioxidant defense. World Allergy Organ J *5*, 9-19.

- Bonora, M., Patergnani, S., Rimessi, A., De Marchi, E., Suski, J.M., Bononi, A., Giorgi, C., Marchi, S., Missiroli, S., Poletti, F.*, et al.* (2012). ATP synthesis and storage. Purinergic Signal *8*, 343-357.
- Boothby, M., and Rickert, R.C. (2017). Metabolic Regulation of the Immune Humoral Response. Immunity *46*, 743-755.
- Borges da Silva, H., Fonseca, R., Pereira, R.M., Cassado Ados, A., Alvarez, J.M., and D'Imperio Lima, M.R. (2015). Splenic Macrophage Subsets and Their Function during Blood-Borne Infections. Front Immunol *6*, 480.
- Borrow, P., Evans, C.F., and Oldstone, M.B. (1995). Virus-induced immunosuppression: immune system-mediated destruction of virus-infected dendritic cells results in generalized immune suppression. J Virol *69*, 1059-1070.
- Bottazzi, B., Doni, A., Garlanda, C., and Mantovani, A. (2010). An integrated view of humoral innate immunity: pentraxins as a paradigm. Annu Rev Immunol *28*, 157-183.
- Boveris, A., Oshino, N., and Chance, B. (1972). The cellular production of hydrogen peroxide. Biochem J *128*, 617-630.
- Boyland, E., and Chasseaud, L.F. (1969). The role of glutathione and glutathione S-transferases in mercapturic acid biosynthesis. Adv Enzymol Relat Areas Mol Biol *32*, 173-219.
- Brand, M.D. (1990). The proton leak across the mitochondrial inner membrane. Biochimica et Biophysica Acta (BBA) - Bioenergetics *1018*, 128-133.
- Brand, M.D. (2010). The sites and topology of mitochondrial superoxide production. Exp Gerontol *45*, 466-472.
- Bratton, D.L., Fadok, V.A., Richter, D.A., Kailey, J.M., Guthrie, L.A., and Henson, P.M. (1997). Appearance of phosphatidylserine on apoptotic cells requires calcium-

mediated nonspecific flip-flop and is enhanced by loss of the aminophospholipid translocase. J Biol Chem *272*, 26159-26165.

- Bretscher, P.A. (1999). A two-step, two-signal model for the primary activation of precursor helper T cells. Proceedings of the National Academy of Sciences *96*, 185-190.
- Brigelius-Flohe, R., and Maiorino, M. (2013). Glutathione peroxidases. Biochim Biophys Acta *1830*, 3289-3303.
- Briles, D.E., Nahm, M., Schroer, K., Davie, J., Baker, P., Kearney, J., and Barletta, R. (1981). Antiphosphocholine antibodies found in normal mouse serum are protective against intravenous infection with type 3 streptococcus pneumoniae. J Exp Med *153*, 694-705.
- Brown, G.C., Lakin-Thomas, P.L., and Brand, M.D. (1990). Control of respiration and oxidative phosphorylation in isolated rat liver cells. Eur J Biochem *192*, 355-362.
- Buck, M.D., O'Sullivan, D., Klein Geltink, R.I., Curtis, J.D., Chang, C.H., Sanin, D.E., Qiu, J., Kretz, O., Braas, D., van der Windt, G.J*., et al.* (2016). Mitochondrial Dynamics Controls T Cell Fate through Metabolic Programming. Cell *166*, 63-76.
- Burbage, M., Gasparrini, F., Aggarwal, S., Gaya, M., Arnold, J., Nair, U., Way, M., Bruckbauer, A., and Batista, F.D. (2018). Tuning of in vivo cognate B-T cell interactions by Intersectin 2 is required for effective anti-viral B cell immunity. Elife *7*.
- Burnet, F.M. (1959). The Clonal Selection Theory of Acquired Immunity. Cambridge University Press, Cambridge, UK.
- Cairns, R.A., Harris, I.S., and Mak, T.W. (2011). Regulation of cancer cell metabolism. Nat Rev Cancer *11*, 85-95.

- Carey, J.B., Moffatt-Blue, C.S., Watson, L.C., Gavin, A.L., and Feeney, A.J. (2008). Repertoire-based selection into the marginal zone compartment during B cell development. J Exp Med *205*, 2043-2052.
- Cariappa, A., Liou, H.C., Horwitz, B.H., and Pillai, S. (2000). Nuclear factor kappa B is required for the development of marginal zone B lymphocytes. J Exp Med *192*, 1175-1182.
- Cariappa, A., Boboila, C., Moran, S.T., Liu, H., Shi, H.N., and Pillai, S. (2007). The recirculating B cell pool contains two functionally distinct, long-lived, posttransitional, follicular B cell populations. J Immunol *179*, 2270-2281.
- Caro-Maldonado, A., Wang, R., Nichols, A.G., Kuraoka, M., Milasta, S., Sun, L.D., Gavin, A.L., Abel, E.D., Kelsoe, G., Green, D.R.*, et al.* (2014). Metabolic reprogramming is required for antibody production that is suppressed in anergic but exaggerated in chronically BAFF-exposed B cells. J Immunol *192*, 3626-3636.
- Caroll, M.C., and Prodeus, A.P. (1998). Linkages of innate and adaptive immunity. Current Opinion in Immunology *10*, 36-40.
- Carsetti, R. (2000). The development of B cells in the bone marrow is controlled by the balance between cell-autonomous mechanisms and signals from the microenvironment. J Exp Med *191*, 5-8.
- Carsetti, R., Kohler, G., and Lamers, M.C. (1995). Transitional B cells are the target of negative selection in the B cell compartment. J Exp Med *181*, 2129-2140.
- Casali, P., and Schettino, E.W. (1996). Structure and function of natural antibodies. Curr Top Microbiol Immunol *210*, 167-179.
- Cenci, S., and Sitia, R. (2007). Managing and exploiting stress in the antibody factory. FEBS Lett *581*, 3652-3657.

- Cerutti, A., Cols, M., and Puga, I. (2013). Marginal zone B cells: virtues of innate-like antibody-producing lymphocytes. Nat Rev Immunol *13*, 118-132.
- Chance, B., and Williams, G.R. (1955a). Respiratory enzymes in oxidative phosphorylation. II. Difference spectra. J Biol Chem *217*, 395-407.
- Chance, B., and Williams, G.R. (1955b). Respiratory enzymes in oxidative phosphorylation. III. The steady state. J Biol Chem *217*, 409-427.
- Chance, B., and Williams, G.R. (1956). Respiratory Enzymes in Oxidative Phosphorylation. Journal of Biological Chemistry *221*, 477-489.
- Chappell, C.P., Draves, K.E., Giltiay, N.V., and Clark, E.A. (2012). Extrafollicular B cell activation by marginal zone dendritic cells drives T cell-dependent antibody responses. J Exp Med *209*, 1825-1840.
- Chen, Y., Shertzer, H.G., Schneider, S.N., Nebert, D.W., and Dalton, T.P. (2005a). Glutamate cysteine ligase catalysis: dependence on ATP and modifier subunit for regulation of tissue glutathione levels. J Biol Chem *280*, 33766-33774.
- Chen, Y., Pikkarainen, T., Elomaa, O., Soininen, R., Kodama, T., Kraal, G., and Tryggvason, K. (2005b). Defective microarchitecture of the spleen marginal zone and impaired response to a thymus-independent type 2 antigen in mice lacking scavenger receptors MARCO and SR-A. J Immunol *175*, 8173-8180.
- Chen, Y., Yang, Y., Miller, M.L., Shen, D., Shertzer, H.G., Stringer, K.F., Wang, B., Schneider, S.N., Nebert, D.W., and Dalton, T.P. (2007). Hepatocyte-specific Gclc deletion leads to rapid onset of steatosis with mitochondrial injury and liver failure. Hepatology *45*, 1118-1128.

- Choi, S.W., Gerencser, A.A., and Nicholls, D.G. (2009). Bioenergetic analysis of isolated cerebrocortical nerve terminals on a microgram scale: spare respiratory capacity and stochastic mitochondrial failure. J Neurochem *109*, 1179-1191.
- Choi, Y.S., Dieter, J.A., Rothaeusler, K., Luo, Z., and Baumgarth, N. (2012). B-1 cells in the bone marrow are a significant source of natural IgM. Eur J Immunol *42*, 120-129.
- Chung, J.B., Silverman, M., and Monroe, J.G. (2003). Transitional B cells: step by step towards immune competence. Trends in Immunology *24*, 342-348.
- Ci, X., Kuraoka, M., Wang, H., Carico, Z., Hopper, K., Shin, J., Deng, X., Qiu, Y., Unniraman, S., Kelsoe, G*., et al.* (2015). TSC1 Promotes B Cell Maturation but Is Dispensable for Germinal Center Formation. PLoS One *10*, e0127527.
- Cinamon, G., Zachariah, M.A., Lam, O.M., Foss, F.W., Jr., and Cyster, J.G. (2008). Follicular shuttling of marginal zone B cells facilitates antigen transport. Nat Immunol *9*, 54-62.
- Cinamon, G., Matloubian, M., Lesneski, M.J., Xu, Y., Low, C., Lu, T., Proia, R.L., and Cyster, J.G. (2004). Sphingosine 1-phosphate receptor 1 promotes B cell localization in the splenic marginal zone. Nat Immunol *5*, 713-720.
- Cooper, M.D., Peterson, R.D., and Good, R.A. (1965). Delineation of the Thymic and Bursal Lymphoid Systems in the Chicken. Nature *205*, 143-146.
- Cornall, R.J., Goodnow, C.C., and Cyster, J.G. (1995). The regulation of self-reactive B cells. Current Opinion in Immunology *7*, 804-811.
- Cossarizza, A., Ferraresi, R., Troiano, L., Roat, E., Gibellini, L., Bertoncelli, L., Nasi, M., and Pinti, M. (2009). Simultaneous analysis of reactive oxygen species and reduced glutathione content in living cells by polychromatic flow cytometry. Nat Protoc *4*, 1790-1797.

- Cossarizza, A., Chang, H.D., Radbruch, A., Acs, A., Adam, D., Adam-Klages, S., Agace, W.W., Aghaeepour, N., Akdis, M., Allez, M.*, et al.* (2019). Guidelines for the use of flow cytometry and cell sorting in immunological studies (second edition). Eur J Immunol *49*, 1457-1973.
- Cua, D.J., Sherlock, J., Chen, Y., Murphy, C.A., Joyce, B., Seymour, B., Lucian, L., To, W., Kwan, S., Churakova, T.*, et al.* (2003). Interleukin-23 rather than interleukin-12 is the critical cytokine for autoimmune inflammation of the brain. Nature *421*, 744-748.
- Cui, Z., and Houweling, M. (2002). Phosphatidylcholine and cell death. Biochimica et Biophysica Acta (BBA) - Molecular and Cell Biology of Lipids *1585*, 87-96.
- Dalton, T.P., Chen, Y., Schneider, S.N., Nebert, D.W., and Shertzer, H.G. (2004). Genetically altered mice to evaluate glutathione homeostasis in health and disease. Free Radic Biol Med *37*, 1511-1526.
- Dambuza, I.M., and Brown, G.D. (2015). C-type lectins in immunity: recent developments. Curr Opin Immunol *32*, 21-27.
- Dempsey, P.W., Allison, M.E., Akkaraju, S., Goodnow, C.C., and Fearon, D.T. (1996). C3d of complement as a molecular adjuvant: bridging innate and acquired immunity. Science *271*, 348-350.
- Deponte, M. (2013). Glutathione catalysis and the reaction mechanisms of glutathione-dependent enzymes. Biochim Biophys Acta *1830*, 3217-3266.
- Di Gioia, M., Spreafico, R., Springstead, J.R., Mendelson, M.M., Joehanes, R., Levy, D., and Zanoni, I. (2020). Endogenous oxidized phospholipids reprogram cellular metabolism and boost hyperinflammation. Nat Immunol *21*, 42-53.
- DiLillo, D.J., Horikawa, M., and Tedder, T.F. (2011). B-lymphocyte effector functions in health and disease. Immunol Res *49*, 281-292.

- Dobzhansky, T. (1973). Nothing in Biology Makes Sense except in the Light of Evolution. The American Biology Teacher *35*, 125-129.
- Donahue, A.C., and Fruman, D.A. (2007). Distinct signaling mechanisms activate the target of rapamycin in response to different B-cell stimuli. Eur J Immunol *37*, 2923-2936.
- Doyle, A., McGarry, M.P., Lee, N.A., and Lee, J.J. (2012). The construction of transgenic and gene knockout/knockin mouse models of human disease. Transgenic Res *21*, 327-349.
- Droge, W., Pottmeyer-Gerber, C., Schmidt, H., and Nick, S. (1986). Glutathione augments the activation of cytotoxic T lymphocytes in vivo. Immunobiology *172*, 151-156.
- Durand, C.A., Hartvigsen, K., Fogelstrand, L., Kim, S., Iritani, S., Vanhaesebroeck, B., Witztum, J.L., Puri, K.D., and Gold, M.R. (2009). Phosphoinositide 3-kinase p110 delta regulates natural antibody production, marginal zone and B-1 B cell function, and autoantibody responses. J Immunol *183*, 5673-5684.
- Eberl, G., Colonna, M., Di Santo, J.P., and McKenzie, A.N. (2015). Innate lymphoid cells. Innate lymphoid cells: a new paradigm in immunology. Science *348*, aaa6566.
- Ehrlich, P., and Morgenroth, J. (1902). Die Seitenkettentheorie der Immunität. Anleitung zu hygienischen Untersuchungen: nach den im Hygienischen Institut der königl. Ludwig-Maximilians-Universität zu München üblichen Methoden zusammengestellt, 381–394.
- Ernster, L., and Schatz, G. (1981). Mitochondria: a historical review. J Cell Biol *91*, 227s-255s.

- Espinosa-Diez, C., Miguel, V., Mennerich, D., Kietzmann, T., Sanchez-Perez, P., Cadenas, S., and Lamas, S. (2015). Antioxidant responses and cellular adjustments to oxidative stress. Redox Biol *6*, 183-197.
- Esplin, B.L., Welner, R.S., Zhang, Q., Borghesi, L.A., and Kincade, P.W. (2009). A differentiation pathway for B1 cells in adult bone marrow. Proc Natl Acad Sci U S A *106*, 5773-5778.
- Esteve, J.M., Mompo, J., Garcia de la Asuncion, J., Sastre, J., Asensi, M., Boix, J., Vina, J.R., Vina, J., and Pallardo, F.V. (1999). Oxidative damage to mitochondrial DNA and glutathione oxidation in apoptosis: studies in vivo and in vitro. FASEB J *13*, 1055-1064.
- Farmer, J.R., Allard-Chamard, H., Sun, N., Ahmad, M., Bertocchi, A., Mahajan, V.S., Aicher, T., Arnold, J., Benson, M.D., Morningstar, J.*, et al.* (2019). Induction of metabolic quiescence defines the transitional to follicular B cell switch. Sci Signal *12*.
- Feeney, A.J. (1990). Lack of N regions in fetal and neonatal mouse immunoglobulin V-D-J junctional sequences. J Exp Med *172*, 1377-1390.
- Ferguson, A.R., Youd, M.E., and Corley, R.B. (2004). Marginal zone B cells transport and deposit IgM-containing immune complexes onto follicular dendritic cells. Int Immunol *16*, 1411-1422.
- Fernandes, A.P., and Holmgren, A. (2004). Glutaredoxins: glutathione-dependent redox enzymes with functions far beyond a simple thioredoxin backup system. Antioxid Redox Signal *6*, 63-74.
- Fidelus, R.K., and Tsan, M.F. (1986). Enhancement of intracellular glutathione promotes lymphocyte activation by mitogen. Cell Immunol *97*, 155-163.
- Finkel, T. (2011). Signal transduction by reactive oxygen species. J Cell Biol *194*, 7-15.

- Flannagan, R.S., Cosio, G., and Grinstein, S. (2009). Antimicrobial mechanisms of phagocytes and bacterial evasion strategies. Nat Rev Microbiol *7*, 355-366.
- Forman, H.J., Fukuto, J.M., and Torres, M. (2004). Redox signaling: thiol chemistry defines which reactive oxygen and nitrogen species can act as second messengers. Am J Physiol Cell Physiol *287*, C246-256.
- Forman, H.J., Zhang, H., and Rinna, A. (2009). Glutathione: overview of its protective roles, measurement, and biosynthesis. Mol Aspects Med *30*, 1-12.
- Franchina, D.G., Dostert, C., and Brenner, D. (2018a). Reactive Oxygen Species: Involvement in T Cell Signaling and Metabolism. Trends Immunol *39*, 489-502.
- Franchina, D.G., Grusdat, M., and Brenner, D. (2018b). B-Cell Metabolic Remodeling and Cancer. Trends Cancer *4*, 138-150.
- Friedman, J.R., and Nunnari, J. (2014). Mitochondrial form and function. Nature *505*, 335-343.
- Fujinami, R.S., von Herrath, M.G., Christen, U., and Whitton, J.L. (2006). Molecular mimicry, bystander activation, or viral persistence: infections and autoimmune disease. Clin Microbiol Rev *19*, 80-94.
- Garcia, J., Han, D., Sancheti, H., Yap, L.P., Kaplowitz, N., and Cadenas, E. (2010). Regulation of mitochondrial glutathione redox status and protein glutathionylation by respiratory substrates. J Biol Chem *285*, 39646-39654.
- Garside, P., Ingulli, E., Merica, R.R., Johnson, J.G., Noelle, R.J., and Jenkins, M.K. (1998). Visualization of specific B and T lymphocyte interactions in the lymph node. Science *281*, 96-99.

- Gaudette, B.T., Jones, D.D., Bortnick, A., Argon, Y., and Allman, D. (2020). mTORC1 coordinates an immediate unfolded protein response-related transcriptome in activated B cells preceding antibody secretion. Nat Commun *11*, 723.
- Gavin, A.L., Hoebe, K., Duong, B., Ota, T., Martin, C., Beutler, B., and Nemazee, D. (2006). Adjuvant-enhanced antibody responses in the absence of toll-like receptor signaling. Science *314*, 1936-1938.
- Girkontaite, I., Missy, K., Sakk, V., Harenberg, A., Tedford, K., Potzel, T., Pfeffer, K., and Fischer, K.D. (2001). Lsc is required for marginal zone B cells, regulation of lymphocyte motility and immune responses. Nat Immunol *2*, 855-862.
- Goodwin, R.G., Lupton, S., Schmierer, A., Hjerrild, K.J., Jerzy, R., Clevenger, W., Gillis, S., Cosman, D., and Namen, A.E. (1989). Human interleukin 7: molecular cloning and growth factor activity on human and murine B-lineage cells. Proc Natl Acad Sci U S A *86*, 302-306.
- Gray, D., MacLennan, I.C., Bazin, H., and Khan, M. (1982). Migrant mu+ delta+ and static mu+ delta- B lymphocyte subsets. Eur J Immunol *12*, 564-569.
- Guinamard, R., Okigaki, M., Schlessinger, J., and Ravetch, J.V. (2000). Absence of marginal zone B cells in Pyk-2-deficient mice defines their role in the humoral response. Nat Immunol *1*, 31-36.
- Gunn, K.E., and Brewer, J.W. (2006). Evidence that marginal zone B cells possess an enhanced secretory apparatus and exhibit superior secretory activity. J Immunol *177*, 3791-3798.
- Haas, K.M., Poe, J.C., Steeber, D.A., and Tedder, T.F. (2005). B-1a and B-1b cells exhibit distinct developmental requirements and have unique functional roles in innate and adaptive immunity to S. pneumoniae. Immunity *23*, 7-18.

- Haas, K.M., Johnson, K.L., Phipps, J.P., and Do, C. (2018). CD22 Promotes B-1b Cell Responses to T Cell-Independent Type 2 Antigens. J Immunol *200*, 1671-1681.
- Haas, K.M., Hasegawa, M., Steeber, D.A., Poe, J.C., Zabel, M.D., Bock, C.B., Karp, D.R., Briles, D.E., Weis, J.H., and Tedder, T.F. (2002). Complement Receptors CD21/35 Link Innate and Protective Immunity during Streptococcus pneumoniae Infection by Regulating IgG3 Antibody Responses. Immunity *17*, 713-723.
- Haines, R.R., Scharer, C.D., Lobby, J.L., and Boss, J.M. (2019). LSD1 Cooperates with Noncanonical NF-kappaB Signaling to Regulate Marginal Zone B Cell Development. J Immunol *203*, 1867-1881.
- Hamilos, D.L., and Wedner, H.J. (1985). The role of glutathione in lymphocyte activation. I. Comparison of inhibitory effects of buthionine sulfoximine and 2-cyclohexene-1-one by nuclear size transformation. J Immunol *135*, 2740-2747.
- Hamilos, D.L., Zelarney, P., and Mascali, J.J. (1989). Lymphocyte proliferation in glutathione-depleted lymphocytes: direct relationship between glutathione availability and the proliferative response. Immunopharmacology *18*, 223-235.
- Hangartner, L., Zinkernagel, R.M., and Hengartner, H. (2006). Antiviral antibody responses: the two extremes of a wide spectrum. Nat Rev Immunol *6*, 231-243.
- Hao, Z., and Rajewsky, K. (2001). Homeostasis of peripheral B cells in the absence of B cell influx from the bone marrow. J Exp Med *194*, 1151-1164.
- Haque, A., Engel, J., Teichmann, S.A., and Lonnberg, T. (2017). A practical guide to single-cell RNA-sequencing for biomedical research and clinical applications. Genome Med *9*, 75.
- Hardy, R.R., and Hayakawa, K. (1986). Development and physiology of Ly-1 B and its human homolog, Leu-1 B. Immunol Rev *93*, 53-79.

- Hardy, R.R., and Hayakawa, K. (2001). B cell development pathways. Annu Rev Immunol *19*, 595-621.
- Hardy, R.R., Carmack, C.E., Shinton, S.A., Kemp, J.D., and Hayakawa, K. (1991). Resolution and characterization of pro-B and pre-pro-B cell stages in normal mouse bone marrow. J Exp Med *173*, 1213-1225.
- Hatefi, Y. (1985). The mitochondrial electron transport and oxidative phosphorylation system. Annu Rev Biochem *54*, 1015-1069.
- Hayakawa, K., Hardy, R.R., Parks, D.R., and Herzenberg, L.A. (1983). The "Ly-1 B" cell subpopulation in normal immunodefective, and autoimmune mice. J Exp Med *157*, 202-218.
- Hayakawa, K., Hardy, R.R., Herzenberg, L.A., and Herzenberg, L.A. (1985). Progenitors for Ly-1 B cells are distinct from progenitors for other B cells. J Exp Med *161*, 1554-1568.
- Hayakawa, K., Li, Y.S., Wasserman, R., Sauder, S., Shinton, S., and Hardy, R.R. (1997). B lymphocyte developmental lineages. Ann N Y Acad Sci *815*, 15-29.
- Hayakawa, K., Asano, M., Shinton, S.A., Gui, M., Wen, L.J., Dashoff, J., and Hardy, R.R. (2003). Positive selection of anti-thy-1 autoreactive B-1 cells and natural serum autoantibody production independent from bone marrow B cell development. J Exp Med *197*, 87-99.
- Hayakawa, K., Asano, M., Shinton, S.A., Gui, M., Allman, D., Stewart, C.L., Silver, J., and Hardy, R.R. (1999). Positive selection of natural autoreactive B cells. Science *285*, 113-116.
- Haynes, C.M., Titus, E.A., and Cooper, A.A. (2004). Degradation of misfolded proteins prevents ER-derived oxidative stress and cell death. Mol Cell *15*, 767-776.

- Helmreich, E., Kern, M., and Eisen, H.N. (1961). The secretion of antibody by isolated lymph node cells. J Biol Chem *236*, 464-473.
- Herzenberg, L.A., and Herzenberg, L.A. (1989). Toward a layered immune system. Cell *59*, 953-954.
- Herzenberg, L.A., Stall, A.M., Lalor, P.A., Sidman, C., Moore, W.A., Parks, D.R., and Herzenberg, L.A. (1986). The Ly-1 B cell lineage. Immunol Rev *93*, 81-102.
- Herzenberg, L.A., De Rosa, S.C., Dubs, J.G., Roederer, M., Anderson, M.T., Ela, S.W., Deresinski, S.C., and Herzenberg, L.A. (1997). Glutathione deficiency is associated with impaired survival in HIV disease. Proc Natl Acad Sci U S A *94*, 1967-1972.
- Hibi, T., and Dosch, H.M. (1986). Limiting dilution analysis of the B cell compartment in human bone marrow. Eur J Immunol *16*, 139-145.
- Hill, B.G., Benavides, G.A., Lancaster, J.R., Jr., Ballinger, S., Dell'Italia, L., Jianhua, Z., and Darley-Usmar, V.M. (2012). Integration of cellular bioenergetics with mitochondrial quality control and autophagy. Biol Chem *393*, 1485-1512.
- Hobeika, E., Thiemann, S., Storch, B., Jumaa, H., Nielsen, P.J., Pelanda, R., and Reth, M. (2006). Testing gene function early in the B cell lineage in mb1-cre mice. Proc Natl Acad Sci U S A *103*, 13789-13794.
- Holmgren, A. (1976). Hydrogen donor system for Escherichia coli ribonucleoside-diphosphate reductase dependent upon glutathione. Proc Natl Acad Sci U S A *73*, 2275-2279.
- Holmgren, A., Johansson, C., Berndt, C., Lonn, M.E., Hudemann, C., and Lillig, C.H. (2005). Thiol redox control via thioredoxin and glutaredoxin systems. Biochem Soc Trans *33*, 1375-1377.

- Hwang, B., Lee, J.H., and Bang, D. (2018). Single-cell RNA sequencing technologies and bioinformatics pipelines. Exp Mol Med *50*, 1-14.
- Ichikawa, D., Asano, M., Shinton, S.A., Brill-Dashoff, J., Formica, A.M., Velcich, A., Hardy, R.R., and Hayakawa, K. (2015). Natural anti-intestinal goblet cell autoantibody production from marginal zone B cells. J Immunol *194*, 606-614.
- Inoue, T., Moran, I., Shinnakasu, R., Phan, T.G., and Kurosaki, T. (2018). Generation of memory B cells and their reactivation. Immunol Rev *283*, 138-149.
- Janeway CA Jr, Murphy K, and Weaver C (2016a). Janeway's Immunobiology. Chapter 7. Garland Science/Taylor & Francis Group, LLC.
- Janeway CA Jr, Murphy K, and Weaver C (2016b). Janeway's Immunobiology. Chapter 1. Garland Science/Taylor & Francis Group, LLC.
- Janeway CA Jr, Murphy K, and Weaver C (2016c). Janeway's Immunobiology. Chapter 8. Garland Science/Taylor & Francis Group, LLC.
- Janeway CA Jr, Murphy K, and Weaver C (2016d). Janeway's Immunobiology. Chapter 10. Garland Science/Taylor & Francis Group, LLC.
- Janeway CA Jr, Murphy K, and Weaver C (2016e). Janeway's Immunobiology. Chapter 4. Garland Science/Taylor & Francis Group, LLC.
- Janeway CA Jr, Murphy K, and Weaver C (2016f). Janeway's Immunobiology. Chapter 2. Garland Science/Taylor & Francis Group, LLC.
- Jang, K.J., Mano, H., Aoki, K., Hayashi, T., Muto, A., Nambu, Y., Takahashi, K., Itoh, K., Taketani, S., Nutt, S.L.*, et al.* (2015). Mitochondrial function provides instructive signals for activation-induced B-cell fates. Nat Commun *6*, 6750.

- Jellusova, J., Cato, M.H., Apgar, J.R., Ramezani-Rad, P., Leung, C.R., Chen, C., Richardson, A.D., Conner, E.M., Benschop, R.J., Woodgett, J.R*., et al.* (2017). Gsk3 is a metabolic checkpoint regulator in B cells. Nat Immunol *18*, 303-312.
- Kantor, A.B., Stall, A.M., Adams, S., Herzenberg, L.A., and Herzenberg, L.A. (1992). Differential development of progenitor activity for three B-cell lineages. Proc Natl Acad Sci U S A *89*, 3320-3324.
- Kaplowitz, N., Aw, T.Y., and Ookhtens, M. (1985). The regulation of hepatic glutathione. Annu Rev Pharmacol Toxicol *25*, 715-744.
- Karlsson, M.C., Guinamard, R., Bolland, S., Sankala, M., Steinman, R.M., and Ravetch, J.V. (2003). Macrophages control the retention and trafficking of B lymphocytes in the splenic marginal zone. J Exp Med *198*, 333-340.
- Kearney, J.F. (2005). Innate-like B cells. Springer Semin Immunopathol *26*, 377-383.
- Khodadadi, L., Cheng, Q., Radbruch, A., and Hiepe, F. (2019). The Maintenance of Memory Plasma Cells. Front Immunol *10*, 721.
- Kirk, S.J., Cliff, J.M., Thomas, J.A., and Ward, T.H. (2010). Biogenesis of secretory organelles during B cell differentiation. J Leukoc Biol *87*, 245-255.
- Kleiman, E., Salyakina, D., De Heusch, M., Hoek, K.L., Llanes, J.M., Castro, I., Wright, J.A., Clark, E.S., Dykxhoorn, D.M., Capobianco, E*., et al.* (2015). Distinct Transcriptomic Features are Associated with Transitional and Mature B-Cell Populations in the Mouse Spleen. Front Immunol *6*, 30.
- Kominsky, D.J., Campbell, E.L., and Colgan, S.P. (2010). Metabolic shifts in immunity and inflammation. J Immunol *184*, 4062-4068.
- Kraal, G. (1992). Cells in the marginal zone of the spleen. Int Rev Cytol *132*, 31-74.
- Krebs, H.A. (1936). Intermediate Metabolism of Carbohydrates. Nature *138*, 288-289.

- Krebs, H.A., Salvin, E., and Johnson, W.A. (1938). The formation of citric and alpha-ketoglutaric acids in the mammalian body. Biochem J *32*, 113-117.
- Kretschmer, K., Jungebloud, A., Stopkowicz, J., Kleinke, T., Hoffmann, R., and Weiss, S. (2003). The selection of marginal zone B cells differs from that of B-1a cells. J Immunol *171*, 6495-6501.
- Kruetzmann, S., Rosado, M.M., Weber, H., Germing, U., Tournilhac, O., Peter, H.H., Berner, R., Peters, A., Boehm, T., Plebani, A.*, et al.* (2003). Human immunoglobulin M memory B cells controlling Streptococcus pneumoniae infections are generated in the spleen. J Exp Med *197*, 939-945.
- Kumararatne, D.S., MacLennan, I.C., Bazin, H., and Gray, D. (1982). Marginal zones: the largest B cell compartment of the rat spleen. Adv Exp Med Biol *149*, 67-73.
- Kurniawan, H., Franchina, D.G., Guerra, L., Bonetti, L., Baguet, L.S., Grusdat, M., Schlicker, L., Hunewald, O., Dostert, C., Merz, M.P.*, et al.* (2020). Glutathione Restricts Serine Metabolism to Preserve Regulatory T Cell Function. Cell Metab *31*, 920-936 e927.
- Lalor, P.A., Herzenberg, L.A., Adams, S., and Stall, A.M. (1989). Feedback regulation of murine Ly-1 B cell development. Eur J Immunol *19*, 507-513.
- Lam, J.H., Smith, F.L., and Baumgarth, N. (2020). B Cell Activation and Response Regulation During Viral Infections. Viral Immunol.
- Lash, L.H. (2006). Mitochondrial glutathione transport: physiological, pathological and toxicological implications. Chem Biol Interact *163*, 54-67.
- LeBien, T.W., and Tedder, T.F. (2008). B lymphocytes: how they develop and function. Blood *112*, 1570-1580.

- Lefrancois, L. (1984). Protection against lethal viral infection by neutralizing and nonneutralizing monoclonal antibodies: distinct mechanisms of action in vivo. J Virol *51*, 208-214.
- Limon, J.J., and Fruman, D.A. (2012). Akt and mTOR in B Cell Activation and Differentiation. Front Immunol *3*, 228.
- Little, A.C., Kovalenko, I., Goo, L.E., Hong, H.S., Kerk, S.A., Yates, J.A., Purohit, V., Lombard, D.B., Merajver, S.D., and Lyssiotis, C.A. (2020). High-content fluorescence imaging with the metabolic flux assay reveals insights into mitochondrial properties and functions. Commun Biol *3*, 271.
- Liu, Y.J., Zhang, J., Lane, P.J., Chan, E.Y., and MacLennan, I.C. (1991). Sites of specific B cell activation in primary and secondary responses to T cell-dependent and T cell-independent antigens. Eur J Immunol *21*, 2951-2962.
- Locasale, J.W., and Cantley, L.C. (2011). Metabolic flux and the regulation of mammalian cell growth. Cell Metab *14*, 443-451.
- Loder, F., Mutschler, B., Ray, R.J., Paige, C.J., Sideras, P., Torres, R., Lamers, M.C., and Carsetti, R. (1999). B cell development in the spleen takes place in discrete steps and is determined by the quality of B cell receptor-derived signals. J Exp Med *190*, 75-89.
- Loffert, D., Schaal, S., Ehlich, A., Hardy, R.R., Zou, Y.R., Muller, W., and Rajewsky, K. (1994). Early B-cell development in the mouse: insights from mutations introduced by gene targeting. Immunol Rev *137*, 135-153.
- Lu, S.C. (2013). Glutathione synthesis. Biochim Biophys Acta *1830*, 3143-3153.
- Lu, T.T., and Cyster, J.G. (2002). Integrin-mediated long-term B cell retention in the splenic marginal zone. Science *297*, 409-412.

- Lunt, S.Y., and Vander Heiden, M.G. (2011). Aerobic glycolysis: meeting the metabolic requirements of cell proliferation. Annu Rev Cell Dev Biol *27*, 441-464.
- Ma, X.M., and Blenis, J. (2009). Molecular mechanisms of mTOR-mediated translational control. Nat Rev Mol Cell Biol *10*, 307-318.
- Mabbott, N.A., and Gray, D. (2014). Identification of co-expressed gene signatures in mouse B1, marginal zone and B2 B-cell populations. Immunology *141*, 79-95.
- MacLennan, I.C. (1994). Germinal centers. Annu Rev Immunol *12*, 117-139.
- MacLennan, I.C., Toellner, K.M., Cunningham, A.F., Serre, K., Sze, D.M., Zuniga, E., Cook, M.C., and Vinuesa, C.G. (2003). Extrafollicular antibody responses. Immunol Rev *194*, 8-18.
- Mailloux, R.J., McBride, S.L., and Harper, M.E. (2013). Unearthing the secrets of mitochondrial ROS and glutathione in bioenergetics. Trends Biochem Sci *38*, 592-602.
- Mak, T.W., Grusdat, M., Duncan, G.S., Dostert, C., Nonnenmacher, Y., Cox, M., Binsfeld, C., Hao, Z., Brustle, A., Itsumi, M.*, et al.* (2017). Glutathione Primes T Cell Metabolism for Inflammation. Immunity *46*, 675-689.
- Martensson, J., Lai, J.C., and Meister, A. (1990). High-affinity transport of glutathione is part of a multicomponent system essential for mitochondrial function. Proc Natl Acad Sci U S A *87*, 7185-7189.
- Martin, F., and Kearney, J.F. (2000a). Positive Selection from Newly Formed to Marginal Zone B Cells Depends on the Rate of Clonal Production, CD19, and btk. Immunity *12*, 39-49.
- Martin, F., and Kearney, J.F. (2000b). B-cell subsets and the mature preimmune repertoire. Marginal zone and B1 B cells as part of a "natural immune memory". Immunol Rev *175*, 70-79.

- Martin, F., and Kearney, J.F. (2002). Marginal-zone B cells. Nat Rev Immunol *2*, 323-335.
- Martin, F., Oliver, A.M., and Kearney, J.F. (2001). Marginal Zone and B1 B Cells Unite in the Early Response against T-Independent Blood-Borne Particulate Antigens. Immunity *14*, 617-629.
- Martinez-Reyes, I., and Chandel, N.S. (2020). Mitochondrial TCA cycle metabolites control physiology and disease. Nat Commun *11*, 102.
- Masciarelli, S., and Sitia, R. (2008). Building and operating an antibody factory: redox control during B to plasma cell terminal differentiation. Biochim Biophys Acta *1783*, 578-588.
- Masini, A., Ceccarelli, D., Trenti, T., Gallesi, D., and Muscatello, U. (1992). Mitochondrial inner membrane permeability changes induced by octadecadienoic acid hydroperoxide. Role of mitochondrial GSH pool. Biochim Biophys Acta *1101*, 84-89.
- Matloubian, M., Kolhekar, S.R., Somasundaram, T., and Ahmed, R. (1993). Molecular determinants of macrophage tropism and viral persistence: importance of single amino acid changes in the polymerase and glycoprotein of lymphocytic choriomeningitis virus. J Virol *67*, 7340-7349.
- Matloubian, M., Somasundaram, T., Kolhekar, S.R., Selvakumar, R., and Ahmed, R. (1990). Genetic basis of viral persistence: single amino acid change in the viral glycoprotein affects ability of lymphocytic choriomeningitis virus to persist in adult mice. J Exp Med *172*, 1043-1048.
- McGhee, J.R. (2005). The world of TH1/TH2 subsets: first proof. J Immunol *175*, 3-4.

- McIlwain, D.R., Grusdat, M., Pozdeev, V.I., Xu, H.C., Shinde, P., Reardon, C., Hao, Z., Beyer, M., Bergthaler, A., Haussinger, D.*, et al.* (2015). T-cell STAT3 is required for the maintenance of humoral immunity to LCMV. Eur J Immunol *45*, 418-427.
- Meister, A. (1988). Glutathione metabolism and its selective modification. J Biol Chem *263*, 17205-17208.
- Meister, A. (1991). Glutathione deficiency produced by inhibition of its synthesis, and its reversal; Applications in research and therapy. Pharmacology & Therapeutics *51*, 155-194.
- Meister, A., and Anderson, M.E. (1983). Glutathione. Annu Rev Biochem *52*, 711-760.
- Melamed, D., Benschop, R.J., Cambier, J.C., and Nemazee, D. (1998). Developmental regulation of B lymphocyte immune tolerance compartmentalizes clonal selection from receptor selection. Cell *92*, 173-182.
- Merle, N.S., Church, S.E., Fremeaux-Bacchi, V., and Roumenina, L.T. (2015). Complement System Part I - Molecular Mechanisms of Activation and Regulation. Front Immunol *6*, 262.
- Mesin, L., Ersching, J., and Victora, G.D. (2016). Germinal Center B Cell Dynamics. Immunity *45*, 471-482.
- Messina, J.P., and Lawrence, D.A. (1989). Cell cycle progression of glutathione-depleted human peripheral blood mononuclear cells is inhibited at S phase. *143*, 1974-1981.
- Moir, S., and Fauci, A.S. (2009). B cells in HIV infection and disease. Nat Rev Immunol *9*, 235-245.
- Mond, J. (1995). T cell independent antigens. Current Opinion in Immunology *7*, 349-354.

- Montecino-Rodriguez, E., and Dorshkind, K. (2012). B-1 B cell development in the fetus and adult. Immunity *36*, 13-21.
- Monteiro, L.B., Davanzo, G.G., de Aguiar, C.F., and Moraes-Vieira, P.M.M. (2020). Using flow cytometry for mitochondrial assays. MethodsX *7*, 100938.
- Morelli, A.M., Ravera, S., Calzia, D., and Panfoli, I. (2019). An update of the chemiosmotic theory as suggested by possible proton currents inside the coupling membrane. Open Biol *9*, 180221.
- Muri, J., and Kopf, M. (2020). Redox regulation of immunometabolism. Nat Rev Immunol.
- Muri, J., Thut, H., Heer, S., Krueger, C.C., Bornkamm, G.W., Bachmann, M.F., and Kopf, M. (2019). The thioredoxin-1 and glutathione/glutaredoxin-1 systems redundantly fuel murine B-cell development and responses. Eur J Immunol *49*, 709-723.
- Murphy, K.M., and Stockinger, B. (2010). Effector T cell plasticity: flexibility in the face of changing circumstances. Nat Immunol *11*, 674-680.
- Murphy, M.P. (2009). How mitochondria produce reactive oxygen species. Biochem J *417*, 1-13.
- Nebert, D.W., and Vasiliou, V. (2004). Analysis of the glutathione S-transferase (GST) gene family. Hum Genomics *1*, 460-464.
- Nguyen, T.T., Elsner, R.A., and Baumgarth, N. (2015). Natural IgM prevents autoimmunity by enforcing B cell central tolerance induction. J Immunol *194*, 1489-1502.
- Nieuwenhuis, P., and Opstelten, D. (1984). Functional anatomy of germinal centers. Am J Anat *170*, 421-435.

- Nossal, G.J.V., Ada, G.L., and Austin, C.M. (1964). Antigens in Immunity. Australian Journal of Experimental Biology and Medical Science *42*, 311-330.
- Notkins, A.L. (2004). Polyreactivity of antibody molecules. Trends Immunol *25*, 174-179.
- O'Neill, J.P. (2000). DNA damage, DNA repair, cell proliferation, and DNA replication: how do gene mutations result? Proc Natl Acad Sci U S A *97*, 11137-11139.
- O'Neill, L.A., and Pearce, E.J. (2016). Immunometabolism governs dendritic cell and macrophage function. J Exp Med *213*, 15-23.
- O'Neill, L.A., Kishton, R.J., and Rathmell, J. (2016). A guide to immunometabolism for immunologists. Nat Rev Immunol *16*, 553-565.
- Ochsenbein, A.F., and Zinkernagel, R.M. (2000). Natural antibodies and complement link innate and acquired immunity. Immunology Today *21*, 624-630.
- Ochsenbein, A.F., Fehr, T., Lutz, C., Suter, M., Brombacher, F., Hengartner, H., and Zinkernagel, R.M. (1999a). Control of early viral and bacterial distribution and disease by natural antibodies. Science *286*, 2156-2159.
- Ochsenbein, A.F., Karrer, U., Klenerman, P., Althage, A., Ciurea, A., Shen, H., Miller, J.F., Whitton, J.L., Hengartner, H., and Zinkernagel, R.M. (1999b). A comparison of T cell memory against the same antigen induced by virus versus intracellular bacteria. Proc Natl Acad Sci U S A *96*, 9293-9298.
- Oliver, A.M., Martin, F., and Kearney, J.F. (1999). IgMhighCD21high Lymphocytes Enriched in the Splenic Marginal Zone Generate Effector Cells More Rapidly Than the Bulk of Follicular B Cells. J Immunol *162*, 7198-7207.

- Oliver, A.M., Martin, F., Gartland, G.L., Carter, R.H., and Kearney, J.F. (1997). Marginal zone B cells exhibit unique activation, proliferative and immunoglobulin secretory responses. Eur J Immunol *27*, 2366-2374.
- Oppenheimer, L., Wellner, V.P., Griffith, O.W., and Meister, A. (1979). Glutathione synthetase. Purification from rat kidney and mapping of the substrate binding sites. J Biol Chem *254*, 5184-5190.
- Papavasiliou, F.N., and Schatz, D.G. (2002). Somatic Hypermutation of Immunoglobulin Genes. Cell *109*, S35-S44.
- Pape, K.A., Catron, D.M., Itano, A.A., and Jenkins, M.K. (2007). The humoral immune response is initiated in lymph nodes by B cells that acquire soluble antigen directly in the follicles. Immunity *26*, 491-502.
- Pearce, E.L., and Pearce, E.J. (2013). Metabolic pathways in immune cell activation and quiescence. Immunity *38*, 633-643.
- Penalver Bernabe, B., Thiele, I., Galdones, E., Siletz, A., Chandrasekaran, S., Woodruff, T.K., Broadbelt, L.J., and Shea, L.D. (2019). Dynamic genome-scale cell-specific metabolic models reveal novel inter-cellular and intra-cellular metabolic communications during ovarian follicle development. BMC Bioinformatics *20*, 307.
- Peschon, J.J., Morrissey, P.J., Grabstein, K.H., Ramsdell, F.J., Maraskovsky, E., Gliniak, B.C., Park, L.S., Ziegler, S.F., Williams, D.E., Ware, C.B.*, et al.* (1994). Early lymphocyte expansion is severely impaired in interleukin 7 receptor-deficient mice. J Exp Med *180*, 1955-1960.
- Phan, T.G., Grigorova, I., Okada, T., and Cyster, J.G. (2007). Subcapsular encounter and complement-dependent transport of immune complexes by lymph node B cells. Nat Immunol *8*, 992-1000.

- Pieper, K., Grimbacher, B., and Eibel, H. (2013). B-cell biology and development. J Allergy Clin Immunol *131*, 959-971.
- Pillai, S., and Cariappa, A. (2009). The follicular versus marginal zone B lymphocyte cell fate decision. Nat Rev Immunol *9*, 767-777.
- Pillai, S., Cariappa, A., and Moran, S.T. (2005). Marginal zone B cells. Annu Rev Immunol *23*, 161-196.
- Pollak, N., Dolle, C., and Ziegler, M. (2007). The power to reduce: pyridine nucleotides--small molecules with a multitude of functions. Biochem J *402*, 205-218.
- Qi, H., Egen, J.G., Huang, A.Y., and Germain, R.N. (2006). Extrafollicular activation of lymph node B cells by antigen-bearing dendritic cells. Science *312*, 1672-1676.
- Quiros, P.M., Goyal, A., Jha, P., and Auwerx, J. (2017). Analysis of mtDNA/nDNA Ratio in Mice. Curr Protoc Mouse Biol *7*, 47-54.
- Raberg, L., Vestberg, M., Hasselquist, D., Holmdahl, R., Svensson, E., and Nilsson, J.A. (2002). Basal metabolic rate and the evolution of the adaptive immune system. Proc Biol Sci *269*, 817-821.
- Recher, M., Lang, K.S., Hunziker, L., Freigang, S., Eschli, B., Harris, N.L., Navarini, A., Senn, B.M., Fink, K., Lotscher, M.*, et al.* (2004). Deliberate removal of T cell help improves virus-neutralizing antibody production. Nat Immunol *5*, 934-942.
- Reczek, C.R., and Chandel, N.S. (2015). ROS-dependent signal transduction. Curr Opin Cell Biol *33*, 8-13.
- Reimold, A.M., Iwakoshi, N.N., Manis, J., Vallabhajosyula, P., Szomolanyi-Tsuda, E., Gravallese, E.M., Friend, D., Grusby, M.J., Alt, F., and Glimcher, L.H. (2001). Plasma cell differentiation requires the transcription factor XBP-1. Nature *412*, 300-307.

- Rock, K.L., Reits, E., and Neefjes, J. (2016). Present Yourself! By MHC Class I and MHC Class II Molecules. Trends Immunol *37*, 724-737.
- Sakaguchi, S., Yamaguchi, T., Nomura, T., and Ono, M. (2008). Regulatory T cells and immune tolerance. Cell *133*, 775-787.
- Salabei, J.K., Gibb, A.A., and Hill, B.G. (2014). Comprehensive measurement of respiratory activity in permeabilized cells using extracellular flux analysis. Nat Protoc *9*, 421-438.
- Savage, H.P., Yenson, V.M., Sawhney, S.S., Mousseau, B.J., Lund, F.E., and Baumgarth, N. (2017). Blimp-1-dependent and -independent natural antibody production by B-1 and B-1-derived plasma cells. J Exp Med *214*, 2777-2794.
- Saxton, R.A., and Sabatini, D.M. (2017). mTOR Signaling in Growth, Metabolism, and Disease. Cell *168*, 960-976.
- Schieber, M., and Chandel, N.S. (2014). ROS function in redox signaling and oxidative stress. Curr Biol *24*, R453-462.
- Schiemann, B., Gommerman, J.L., Vora, K., Cachero, T.G., Shulga-Morskaya, S., Dobles, M., Frew, E., and Scott, M.L. (2001). An essential role for BAFF in the normal development of B cells through a BCMA-independent pathway. Science *293*, 2111-2114.
- Schmidt-Supprian, M., and Rajewsky, K. (2007). Vagaries of conditional gene targeting. Nat Immunol *8*, 665-668.
- Schmidt, E.K., Clavarino, G., Ceppi, M., and Pierre, P. (2009). SUnSET, a nonradioactive method to monitor protein synthesis. Nat Methods *6*, 275-277.
- Sena, L.A., and Chandel, N.S. (2012). Physiological roles of mitochondrial reactive oxygen species. Mol Cell *48*, 158-167.

- Sena, L.A., Li, S., Jairaman, A., Prakriya, M., Ezponda, T., Hildeman, D.A., Wang, C.R., Schumacker, P.T., Licht, J.D., Perlman, H.*, et al.* (2013). Mitochondria are required for antigen-specific T cell activation through reactive oxygen species signaling. Immunity *38*, 225-236.
- Shaffer, A.L., Lin, K.-I., Kuo, T.C., Yu, X., Hurt, E.M., Rosenwald, A., Giltnane, J.M., Yang, L., Zhao, H., Calame, K.*, et al.* (2002). Blimp-1 Orchestrates Plasma Cell Differentiation by Extinguishing the Mature B Cell Gene Expression Program. Immunity *17*, 51-62.
- Shaffer, A.L., Shapiro-Shelef, M., Iwakoshi, N.N., Lee, A.H., Qian, S.B., Zhao, H., Yu, X., Yang, L., Tan, B.K., Rosenwald, A.*, et al.* (2004). XBP1, downstream of Blimp-1, expands the secretory apparatus and other organelles, and increases protein synthesis in plasma cell differentiation. Immunity *21*, 81-93.
- Shaw, P.X., Horkko, S., Chang, M.K., Curtiss, L.K., Palinski, W., Silverman, G.J., and Witztum, J.L. (2000). Natural antibodies with the T15 idiotype may act in atherosclerosis, apoptotic clearance, and protective immunity. J Clin Invest *105*, 1731-1740.
- Shevach, E.M. (2011). The resurrection of T cell-mediated suppression. J Immunol *186*, 3805-3807.
- Shi, W., Liao, Y., Willis, S.N., Taubenheim, N., Inouye, M., Tarlinton, D.M., Smyth, G.K., Hodgkin, P.D., Nutt, S.L., and Corcoran, L.M. (2015). Transcriptional profiling of mouse B cell terminal differentiation defines a signature for antibody-secreting plasma cells. Nat Immunol *16*, 663-673.
- Shimizu, Y., and Hendershot, L.M. (2009). Oxidative folding: cellular strategies for dealing with the resultant equimolar production of reactive oxygen species. Antioxid Redox Signal *11*, 2317-2331.

- Sies, H. (1986). Biochemistry of Oxidative Stress. Angewandte Chemie International Edition in English *25*, 1058-1071.
- Sies, H., and Jones, D.P. (2020). Reactive oxygen species (ROS) as pleiotropic physiological signalling agents. Nat Rev Mol Cell Biol.
- Slifka, M.K., Antia, R., Whitmire, J.K., and Ahmed, R. (1998). Humoral Immunity Due to Long-Lived Plasma Cells. Immunity *8*, 363-372.
- Song, H., and Cerny, J. (2003). Functional heterogeneity of marginal zone B cells revealed by their ability to generate both early antibody-forming cells and germinal centers with hypermutation and memory in response to a T-dependent antigen. J Exp Med *198*, 1923-1935.
- Spitzer, M.H., and Nolan, G.P. (2016). Mass Cytometry: Single Cells, Many Features. Cell *165*, 780-791.
- Srivastava, B., Quinn, W.J., 3rd, Hazard, K., Erikson, J., and Allman, D. (2005). Characterization of marginal zone B cell precursors. J Exp Med *202*, 1225-1234.
- Staal, F.J., Roederer, M., Herzenberg, L.A., and Herzenberg, L.A. (1992a). Glutathione and immunophenotypes of T and B lymphocytes in HIV-infected individuals. Ann N Y Acad Sci *651*, 453-463.
- Staal, F.J., Roederer, M., Israelski, D.M., Bubp, J., Mole, L.A., McShane, D., Deresinski, S.C., Ross, W., Sussman, H., Raju, P.A.*, et al.* (1992b). Intracellular glutathione levels in T cell subsets decrease in HIV-infected individuals. AIDS Res Hum Retroviruses *8*, 305-311.
- Staal, F.J., Roederer, M., Bubp, J., Mole, L.A., Anderson, M.T., Raju, P.A., Israelski, D.M., Deresinski, S.C., Moore, W.A., Herzenberg, L.A.*, et al.* (1992c). CD20 expression

is increased on B lymphocytes from HIV-infected individuals J Acquir Immune Defic Syndr *5*.

- Stall, A.M., Adams, S., Herzenberg, L.A., and Kantor, A.B. (1992). Characteristics and development of the murine B-1b (Ly-1 B sister) cell population. Ann N Y Acad Sci *651*, 33-43.
- Steiniger, B., Timphus, E.M., and Barth, P.J. (2006). The splenic marginal zone in humans and rodents: an enigmatic compartment and its inhabitants. Histochem Cell Biol *126*, 641-648.
- Stockwin, L.H., McGonagle, D., Martin, I.G., and Blair, G.E. (2000). Dendritic cells: immunological sentinels with a central role in health and disease. Immunol Cell Biol *78*, 91-102.
- Stoeckius, M., Hafemeister, C., Stephenson, W., Houck-Loomis, B., Chattopadhyay, P.K., Swerdlow, H., Satija, R., and Smibert, P. (2017). Simultaneous epitope and transcriptome measurement in single cells. Nat Methods *14*, 865-868.
- Stoeckius, M., Zheng, S., Houck-Loomis, B., Hao, S., Yeung, B.Z., Mauck, W.M., 3rd, Smibert, P., and Satija, R. (2018). Cell Hashing with barcoded antibodies enables multiplexing and doublet detection for single cell genomics. Genome Biol *19*, 224.
- Strassmann, J.E., Queller, D.C., Avise, J.C., and Ayala, F.J. (2011). In the light of evolution V: cooperation and conflict. Proc Natl Acad Sci U S A *108 Suppl 2*, 10787-10791.
- Su, T.T., and Rawlings, D.J. (2002). Transitional B lymphocyte subsets operate as distinct checkpoints in murine splenic B cell development. J Immunol *168*, 2101-2110.
- Sullivan, B.M., Emonet, S.F., Welch, M.J., Lee, A.M., Campbell, K.P., de la Torre, J.C., and Oldstone, M.B. (2011). Point mutation in the glycoprotein of lymphocytic

choriomeningitis virus is necessary for receptor binding, dendritic cell infection, and long-term persistence. Proc Natl Acad Sci U S A *108*, 2969-2974.

- Swanson, C.L., Pelanda, R., and Torres, R.M. (2013). Division of labor during primary humoral immunity. Immunol Res *55*, 277-286.
- Szakal, A.K., Holmes, K.L., and Tew, J.G. (1983). Transport of immune complexes from the subcapsular sinus to lymph node follicles on the surface of nonphagocytic cells, including cells with dendritic morphology. J Immunol *131*, 1714-1727.
- Tellier, J., Shi, W., Minnich, M., Liao, Y., Crawford, S., Smyth, G.K., Kallies, A., Busslinger, M., and Nutt, S.L. (2016). Blimp-1 controls plasma cell function through the regulation of immunoglobulin secretion and the unfolded protein response. Nat Immunol *17*, 323-330.
- Tew, J.G., Wu, J., Fakher, M., Szakal, A.K., and Qin, D. (2001). Follicular dendritic cells: beyond the necessity of T-cell help. Trends in Immunology *22*, 361-367.
- Thiele, I., Swainston, N., Fleming, R.M., Hoppe, A., Sahoo, S., Aurich, M.K., Haraldsdottir, H., Mo, M.L., Rolfsson, O., Stobbe, M.D.*, et al.* (2013). A community-driven global reconstruction of human metabolism. Nat Biotechnol *31*, 419-425.
- Tiscornia, G., Singer, O., Ikawa, M., and Verma, I.M. (2003). A general method for gene knockdown in mice by using lentiviral vectors expressing small interfering RNA. Proc Natl Acad Sci U S A *100*, 1844-1848.
- Trachootham, D., Lu, W., Ogasawara, M.A., Nilsa, R.D., and Huang, P. (2008). Redox regulation of cell survival. Antioxid Redox Signal *10*, 1343-1374.
- Treanor, B. (2012). B-cell receptor: from resting state to activate. Immunology *136*, 21-27.

- Tsubata, T. (2020). Involvement of Reactive Oxygen Species (ROS) in BCR Signaling as a Second Messenger. Adv Exp Med Biol *1254*, 37-46.
- Tu, B.P., and Weissman, J.S. (2002). The FAD- and O2-Dependent Reaction Cycle of Ero1-Mediated Oxidative Protein Folding in the Endoplasmic Reticulum. Molecular Cell *10*, 983-994.
- Tumang, J.R., Frances, R., Yeo, S.G., and Rothstein, T.L. (2005). Spontaneously Ig-secreting B-1 cells violate the accepted paradigm for expression of differentiation-associated transcription factors. J Immunol *174*, 3173-3177.
- Urbanczyk, S., Stein, M., Schuh, W., Jack, H.M., Mougiakakos, D., and Mielenz, D. (2018). Regulation of Energy Metabolism during Early B Lymphocyte Development. Int J Mol Sci *19*.
- van Anken, E., Romijn, E.P., Maggioni, C., Mezghrani, A., Sitia, R., Braakman, I., and Heck, A.J.R. (2003). Sequential Waves of Functionally Related Proteins Are Expressed When B Cells Prepare for Antibody Secretion. Immunity *18*, 243-253.
- Vandepol, S.B., Lefrancois, L., and Holland, J.J. (1986). Sequences of the major antibody binding epitopes of the Indiana serotype of vesicular stomatitis virus. Virology *148*, 312-325.
- Vashist, S., and Ng, D.T. (2004). Misfolded proteins are sorted by a sequential checkpoint mechanism of ER quality control. J Cell Biol *165*, 41-52.
- Vaughan, M. (1997). Oxidative Modification of Macromolecules Minireview Series. J Biol Chem *272*.
- Vene, R., Delfino, L., Castellani, P., Balza, E., Bertolotti, M., Sitia, R., and Rubartelli, A. (2010). Redox remodeling allows and controls B-cell activation and differentiation. Antioxid Redox Signal *13*, 1145-1155.

- Vettermann, C., and Jack, H.M. (2010). The pre-B cell receptor: turning autoreactivity into self-defense. Trends Immunol *31*, 176-183.
- Vettermann, C., Herrmann, K., and Jack, H.M. (2006). Powered by pairing: the surrogate light chain amplifies immunoglobulin heavy chain signaling and pre-selects the antibody repertoire. Semin Immunol *18*, 44-55.
- Victora, G.D., and Nussenzweig, M.C. (2012). Germinal centers. Annu Rev Immunol *30*, 429-457.
- Victora, G.D., Schwickert, T.A., Fooksman, D.R., Kamphorst, A.O., Meyer-Hermann, M., Dustin, M.L., and Nussenzweig, M.C. (2010). Germinal center dynamics revealed by multiphoton microscopy with a photoactivatable fluorescent reporter. Cell *143*, 592-605.
- Vivier, E., Artis, D., Colonna, M., Diefenbach, A., Di Santo, J.P., Eberl, G., Koyasu, S., Locksley, R.M., McKenzie, A.N.J., Mebius, R.E*., et al.* (2018). Innate Lymphoid Cells: 10 Years On. Cell *174*, 1054-1066.
- Vollmers, H.P., and Brandlein, S. (2009). Natural antibodies and cancer. N Biotechnol *25*, 294-298.
- Voss, K., Hong, H.S., Bader, J.E., Sugiura, A., Lyssiotis, C.A., and Rathmell, J.C. (2021). A guide to interrogating immunometabolism. Nat Rev Immunol.
- Wagner, A., Wang, C., Fessler, J., DeTomaso, D., Avila-Pacheco, J., Kaminski, J., Zaghouani, S., Christian, E., Thakore, P., Schellhaass, B*., et al.* (2021). Metabolic modeling of single Th17 cells reveals regulators of autoimmunity. Cell.
- Wahl, D.R., Byersdorfer, C.A., Ferrara, J.L., Opipari, A.W., Jr., and Glick, G.D. (2012). Distinct metabolic programs in activated T cells: opportunities for selective immunomodulation. Immunol Rev *249*, 104-115.

- Wang, C., Wagner, A., Fessler, J., Avila-Pacheco, J., Karminski, J., Thakore, P., Zaghouani, S., Pierce, K., Bod, L., Schnell, A.*, et al.* (2020). Metabolic and Epigenomic Regulation of Th17/Treg Balance by the Polyamine Pathway.
- Wang, S.B., Murray, C.I., Chung, H.S., and Van Eyk, J.E. (2013). Redox regulation of mitochondrial ATP synthase. Trends Cardiovasc Med *23*, 14-18.
- Waters, L.R., Ahsan, F.M., Wolf, D.M., Shirihai, O., and Teitell, M.A. (2018). Initial B Cell Activation Induces Metabolic Reprogramming and Mitochondrial Remodeling. iScience *5*, 99-109.
- Weih, D.S., Yilmaz, Z.B., and Weih, F. (2001). Essential role of RelB in germinal center and marginal zone formation and proper expression of homing chemokines. J Immunol *167*, 1909-1919.
- Weill, J.C., Weller, S., and Reynaud, C.A. (2009). Human marginal zone B cells. Annu Rev Immunol *27*, 267-285.
- Weller, S., Braun, M.C., Tan, B.K., Rosenwald, A., Cordier, C., Conley, M.E., Plebani, A., Kumararatne, D.S., Bonnet, D., Tournilhac, O.*, et al.* (2004). Human blood IgM "memory" B cells are circulating splenic marginal zone B cells harboring a prediversified immunoglobulin repertoire. Blood *104*, 3647-3654.
- Wells, S.M., Kantor, A.B., and Stall, A.M. (1994). CD43 (S7) expression identifies peripheral B cell subsets. J Immunol *153*, 5503-5515.
- Wheeler, M.L., and Defranco, A.L. (2012). Prolonged production of reactive oxygen species in response to B cell receptor stimulation promotes B cell activation and proliferation. J Immunol *189*, 4405-4416.

- Winterbourn, C.C., and Brennan, S.O. (1997). Characterization of the oxidation products of the reaction between reduced glutathione and hypochlorous acid. Biochem J *326 (Pt 1)*, 87-92.
- Won, W.J., and Kearney, J.F. (2002). CD9 is a unique marker for marginal zone B cells, B1 cells, and plasma cells in mice. J Immunol *168*, 5605-5611.
- Wood, Z.A., Schröder, E., Robin Harris, J., and Poole, L.B. (2003). Structure, mechanism and regulation of peroxiredoxins. Trends in Biochemical Sciences *28*, 32-40.
- Wu, G., Fang, Y.Z., Yang, S., Lupton, J.R., and Turner, N.D. (2004). Glutathione metabolism and its implications for health. J Nutr *134*, 489-492.
- Yancopoulos, G.D., Desiderio, S.V., Paskind, M., Kearney, J.F., Baltimore, D., and Alt, F.W. (1984). Preferential utilization of the most JH-proximal VH gene segments in pre-B-cell lines. Nature *311*, 727-733.
- Yang, Y., Bazhin, A.V., Werner, J., and Karakhanova, S. (2013). Reactive oxygen species in the immune system. Int Rev Immunol *32*, 249-270.
- Yang, Y., Dieter, M.Z., Chen, Y., Shertzer, H.G., Nebert, D.W., and Dalton, T.P. (2002). Initial characterization of the glutamate-cysteine ligase modifier subunit Gclm(-/-) knockout mouse. Novel model system for a severely compromised oxidative stress response. J Biol Chem *277*, 49446-49452.
- You, Y., Zhao, H., Wang, Y., and Carter, R.H. (2009). Cutting edge: Primary and secondary effects of CD19 deficiency on cells of the marginal zone. J Immunol *182*, 7343-7347.

- You, Y., Myers, R.C., Freeberg, L., Foote, J., Kearney, J.F., Justement, L.B., and Carter, R.H. (2011). Marginal zone B cells regulate antigen capture by marginal zone macrophages. J Immunol *186*, 2172-2181.
- Yuan, D., and Tucker, P.W. (1984). Transcriptional regulation of the mu-delta heavy chain locus in normal murine B lymphocytes. J Exp Med *160*, 564-583.
- Yumura, W., Sugino, N., Nagasawa, R., Kubo, S., Hirokawa, K., and Maruyama, N. (1989). Age-associated changes in renal glomeruli of mice. Exp Gerontol *24*, 237-249.
- Zamaraeva, M.V., Sabirov, R.Z., Maeno, E., Ando-Akatsuka, Y., Bessonova, S.V., and Okada, Y. (2005). Cells die with increased cytosolic ATP during apoptosis: a bioluminescence study with intracellular luciferase. Cell Death Differ *12*, 1390-1397.
- Zhang, Y., Marcillat, O., Giulivi, C., Ernster, L., and Davies, K.J. (1990). The oxidative inactivation of mitochondrial electron transport chain components and ATPase. J Biol Chem *265*, 16330-16336.
- Zhou, Z.H., Zhang, Y., Hu, Y.F., Wahl, L.M., Cisar, J.O., and Notkins, A.L. (2007). The broad antibacterial activity of the natural antibody repertoire is due to polyreactive antibodies. Cell Host Microbe *1*, 51-61.
- Zinkernagel, R.M., Bachmann, M.F., Kundig, T.M., Oehen, S., Pirchet, H., and Hengartner, H. (1996). On immunological memory. Annu Rev Immunol *14*, 333-367.
- Zinkernagel, R.M., Ehl, S., Aichele, P., Oehen, S., Kundig, T., and Hengartner, H. (1997). Antigen localisation regulates immune responses in a dose- and time-dependent fashion: a geographical view of immune reactivity. Immunol Rev *156*, 199-209.
- Zou, C., Wang, Y., and Shen, Z. (2005). 2-NBDG as a fluorescent indicator for direct glucose uptake measurement. J Biochem Biophys Methods *64*, 207-215.